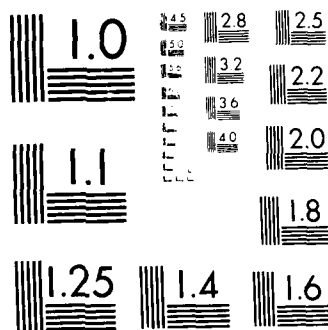ANISOTROPY AND STRESS PATH EFFECTS IN CLAYS WITH
APPLICATIONS TO THE PRES.. (U) PURDUE UNIV LAFAYETTE IN
SCHOOL OF CIVIL ENGINEERING   31 JUL 88 AFOSR-TR-88-1018

UNCLASSIFIED   AFOSR-87-0132   F/G 8/7   NL

AD-A199 628

CUMENTATION PAGE

Form Approved
OMB No 0704-0188

UNCLASSIFIED

1b RESTRICTIVE MARKINGS	

2a. SECURITY CLASSIFICATION AUTHORITY	3. DISTRIBUTION/AVAILABILITY OF REPORT
2b. DECLASSIFICATION/DOWNGRADING SCHEDULE	Approved for Public Release; Distribution Unlimited

4 PERFORMING ORGANIZATION REPORT NUMBER(S)	5 MONITORING ORGANIZATION REPORT NUMBER(S)
	AFOSR·TR· 88-1010

6a NAME OF PERFORMING ORGANIZATION	6b OFFICE SYMBOL (If applicable)	7a NAME OF MONITORING ORGANIZATION
School of Civil Engineering Purdue University		AFOSR/NA

6c. ADDRESS (City, State, and ZIP Code)	7b ADDRESS (City, State, and ZIP Code)
Purdue University West Lafayette, IN 47907	Bldg. 410 Bolling AFB, DC 20332-6448

8a NAME OF FUNDING/SPONSORING ORGANIZATION	8b OFFICE SYMBOL (If applicable)	9 PROCUREMENT INSTRUMENT IDENTIFICATION NUMBER
AFOSR	NA	AFOSR-87-0132

8c. ADDRESS (City, State, and ZIP Code)	10 SOURCE OF FUNDING NUMBERS			
	PROGRAM ELEMENT NO	PROJECT NO	TASK NO	WORK UNIT ACCESSION NO
Bldg. 410 Bolling AFB, DC 20332-6448	6.1102F	2302	C1	

11 TITLE (Include Security Classification) (U)

Anisotropy and Stress Path Effects in Clays with Applications to the Pressuremeter Test

12 PERSONAL AUTHOR(S)
S. Thevanayagam, A. Skandarajah and J. L. Chameau

13a TYPE OF REPORT	13b TIME COVERED	14. DATE OF REPORT (Year, Month, Day)	15 PAGE COUNT
Final	FROM 3/1/87 TO 5/31/88	1988 July 31	146

16 SUPPLEMENTARY NOTATION

17 COSATI CODES			18 SUBJECT TERMS (Continue on reverse if necessary and identify by block number)
FIELD	GROUP	SUB-GROUP	Strength Anisotropy, Stress Path, Pore Pressure, Cohesive Soils, Clays, Shear Strength, Pressuremeter, In Situ Tests

19 ABSTRACT (Continue on reverse if necessary and identify by block number)
The research study undertaken at Purdue focuses towards increasing our understanding of fundamental issues related to the behavior of clays, especially with regard to modelling their anisotropy. There is ample evidence that in situ soils are anisotropic, elasto-plastic, stress path and rate dependent, unlike what is generally assumed in test interpretations. Therefore, the study of mechanisms of deformation of in situ tests and their interpretation must take into account these features, and especially the anisotropic nature of the soil deposit.

Expressions were derived for the normalized shear strength τ_p/σ'_{vo} using the Cam clay model, the modified Cam clay model, and the extended Cam clay and modified Cam clay models with spacing ratio. Both extended models with spacing ratio predict values that compare well with experimental data. Unlike the excellent agreement with experimental results obtained for τ_p/σ'_{vo}, predictions made for Skempton's A parameter at failure A_f were marginal for all models. A_f is very sensitive to Λ, which is a function of C_s and C_c. This severely
(Continued)

20 DISTRIBUTION/AVAILABILITY OF ABSTRACT	21 ABSTRACT SECURITY CLASSIFICATION
☒ UNCLASSIFIED/UNLIMITED ☐ SAME AS RPT ☐ DTIC USERS	UNCLASSIFIED

22a NAME OF RESPONSIBLE INDIVIDUAL	22b TELEPHONE (Include Area Code)	22c OFFICE SYMBOL
Major Steven C. Boyce	(202) 767-6963	AFOSR/NA

DD Form 1473, JUN 86   Previous editions are obsolete   SECURITY CLASSIFICATION OF THIS PAGE

UNCLASSIFIED
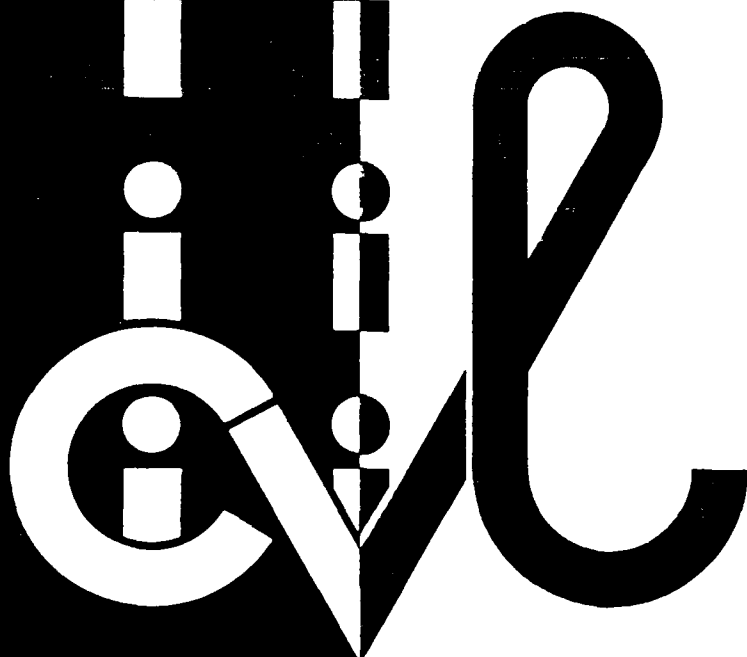
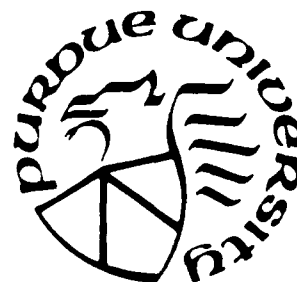# SCHOOL OF CIVIL ENGINEERING

ANISOTROPY AND STRESS PATH EFFECTS
IN CLAYS WITH APPLICATIONS TO THE
PRESSUREMETER TEST

by

S. Thevanayagam
A. Skandarajah
J. L. Chameau

PURDUE UNIVERSITY

88 10 5 294

19. ABSTRACT (continued)

influences Λ and thus affects the predictions of A_f. Using critical state concepts a simplified procedure to predict the overconsolidatio ratio of clays is presented. Since the OCR estimate is not sensitive to the C_r/C_c ratio, a good prediction is possible from the knowledge of e/e_L and σ'_v.

The limitations of existing theories to model the anisotropy of clays were identified. A novel approach is presented that incorporates the essential features of anisotropic behavior of clays, and the theory is validated using experimental data. The model captures the essential features of initial and induced anisotropy, yet yielding close form solutions for all the failure parameters of clay. The proposed theory is applicable to a number of geotechnical problems; in this report, it is used to investigate several important issues related to the determination of in situ properties using the self-boring pressuremeter (SBPM):

(i) The stress state and mode of deformation in pressuremeter tests are identified. The generality of plane strain condition during expansion of an SBPM cavity is shown and conditions where it is far from plane strain are indicated. Experimental data are used to substantiate the theoretical findings. All indications are that these findings can settle the questions regarding the mode of deformation and the role of the vertical stress in expansion of cylindrical cavity.

(ii) The possibility of radial cracking (negative circumferential stress) was analyzed in detail and shown to be unlikely.

(iii) Using the theory developed in this work, the SBPM failure parameters can be used to determine the same parameters for many different modes of failure other than that of the SBPM.

(iv) A procedure has been proposed to evaluate the error in strain induced by initial movement of the pressuremeter cavity. After evaluation of the error in strain, actual strength parameters can be calculated.

ANISOTROPY AND STRESS PATH EFFECTS
IN CLAYS WITH APPLICATIONS TO THE
PRESSUREMETER TEST

by

S. Thevanayagam
A. Skandarajah
J. L. Chameau

PURDUE UNIVERSITY

School of Civil Engineering

West Lafayette, IN 47907

July 31, 1988

A-1

TABLE OF CONTENTS

CHAPTER 1

INTRODUCTION

The research study undertaken at Purdue focuses towards increasing our understanding of fundamental issues related to the behavior of clays, especially with regard to modelling their anisotropy. The information being developed is applicable to most geotechnical problems, however, in illustrating their usefulness, emphasis is placed on interpretation of in situ tests, and in particular pressuremeter and self-boring pressuremeter (SBPM) tests. There is ample evidence that in situ soils are anisotropic, elasto-plastic, stress path and rate dependent, unlike what is generally assumed in test interpretations. Therefore, the study of mechanisms of deformation of in situ tests and their interpretation must take into account these features, and especially the anisotropic nature of the soil deposit. A simple and reliable anisotropic theory will be most useful in the study of several important factors related to pressuremeter testing such as possibility of radial cracking, role of vertical stress, stress conditions at failure, and the effects of initial disturbance which cannot be measured. It will also be possible to estimate undrained strength of the clay in other modes of failure using SBPM data only.

In Chapter 2 of this report, the viability of modelling the anisotropic behavior of clays within the context of the modified cam clay (MCC) model (Roscoe and Burland 1968, Wroth 1984) is stu-

died. Some useful relationships to predict the behavior of clays in triaxial space are presented, and the limitations of the MCC model are indicated. A cuboidal shear device is used to illustrate the influence of stress path and fabric anisotropy on the behavior of clays. In addition, using critical state concepts (Schofield and Wroth 1968, Wroth 1979) a simplified procedure to predict the overconsolidation ratio of clays is presented.

In Chapter 3, the limitations of existing theories to model the anisotropy of clays are identified. A novel approach is presented that incorporates the essential features of anisotropic behavior of clays, and the theory is validated using experimental data. The model captures the essential features of initial and induced anisotropy, yet yielding close form solutions for all the failure parameters of clay. All the facets of anisotropy known to date are incorporated. It can be applied to a number of geotechnical problems, such as stability of embankments, retaining systems, etc. Its potential is demonstrated by studying the following issues in pressuremeter testing of soils. (i) The stress state and mode of deformation in pressuremeter tests are identified. The generality of plane strain condition during expansion of an SBPM cavity is shown and conditions where it is far from plane strain are indicated. Experimental data are used to substantiate the theoretical findings. All indications are that these findings can settle the questions regarding the mode of deformation and the role of the vertical stress in expansion of cylindrical cavity (SBPM).

(ii) Possibility of radial cracking is analyzed in detail, showing little chance for its occurrence. (iii) A method to obtain aniso-tropic failure parameters using SBPM test data is outlined. (iv) An analytical technique to make allowance for the disturbance in test data is presented.

CHAPTER 2

STRESS PATH AND STRENGTH ANISOTROPY

2.1 Experimental Illustration of Anisotropy Effects

Strength anisotropy consists of two major components. One is inherent anisotropy, which occurs due to preferred particle arrangement during sedimentation, resulting in a fabric that is not identical in all directions. The other component is stress induced anisotropy which is caused by an anisotropic state of stress at the end of consolidation. Inherent anisotropy implies that the soil behaves anisotropically even if the initial stress state is isotropic. Stress induced anisotropy means that the soil behaves anisotropically depending on the direction of loading due to its initial anisotropic stress state even if the soil properties such as c' and ϕ' are isotropic. The ratio of triaxial compression strength to that of triaxial extension is often referred to as a measure of anisotropy. Using the cuboidal shear device, anisotropy was illustrated by comparing the strength derived from strain controlled tests on sedimented samples loaded vertically and horizontally under plane strain conditions.

Three tests were carried out on WP Georgia silty clay under essentially plane strain conditions: the first two tests on K_o consolidated samples and the following one on an isotropically consolidated sample. In the first test ($CK_oUC-PSV$), major and minor principal stress increments were applied horizontally, while the intermediate principal stress increment was applied vertically,

ensuring plane strain conditions, with the plane of deformation being horizontal (this situation is typical of a horizontally loaded pile foundation). In the second test (CK_oUC-PSH) intermediate and minor principal stress increments were applied horizontally, while the major principal stress increment was applied vertically, ensuring plane strain conditions, with the plane of deformation being vertical (this is a typical field loading condition, e.g., long embankment strip footing, etc.). The same test was repeated on an isotropically consolidated sample (CIUC-PSH). The results of these plane strain tests are given in Table 2.1.

To quantify strength anisotropy, several techniques have been proposed by previous researchers (e.g. Aas, 1965, Duncan and Seed, 1966, Lo and Morin, 1972, Berre and Bjerrum, 1973, Krishnamurthy, et al., 1980, Nakase and Kamei, 1983). In the experimental program described herein, the specimen is never rotated. The axis remains vertical during consolidation and shear. Anisotropy is measured by the ratio of the shear strength of a horizontally loaded specimen to the strength of a vertically loaded replicate specimen.

From Table 2.1, the three different tests that followed different stress paths and had undergone different consolidation (K_o and isotropic consolidation) yielded different strength values. The first sample (CK_oUC-PSV), K_o consolidated and loaded horizontally, gave the lowest strength. The reason is that the extension test stress path meets the failure envelope before the compression test stress path does. In the other two tests where the plane

<div align="center">

Table 2.1   Plane Strain Test Results
(WP Georgia Silty Clay)

</div>

Sample No.	Test	$(\tau_f/\sigma'_{cv})_{max}$	$\dfrac{[\tau_f/\sigma'_{cv}]_H}{[\tau_f/\sigma'_{cv}]_v}$	$\dfrac{[\tau_f/\sigma'_{cv}]_{K_o}}{[\tau_f/\sigma'_{cv}]_{iso}}$
1	CK_oUC-PSV	0.47		
			0.78	—
2	CK_oUC-PSH	0.60		
			—	0.86
3	CIUC-PSH	0.70		

strain condition was maintained in horizontal direction and the loading was applied vertically (conventional plane strain tests), the samples showed higher strengths than the first one, with the isotropically consolidated sample being stronger than the K_o consolidated one.

The three different stress path tests yielded different strengths which clearly illustrate the stress dependent anisotropic nature of the soil. The anisotropic ratio $[\tau_f/\sigma'_{vc}]_H/[\tau_f/\sigma'_{vc}]_V$ of the K_o consolidated sample is 0.78, which shows that the stress path has a significant influence on the anisotropic strength. The strength ratio between the K_o and isotropically consolidated samples is not unity (= 0.86) which indicates that induced anisotropy effects exist.

2.2 Theoretical Studies of Stress Path and Anisotropy

2.2.1 Predicting Undrained Shear Strengths of CK_oUC from CIUC Tests

Isotropically consolidated undrained compression (CIUC) triaxial tests are the common laboratory tests to determine the undrained shear strength of clays primarily because of the convenience and simplicity of the experimental procedures. Anisotropically consolidated (CAUC) tests are more complicated and take much longer to run. Natural soil deposits, however, are rarely isotropic nor do they often have an in situ $K_o = 1$. Therefore, development of a theoretical expression to predict the actual behavior/strength (i.e. CK_oUC strength) from CIUC test results

would be very beneficial.

Although Ladd (1965) concluded that it is not possible to predict CK_oUC strength from CIUC tests because the tests follow two different stress paths, Sivakugan, et al. (1988b) found that a reasonably good estimate of the CK_oUC strengths may be obtained from a single CIUC test on the same soil. The ratio of $(\tau_f/\sigma_{vo}')_{CK_oUC}$ to $(\tau_f/\sigma_{vo}')_{CIUC}$ was shown to be a function of the coefficient of earth pressure at rest K_o and Skempton's pore pressure parameters at failure A_f for both tests. Thus, τ_f/σ_{vo}' from a CIUC test may be used with estimates of K_o and the A parameters to estimate the normalized shear strength of K_o-consolidated specimens. Although only limited data are available, the procedure appears to be sufficiently accurate for practical purposes. It is briefly summarized here, as details are given in Sivakugan (1987) and Sivakugan, et al. (1988b).

It was shown that for normally consolidated clays, the strength ratio can be given by:

$$\frac{\left(\dfrac{\tau_f}{\sigma_{vo}'}\right)_{CK_oUC}}{\left(\dfrac{\tau_f}{\sigma_{vo}'}\right)_{CIUC}} = \frac{K_o + 2(1 - K_o)\, A_{f,i}}{K_o + 2(1 - K_o)\, A_{f,K_o}} \left[A_{f,K_o}\,(1 - K_o) + K_o\right] \quad (2.1)$$

where $\left(\dfrac{\tau_f}{\sigma_{vo}'}\right)_{CK_oUC}$ = normalized undrained shear strength for CK_oUC test

$\left(\dfrac{\tau_f}{\sigma_{vo}'}\right)_{CIUC}$ = normalized undrained shear strength for CIUC test

$A_{f,i}$ = Skempton's A parameter at failure for the CIUC test;

A_{f,K_o} = Skempton's A parameter at failure for the CK_oUC test

K_o = coefficient of at rest earth pressure.

Typical representations of this strength ratio equation are given in Fig. 2.1 for K_o = 0.4. From this figure and others at different K_o values, it can be seen that $A_{f,i}$ has a much greater influence on the strength ratio than A_{f,K_o}, and even a crude estimate of A_{f,K_o} is usually sufficient for a reasonably good estimate of the strength ratio.

The parameters required for the computation are K_o, $A_{f,i}$ and A_{f,K_o}. It is admittedly not easy to obtain accurate estimates of K_o in practice, e.g. see Massarsch et al. (1975) and Tavaras et al. (1975). In the interim, K_o may be obtained from published correlations (Holtz and Kovacs, 1981) or estimated from Jaky's (1948) relationship. The isotropic A parameter $A_{f,i}$ can be obtained from the CIUC test results, while A_{f,K_o} requires K_o-triaxial tests (just what we want to avoid). Fortunately, as indicated previously, the strength ratio is not very sensitive to A_{f,K_o}, and only crude estimates are required for good estimates of the strength ratio. In the absence of any other information, the mere knowledge of whether $A_{f,i}$ is greater or less than A_{f,K_o} is sufficient for a reasonably good estimate of this parameter. Numerical examples to predict the strength ratio are given in Sivakugan et al. (1988b).
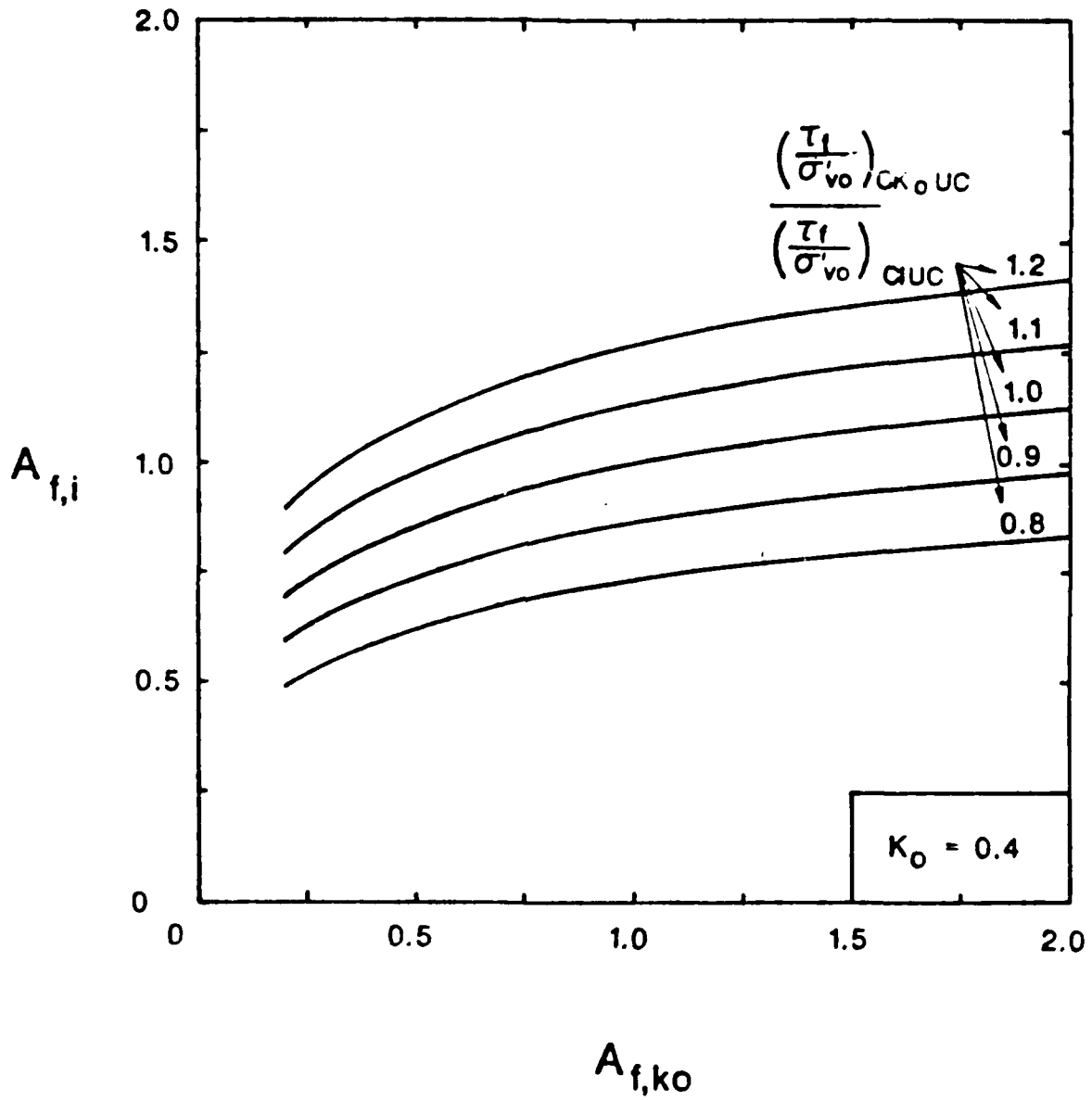
Figure 2.1 Variation of $A_{f,i}$ with A_{f,K_o} for Strength Ratios (Eq. 2.1) of 0.8-1.2 for $K_o = 0.4$

To check the applicability of the proposed technique, calculated values of the strength ratio were compared to experimental data (Table 2.2) for 24 different soils, and the results are plotted in Fig. 2.2. This figure shows that for carefully performed tests on replicate specimens, the assumptions made and equations used to derive Eq. 2.1 are reasonably valid. From Table 2.2, it is seen that A_{f,K_o} can be less or greater than $A_{f,i}$ by as much as 100%. The slight differences in ϕ' between isotropic and K_o tests can be neglected in the procedure. This is justified by a statistical analysis of experimental data from CIUC and CAUC tests by Mayne (1985), which showed that $\phi'_{CAUC} = 0.97\ \phi'_{CIUC}$.

2.2.2 Spacing Ratio

The Cam clay (Roscoe et al., 1963) and the modified Cam clay models (Roscoe and Burland, 1968) are the most widely accepted critical state soil models. They have undergone several developments over the past two decades (e.g., Egan, 1977, Pender 1978, and van Echelen and Potts, 1978). Sivakugan (1987) and Sivakugan et al. (1988a) give a review of the main characteristics of these models. The Cambridge soil models were developed essentially for isotropically consolidated clays, although most soil deposits encountered in nature are one dimensionally consolidated with no lateral deformation.

In the Cambridge soil models, it was hypothesized that the K_o consolidation line (K_o CL) in the $p'-q-v$ space lies on the state

Table 2.2 Experimental and Predicted Strength Ratios

No.	Soil	K_o	$A_{f,1}$	A_{f,K_o}	ϕ'		Strength Ratio		Ref.
					CIUC	$CK_o UC$	Predicted	Expt'l	
1	Boston Blue Clay	0.54	1.10	0.60	27.5	26.5	1.16	1.10	36
2	Weald Clay	0.61	0.92	1.80	26.0	26.0	0.87	0.84	36
3	Vicksburg Buckshot Clay	0.54	1.05	1.05	24.0	23.5	1.02	1.00	36
4	Undist. Kawasaki Clay	0.52	0.80	0.50	37.0	33.0	0.98	0.93	36
5	Undist. Brobekkveien Oslo Clay	0.47	0.95	0.75	30.5	27.0	0.69	0.91	36
6	Undist. Skabo Clay	0.47	1.05	0.75	30.0	26.5	1.09	1.00	36
7	Hokkaido silt 1	0.45	0.84	0.58	37.2	35.1	0.97	0.95	49
8	Hokkaido silt 2	0.45	1.03	2.0	35.1	34.9	0.93	0.94	49
9	Hokkaido Clay	0.47	0.82	1.03	36.1	34.0	0.87	0.88	49
10	Illite	0.50	0.43	0.10	22.3[a]	24.9[a]	0.85	0.88	28
11	Spestone Kaolinite	0.64	1.55	3.60	22.6	20.8	1.05	0.95	61
12	Nagoya Clay	0.47	0.70	0.50	33.9[a]	32.4[a]	0.89	0.86	56

Table 2.2, continued

No.	Soil	K_o	$A_{f,1}$	A_{f,K_o}	ϕ'		Strength Ratio		Ref.
					CIUC	$CK_o UC$	Predicted	Expt'l	
13	Kawasaki M-10	0.42	0.61	0.31	39.2	39.3	0.87	0.68	57
14	Kawasaki M-15	0.40	0.65	0.39	38.7	40.1	0.86	0.74	57
15	Kawasaki M-20	0.41	0.71	0.44	40.6	40.1	0.90	0.78	57
16	Kawasaki Clay	0.41	0.72	0.48	40.8	41.0	0.89	0.80	57
17	Whitefish Falls	0.48	1.03	0.68	27.0	26.0	1.09	1.06	15
18	Wallaceburg	0.51	0.70	0.44	23.0	25.0	0.92	0.97	15
19	Boston Blue Clay	0.50	1.0	0.5	25.4[a]	26.1[a]	1.13	1.07	14
20	Marine Clay	0.51	1.08	1.25	34.0	29.0	1.01	0.94	31
21	Vicksburg Buckshot Clay	0.55	0.88	0.41	26.7	24.9	1.07	0.96	18
22	EABPL clay	0.64	0.92	0.60	21.7	20.2	1.04	0.98	18
23	K50	0.47	1.06	1.05	32.0	29.1	1.03	0.94	77
24	Kaolinite	0.49	1.15	1.03	26.9	24.2	1.09	0.93	77

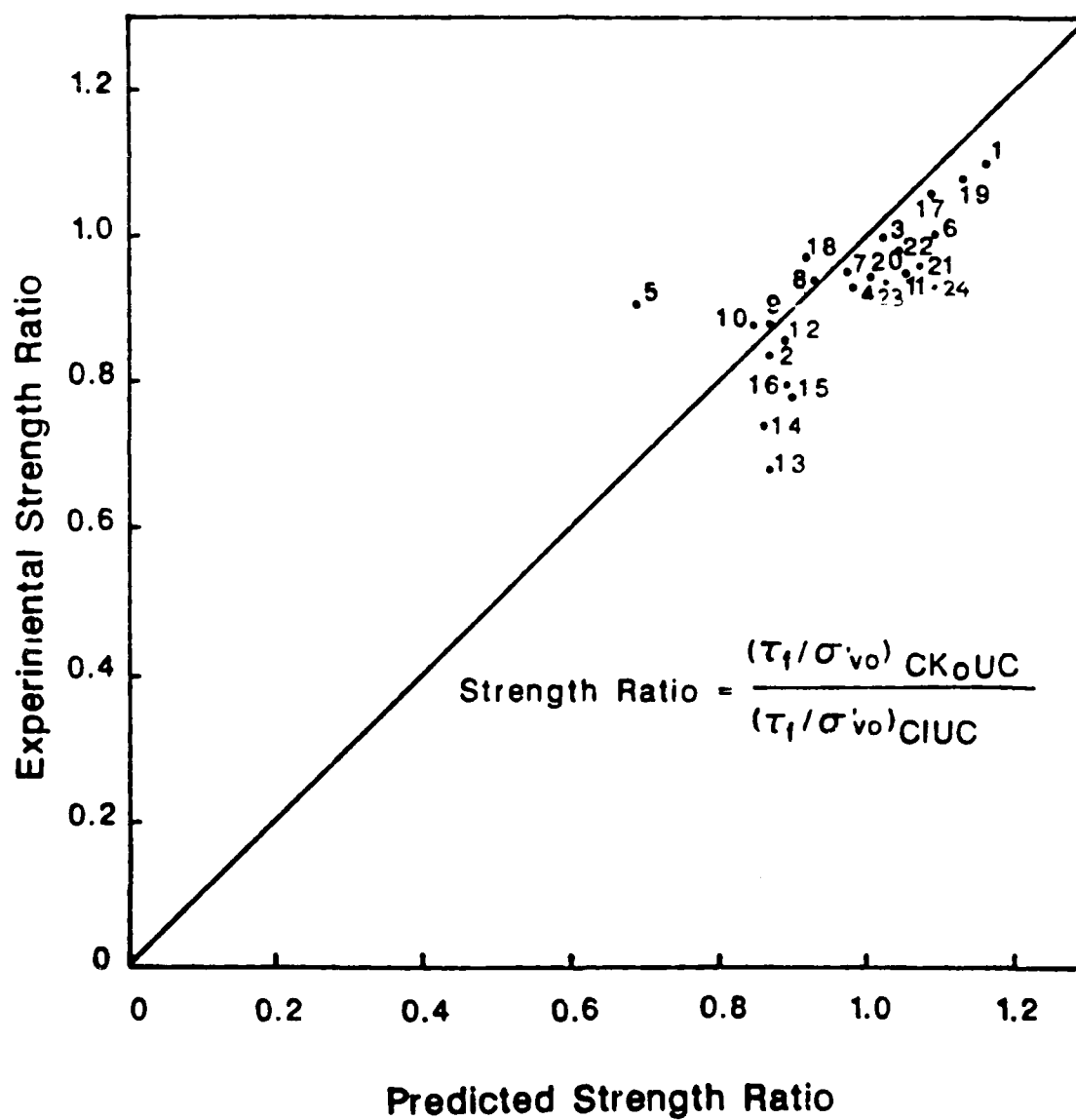[a] Computed from Eq. 1 of Bjerrum and Simmons (1960).

Figure 2.2 Experimental versus Predicted Strength Ratio

boundary surface between the critical state line (CSL) and the iso-
tropic consolidation line (ICL) (Atkinson and Bransby, 1978, and
Roscoe and Poorooshasb, 1963). Furthermore, ICL, K_oCL, and CSL are
assumed to be three parallel lines with a negative slope of λ in
the v-ln p' plane, as shown in Fig. 2.3 (Atkinson and Bransby,
1978), resulting in the following equations, respectively:

$$v = N - \lambda \ln p' \qquad (2.2a)$$

$$v = N_o - \lambda \ln p' \qquad (2.2b)$$

$$v = \Gamma - \lambda \ln p' \qquad (2.2c)$$

where N = the specific volume (v = 1 + e) of a specimen isotropi-
cally (hydrostatically) consolidated under p' = 1 kN/m^2. N_o is the
specific volume of a specimen one dimensionally consolidated with
p' = 1 kN/m^2, and Γ is the specific volume at the critical state
when p' = 1 kN/m^2.

A new state parameter, called spacing ratio and denoted by r,
is introduced herein (Sivakugan et al., 1988a) to represent the
relative position of K_oCL with respect to ICL and CSL. The stress
path of a CK_oUC test is AF (Fig. 2.3), and the spacing ratio can be
defined as:

$$r = \frac{N_o - \Gamma}{N - \Gamma} \qquad (0 < r < 1) \qquad (2.3)$$

When this ratio takes its extreme values of 0 or 1, K_oCL coincides
with the CSL or ICL, respectively.

Expressions were derived for spacing ratios for extended Cam
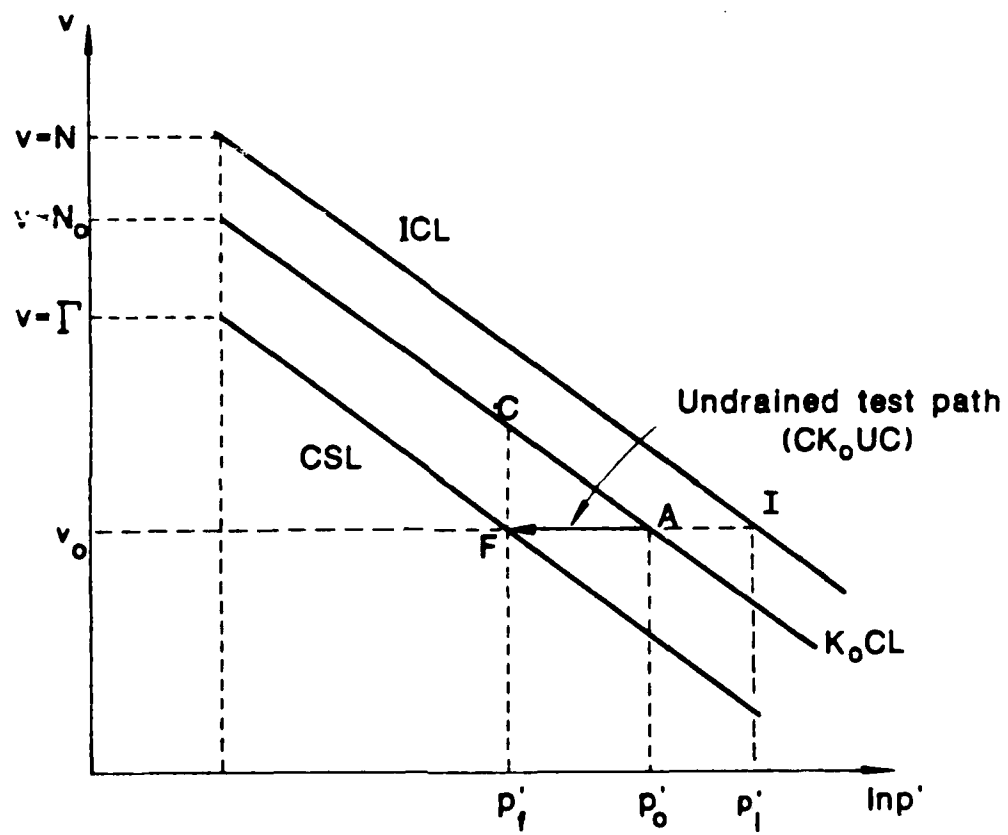clay model and for extended modified Cam clay model in order to

Figure 2.3   ICL, K_oCL, CSL, and CK_oUC Test Path on
$v - \ln p'$ Plane

consider K_o consolidated soils instead of isotropically consoli-
dated soils. The spacing ratio for both extended models are given
in Table 2.3. Sivakugan et al. (1988a) have derived expressions
for the normalized shear strength τ_f/σ_{vo} using the Cam clay model,
modified Cam clay model and the extended models with spacing ratio.
The derived expressions are summarized in Table 2.3. For detailed
derivations the reader is referred to Sivakugan (1987). The nor-
malized shear strength is a function of tne friction angle and the
consolidation characteristics of the soil. The expressions are
derived assuming that the normally consolidated clay is idealized
as an elasto-plastic material exhibiting isotropic strain harden-
ing. Based on constitutive equations proposed by Sekigushi and
Ohta (1977), Ohta and Nishihara (1985) developed similar equations
for the normalized shear strength but using rheological and dila-
tancy characteristics of soils.

A typical variation of normalized undrained shear strength
with ϕ' predicted by the extended models is shown in Fig. 2.4. The
extended modified Cam clay model gives slightly higher values than
the extended Cam clay model for all values of K_o and Λ, however,
the differences are small. The normalized undrained shear strength
varies approximately linearly with ϕ'_{CIUC}. It varies between 0.25
and 0.45 for typical values of K_o, Λ and ϕ' (Sivakugan et al.,
1988a).

For the limited data available in the literature, predictions
of τ_f/σ_{vo} for K_o consolidated clays were made from the extension of

Table 2.3   Expressions for Spacing Ratio, Normalized Shear
Strength and Skempton's A-Parameter at Failure

	Cam Clay Model	Modified Cam Clay Model	Extended Models with Spacing Ratio	
			Cam Clay	Modified Cam Clay
Spacing Ratio, r	—	—	$1 - \dfrac{\eta_o}{M}$	$\dfrac{\ln\left(\dfrac{2M^2}{M^2 + \eta_o^2}\right)}{\ln 2}$
Normalized Shear Strength τ_f/σ_{vo}	$\dfrac{1}{2} M e^{-\Lambda}$	$\dfrac{1}{2} M 2^{-\Lambda}$	$\dfrac{M}{6}(1 + 2K_o) e^{-r\Lambda}$	$\dfrac{M}{6}(1 + 2K_o) 2^{-r\Lambda}$
Skempton's Pore-Pressure Parameter A_f	$\dfrac{1}{3} - \dfrac{1}{M} + \dfrac{1}{M} e^{\Lambda}$	$\dfrac{1}{3} - \dfrac{1}{M} + \dfrac{1}{M} 2^{\Lambda}$	$\dfrac{1}{3} + \dfrac{e^{r\Lambda} - 1}{M - \eta_o e^{r\Lambda}}$	$\dfrac{1}{3} + \dfrac{2^{r\Lambda} - 1}{M - \eta_o 2^{r\Lambda}}$

M = stress ratio q/p' at critical state = $\dfrac{6 \sin \phi'}{3 - \sin \phi'}$

η_o = stress ratio q/p' immediately after K_o consolidation = $\dfrac{q_o}{p_o'} = \dfrac{3(1 - K_o)}{(1 + 2K_o)}$

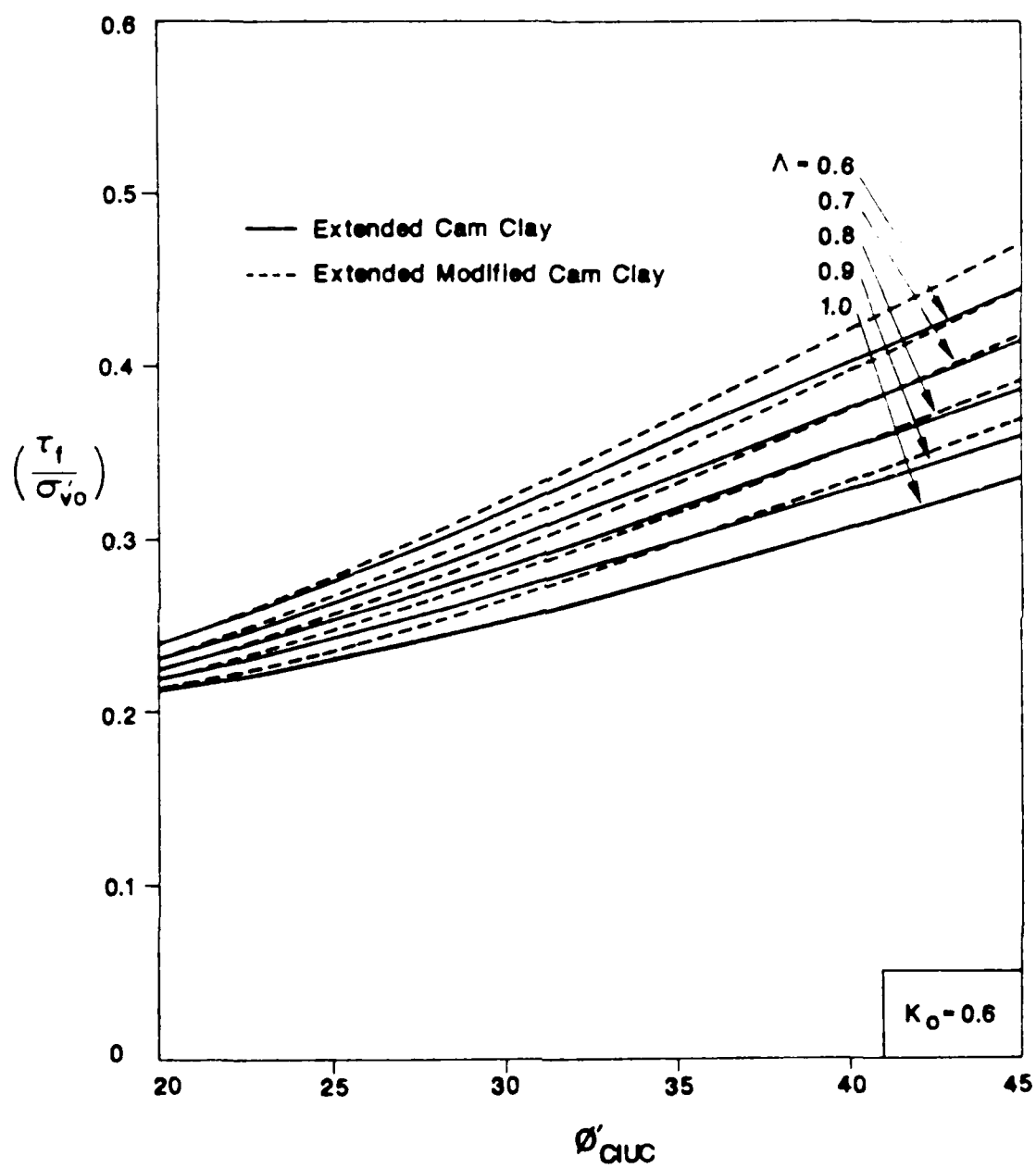$\Lambda = 1 - \dfrac{C_r}{C_c} = 1 - \dfrac{k}{\lambda}$

Figure 2.4 Variation of τ_f/σ'_{vo} with ϕ' for $K_o = 0.6$

the Cam clay and modified Cam clay models. The data and the predicted values are given in Table 2.4. Both extended models show excellent agreement with the experimental results as illustrated in Fig. 2.5.

The Cam clay models as well as the extended models can also be used to predict the pore pressures at failure by evaluating Skempton's A parameter at failure, A_f. This parameter is given by:

$$A_f = \frac{\Delta u_f}{q_f}$$

$$= \frac{p_o' + \frac{1}{3} q_f - p_f'}{q_f} \tag{2.4}$$

At failure $q_f = Mp_f'$. Therefore,

$$A_f = \frac{1}{3} - \frac{1}{M} + \frac{1}{M} \frac{p_o'}{p_f'} \tag{2.5}$$

The resulting relationships between A_f and M, r_o, r, and Λ, are given in Table 2.3 (see Sivakugan, 1987, for a detailed derivation). A typical variation of A_{f,K_o}, the A parameter at failure for K_o consolidated clays, with ϕ' predicted from the extended models is shown in Fig. 2.6. For low values of Λ both models predict about the same A_{f,K_o}. For higher Λ, the extended modified Cam clay model gives lower values than the extended Cam clay model. A_{f,K_o} decreases with increasing ϕ', decreasing Λ, and increasing K_o. For typical values of ϕ', Λ and K_o, A_{f,K_o} varies between 0.9

Table 2.4   Experimental and Predicted Values of τ_f/σ'_{vo} and A_f

| No. | Soil | K_o | ϕ'_{CIUC} deg. | Λ | Expt'l | | Predicted | | | | Ref. |
					$\dfrac{\tau_f}{\sigma'_{vo}}$	A_f	Ext. Cam Clay		Ext. Mod. Cam Clay		
							$\dfrac{\tau_f}{\sigma'_{vo}}$	A_f	$\dfrac{\tau_f}{\sigma'_{vo}}$	A_f	
1	Hokkaido Silt 1	0.45	37.2	0.80	0.40	0.58	0.34	1.71	0.35	1.57	49
2	Hokkaido Silt 2	0.45	35.1	0.84	0.34	2.00	0.32	2.11	0.33	1.94	49
3	Hokkaido Clay	0.47	36.1	0.89	0.36	1.03	0.30	2.60	0.32	1.89	49
4	Spestone Kaolinite	0.64	22.6	0.89	0.21	3.60	0.22	3.39	0.23	2.97	62
5	Kaolinite	0.50	26.9	0.85	0.27	1.03	0.28	3.14	0.28	2.97	77
6	K50	0.50	32.0	0.90	0.32	1.05	0.29	2.66	0.30	2.40	77
7	Weald Clay	0.59	25.9	0.66	0.27	1.80	0.28	1.63	0.28	1.52	22
8	Sapporo Clay	0.52	3.6	0.49	0.30	1.24	0.34	0.98	0.34	0.94	50,51
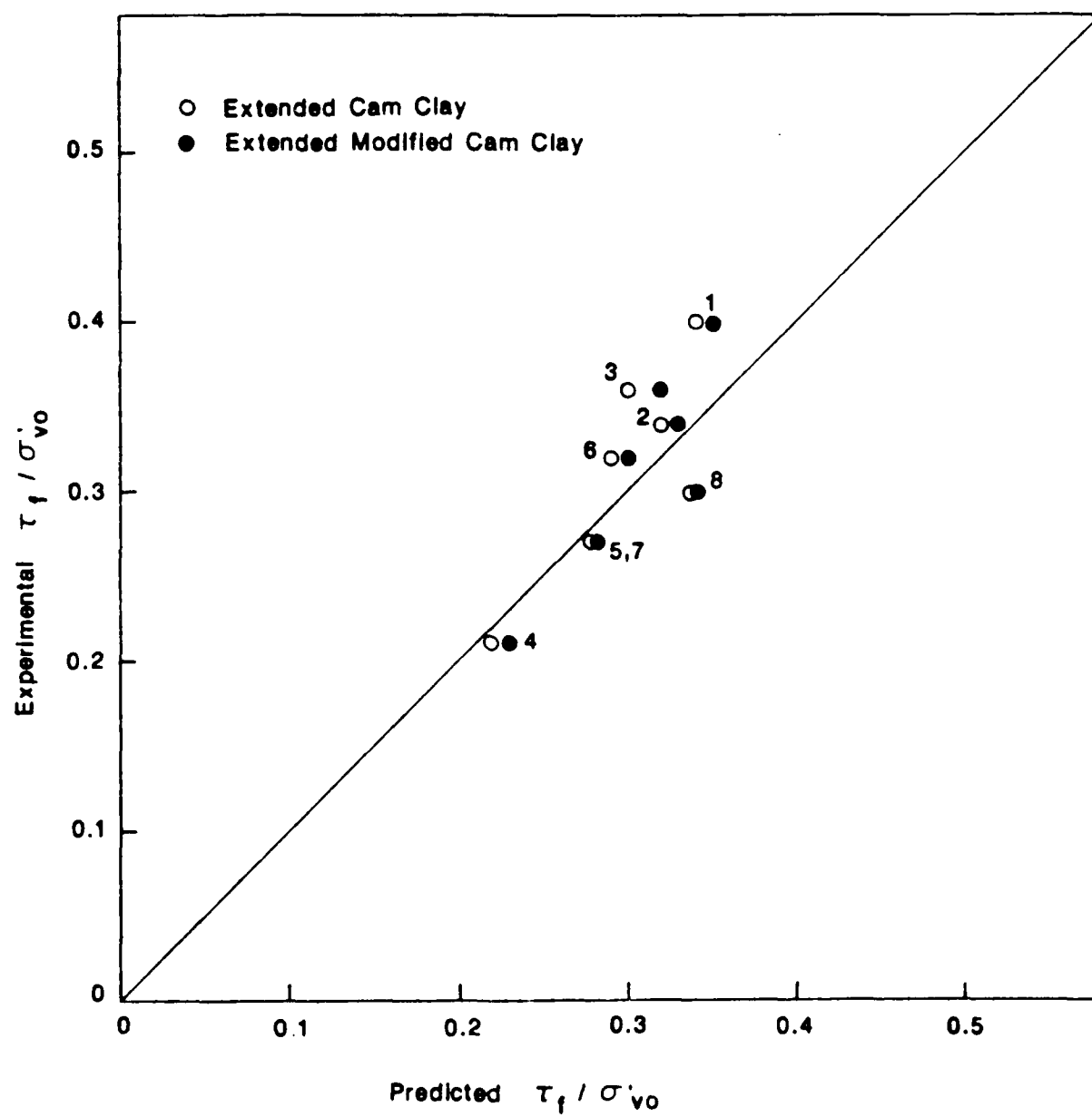
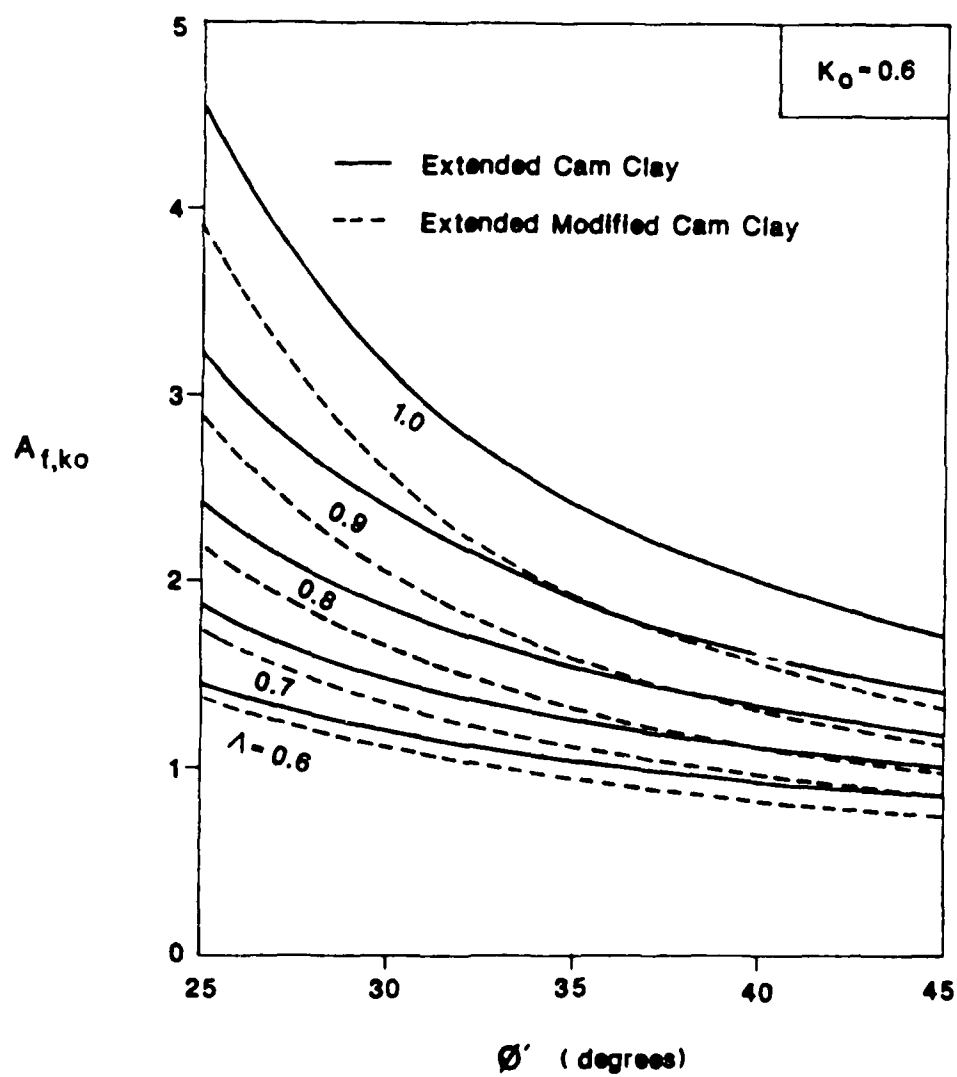Figure 2.5   Predicted vs. Measured Normalized Strength Ratio

Figure 2.6 Variation of A_{f,K_o} with ϕ' for $K_o = 0.6$

and 4.0 (Sivakugan et al., 1988a).

Predictions of A_f for K_o consolidated clays were made for the eight soils given in Table 2.4. The data and results are given in Table 2.4 for both the extended Cam clay model and extended modified Cam clay models. Unlike the excellent agreement obtained for the τ_f/σ_{vo} ratio, the A_f prediction from both models are inconsistent, being excellent for some tests and poor for others (Fig. 2.7). It seems that A_f is very sensitive to Λ, which is a function of both C_c and C_r, the compression index and the swelling index, respectively. Measurement of C_c is rather straight forward; however, C_r varies with OCR and no standard procedure is generally adopted in measuring C_r. This severely influences Λ and thus significantly affects the predictions of A_f. To avoid the problems in determining Λ from C_r, Mayne (1980) has proposed to redefine Λ in terms of overconsolidated strength data as:

$$\Lambda = \frac{\log \left[(\tau_f/\sigma_{vo})_{OC}\right] - \log \left[(\tau_f/\sigma_{vo})_{NC}\right]}{\log \text{ OCR}} \qquad (2.6)$$

where $(\tau_f/\sigma_{vo})_{OC}$ and $(\tau_f/\sigma_{vo})_{NC}$ are the normalized shear strength of overconsolidated and normally consolidated clays, respectively. The normalized undrained strength values at two different OCR's are required for this determination. For the data given in Table 2.4, such information was not available, and thus it was not possible to compute Λ by this method.

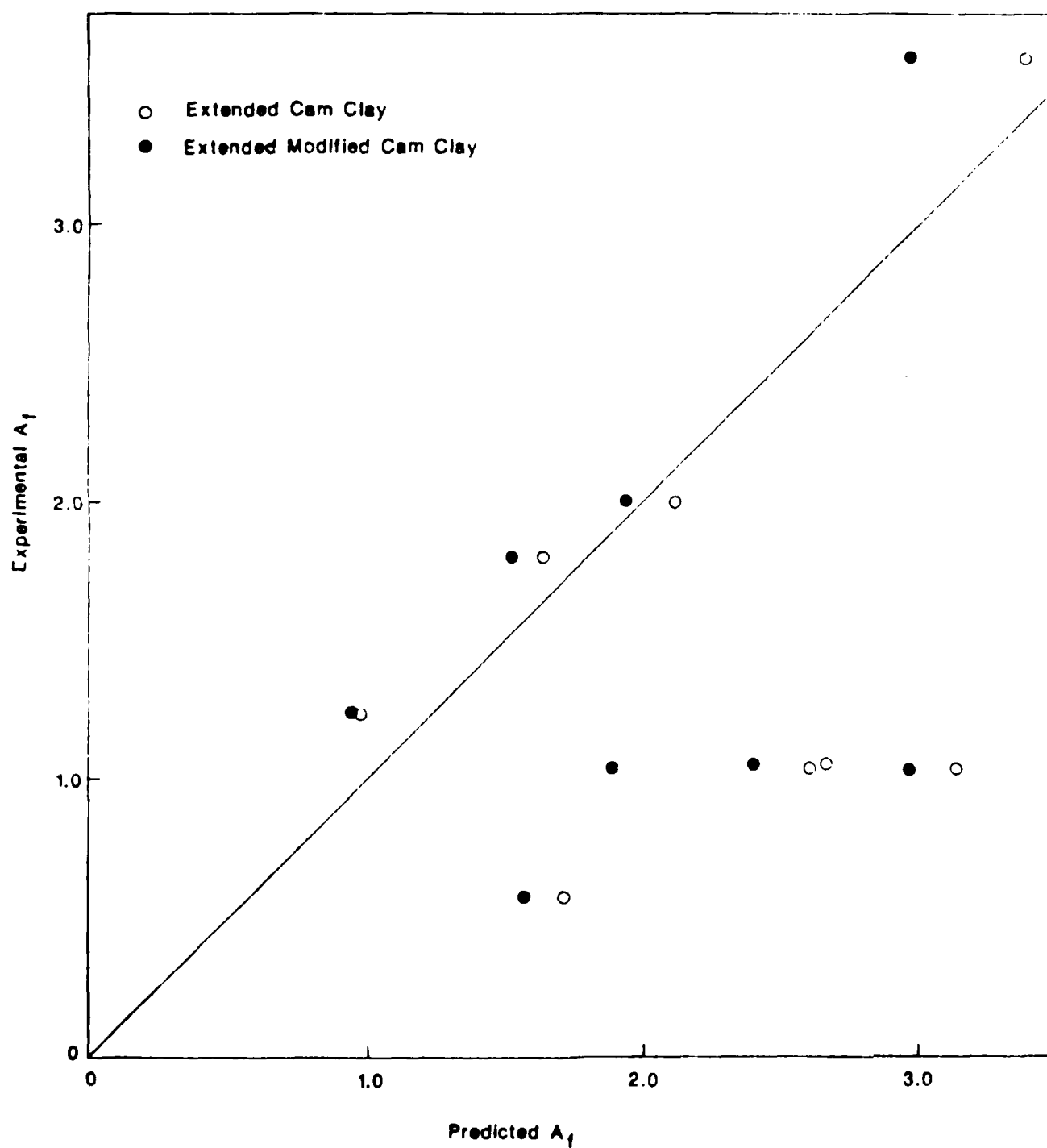It has also been suggested to determine Λ from correlations.

Figure 2.7   Predicted vs. Measured A-parameter at Failure

Few empirical correlations have been cited in the literature relating M with Λ. Schofield and Wroth (1968) proposed that $M/\Lambda = 1.5$; Karube (1975) suggested that it is 1.75. However, based on experimental data from literature, Sivakugan and Holtz (1986) showed that there appears to be no correlation between M and Λ. As shown in Fig. 2.8, the rather large scatter makes a linear correlation questionable.

2.2.3 Conclusions

Although CK_oUC and CIUC tests follow different stress paths, it has been shown that a good estimate of the CK_oUC strength can be obtained from a single CIUC test. The normalized strength ratio, $(\tau_f/\sigma'_{vo})_{CK_oUC}/(\tau_f/\sigma'_{vo})_{CIUC}$, was found to be a function of earth pressure at rest K_o and Skempton's pore pressure parameters at failure A_f for both tests. K_o may be obtained from published correlations or estimated from Jaky's relationship. The isotropic A parameter $A_{f,i}$ can be obtained from the CIUC test results. Since the strength ratio is not very sensitive to A_{f,K_o}, an estimate of A_{f,K_o} is sufficient for the calculation.

Expressions were derived for the normalized shear strength τ_f/σ'_{vo} using the Cam clay model, the modified Cam clay model, and the extended Cam clay and modified Cam clay models with spacing ratio. The normalized shear strength is a function of the friction angle and the consolidation characteristics of the soil. Both extended models with spacing ratio predict values that compare well
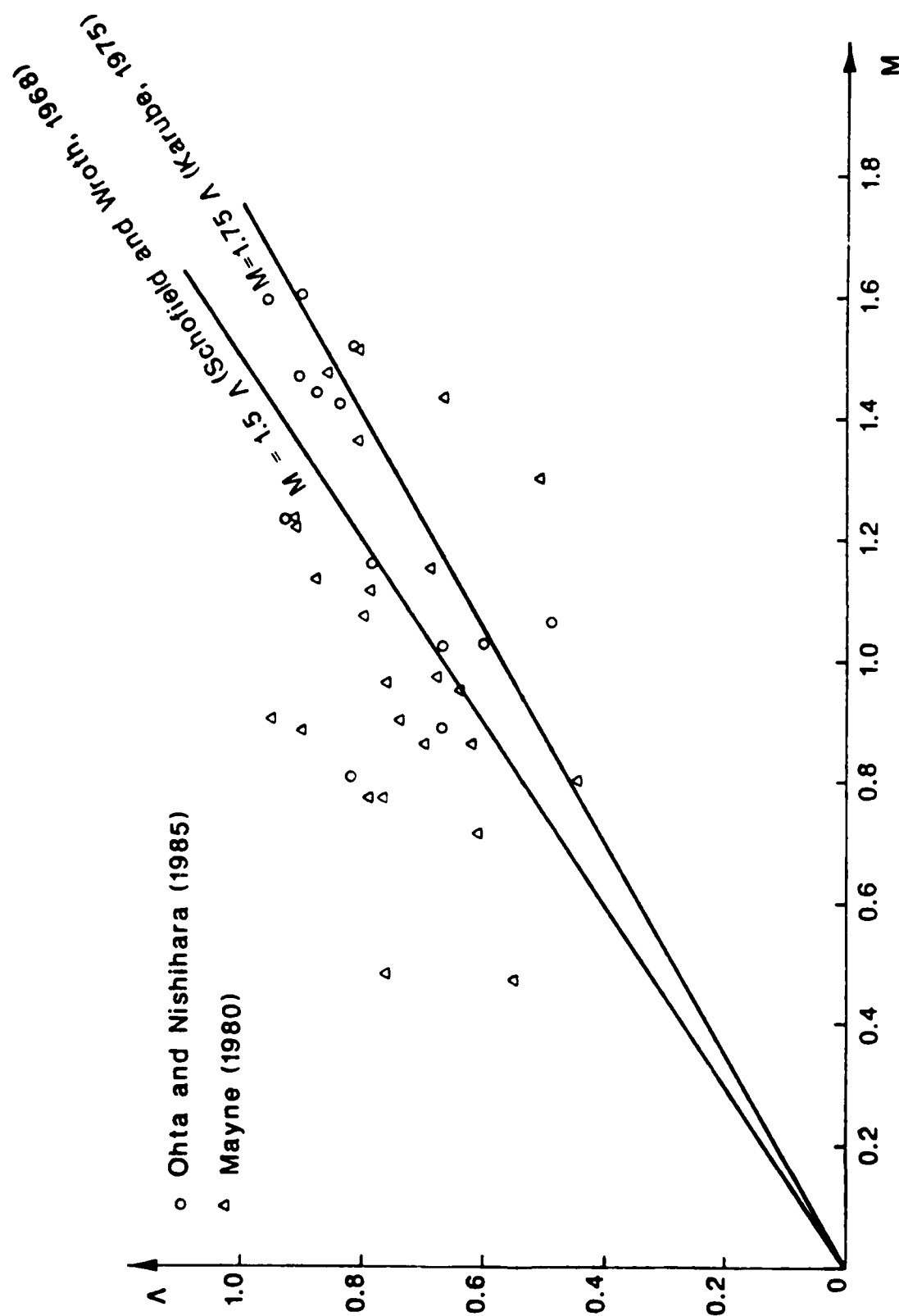
Figure 2.8 Variation of A with M (after Sivakugan & Holtz, 1986)

with experimental data.

Expressions were also derived for estimating Skempton's A parameter at failure for isotropically consolidated soils and K_o consolidated soils. Unlike the excellent agreement with experimental results obtained for the strength ratio, the A_f prediction is marginal for all models. A_f is very sensitive to Λ, which is a function of C_c and C_r. This severely influences Λ and thus affects the predictions of A_f.

2.3 Normalization of Consolidation Lines

2.3.1 Introduction

A good estimate of compression index, C_c, recompression index, C_r, and preconsolidation pressure, p_c, are prerequisites for settlement analysis of embankments or buildings on cohesive soils. For this, it is common practice to perform consolidation tests on specimens prepared from undisturbed samples taken at various locations within the clay stratum. From the consolidation test results, $e-\log\sigma_v$ plots are generated, and C_c, C_r and p_c are obtained. These steps involve effort and expense, and, for preliminary designs, empirical correlations are often used to estimate these parameters (e.g. Holtz and Kovacs, 1981). C_c has been correlated with natural water content, liquid limit and initial void ratio (e.g. Skempton, 1944, Nishida, 1956, Cozzolino, 1961, Azzouz et al., 1976, and Koppula, 1981). C_r is often assumed to be 0.1 to 0.2 times C_c. Estimating p_c from correlations remains a problem

yet.

The slope and position of virgin consolidation lines in the e-logσ_v space depend primarily on liquid limit (or initial void ratio) and sensitivity of the soil. Therefore, for clays of low to medium sensitivity, the slope and the intercept on the e-axis depend mainly on the liquid limit. When e-logσ_v lines for several normally consolidated clays are plotted together, a wide range of void ratios may be observed for a given σ_v, depending upon their respective liquid limits. Based on the Gouy-Chapman diffuse double layer theory, Nagaraj and Srinivasamurthy (1983 and 1986) showed that when e is normalized with respect to the void ratio at the liquid limit, e_L, all the lines tend to fall into a narrow band irrespective of the clay mineral type or pore fluid characteristics.

This is confirmed from published consolidation test data for 16 different clays and experimental data from three artificially sedimented clays. The existence of such a normalized relationship facilitates predictions of the overconsolidation ratio (OCR). A simple procedure to predict OCR is proposed. A summary of this study and its conclusions are given below.

2.3.2 Critical State Model

The virgin consolidation line is often assumed to be linear (i.e. constant C_c) for settlement calculations. An idealized virgin consolidation line in e-logσ_v space is shown in Fig. 2.9. In
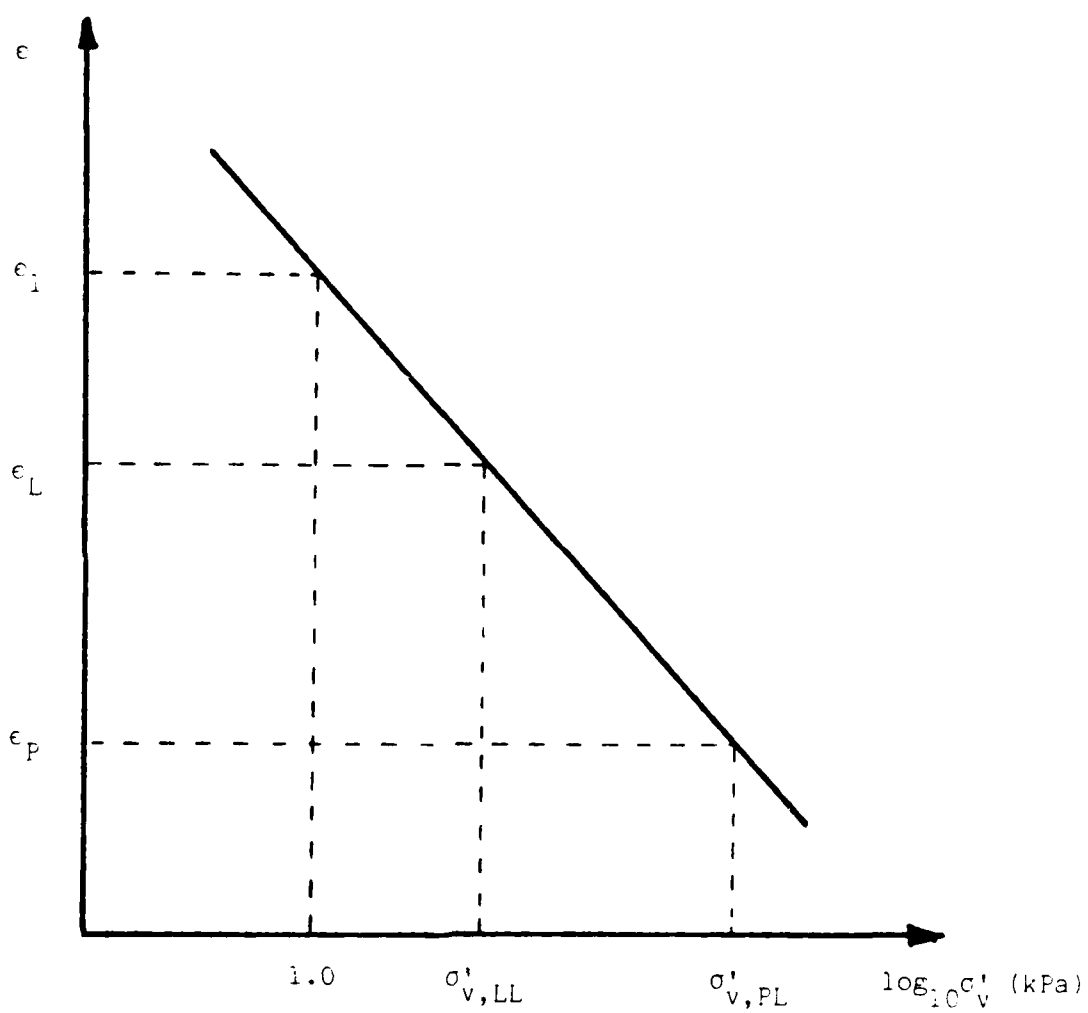
Figure 2.9 Idealized Virgin Consolidation Line in ϵ-log σ_v' Space

reality, it may be slightly curved as the plastic limit is approached. The equation of the virgin consolidation line is given by:

$$e = - C_c \log \sigma_v' + e_1 \qquad (2.7)$$

Normalizing Eq. 2.7 by $e_L - e_P$:

$$\frac{e}{e_L - e_P} = \frac{-C_c}{e_L - e_P} \log \sigma_v' + \frac{e_1}{e_L - e_P} \qquad (2.8)$$

where e_P is the void ratio at plastic limit. The liquidity index LI is defined by:

$$LI = \frac{w - PL}{LL - PL}$$

$$= \frac{e - e_P}{e_L - e_P} \qquad (2.9)$$

From Eqs. 2.8 and 2.9:

$$LI = - \frac{C_c}{e_L - e_P} \log \sigma_v' + \frac{e_1 - e_P}{e_L - e_P} \qquad (2.10)$$

Thus, if e versus $\log \sigma_v'$ is a straight line, so is LI versus $\log \sigma_v'$ and vice versa.

There is experimental evidence that when the liquidity index is plotted against logarithm of undrained shear strength, all the points fall within a narrow band (e.g. Skempton and Northey, 1953, Houston and Mitchell, 1969, Mitchell, 1976). Based on the large number of experimental results given by Skempton and Northey (1953) and Youssef et al. (1965), Schofield and Wroth (1968) adopted a value of 1.7 kN/m^2 as the best estimate of the undrained shear

strength at the liquid limit, and estimated the shear strength at the plastic limit to be 100 times that at the liquid limit, i.e., $c_u = 170$ kN/m^2 at the plastic limit. The idealized relationship often used in critical state models (Atkinson and Bransby, 1978, Wroth and Wood, 1978, and Wroth, 1979) is shown in Fig. 2.10(a). Using the critical state model and the above LI versus c_u relationship, Wroth (1979) developed an idealized relationship between vertical effective stress and liquidity index which is shown in Fig. 2.10(b). Based on the experimental evidence Wroth estimated that $\sigma_v' = 6.3$ kPa at the liquid limit (or LI = 1) and $\sigma_v' = 630$ kPa at the plastic limit (LI = 0).

2.3.3 Normalized Virgin Consolidation Lines

Normalizing Eq. 2.7 by e_L:

$$\frac{e}{e_L} = \frac{-C_c}{e_L} \log \sigma_v' + \frac{e_1}{e_L} \qquad (2.11)$$

where e_L, the void ratio at liquid limit, is obtained from:

$$e_L = \frac{LL}{100} G_s \qquad (2.12)$$

and G_s is the specific gravity of the soil grains.

With the diffuse double layer theory, Nagaraj and Srinivasamurthy (1963) analytically developed and supported with experimental data that the half-space distance, d, is linearly correlated with e/e_L, and linearly correlated with $\log \sigma_v'$. This aspect was examined further using the e-$\log \sigma_v'$ curves of six natural

a) Undrained Shear Strength

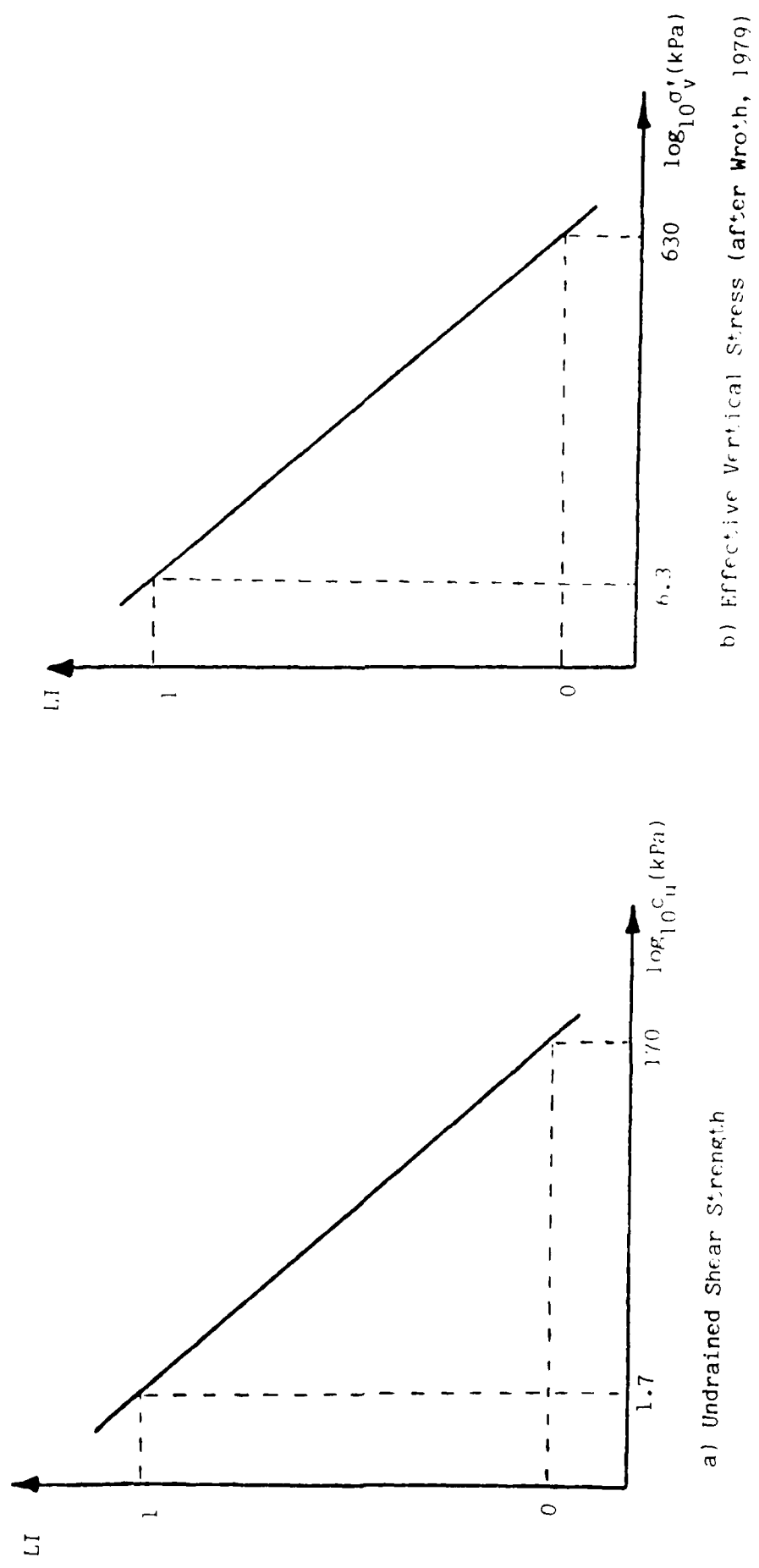b) Effective Vertical Stress (after Wroth, 1979)

Figure 2.10 Idealized Relationship Between Liquidity Index and (a) Remolded Shear Strength (b) Vertical Effective Stress

soils, the liquid limit water contents of which varied over a four fold range. All six curves fell into a narrow range, and, with a correlation coefficient of 0.953, the best fit straight line was functionally expressed as:

$$e/e_L = 1.099 - 0.2237 \log_{10} \sigma_v' \qquad (2.13)$$

where σ_v' is in kN/m^2. With additional data for eleven soils, Nagaraj and Srinivasamurthy (1986) further refined the above equation (correlation coefficient of 0.962) and expressed it as:

$$e/e_L = 1.122 - 0.2343 \log_{10} \sigma_v' \qquad (2.14)$$

This was further confirmed in this study, using the critical state model and the data obtained from Skempton (1944) for 16 clays of different geological origin (Table 2.5). When the wide scattered consolidation lines were normalized by their corresponding e_L's, they fell into a narrow range as shown in Fig. 2.11. The equation of the best fit straight line was found as:

$$e/e_L = 1.084 - 0.2154 \log_{10} \sigma_v' \qquad (2.15)$$

where σ_v' is in kN/m^2.

In addition, conventional consolidation tests were performed on three different artificially sedimented soils, kaolinite, "K50" containing 50% kaolinite and 50% silt, and grundite, an illitic clay. The soil slurries were made to a water content of approximately 2 1/2 times the liquid limit, and were consolidated in a

Table 2.5 Properties of Skempton's (1944) Clays

| No.	Soil	LL	PI	G_s	e_1	C_c	e_L	e_P
1	Boulder Clay	28	14	2.69	0.76	0.12	0.75	0.38
2	Wealden Clay	39	20	2.73	1.25	0.24	1.06	0.52
3	R. Severn Alluvium	46	21	2.59	1.22	0.21	1.19	0.65
4	Kaolin	50	18	2.64	1.51	0.23	1.32	0.84
5	Oxford Clay	53	26	2.57	1.56	0.30	1.36	0.69
6	Belfast Clay	67	37	2.66	1.64	0.32	1.78	0.80
7	Ganges Clay	69	41	2.77	2.06	0.42	1.91	0.78
8	Gosport Clay	75	46	2.67	2.03	0.46	2.00	0.77
9	London Blue Clay	77	49	2.71	2.26	0.49	2.09	0.76
10	London Brown Clay	88	56	2.65	2.44	0.56	2.27	0.85
11	Argille Plastique	128	97	2.58	3.44	0.81	3.30	0.80
12	Bosporous	36	18	2.71	1.24	0.25	0.98	0.49
13	Boston Blue Cla.	39	16	2.78	1.22	0.21	1.08	0.64
14	Vienna Miocene	47	25	2.76	1.47	0.30	1.30	0.61
15	Bosporous Blue Clay	58	32	2.85	1.61	0.32	1.65	0.74
16	Denmark Marine Clay	127	91	2.77	4.00	0.91	3.52	1.00
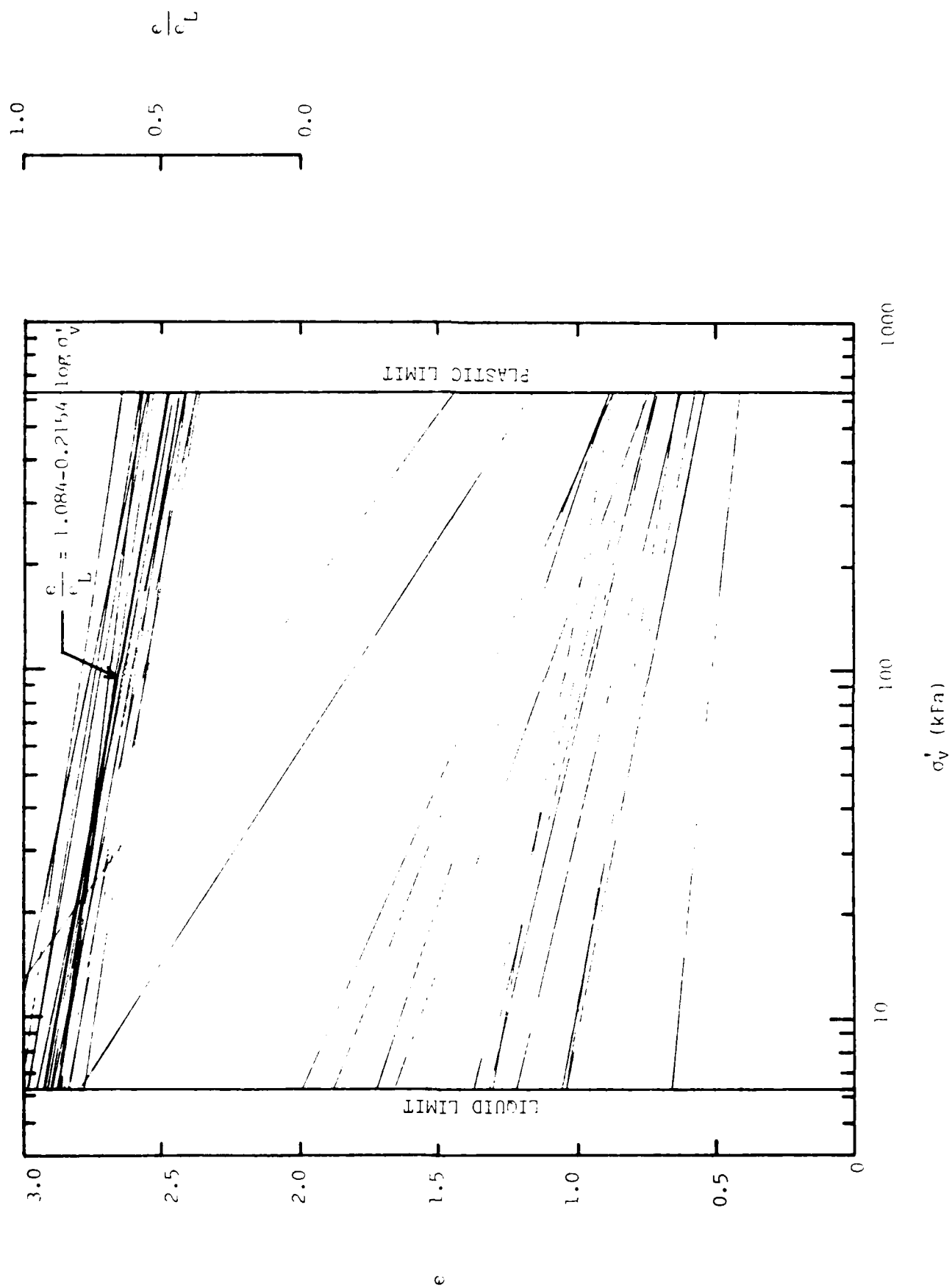
Figure 2.11 e versus log σ'_v and Normalized (e/e_L) Consolidation Lines (After Skempton, 1944)

consolidation chamber. Details of the slurry preparation method,
consolidation chamber etc. are available in Sivakugan (1987) and
Sivakugan et al. (1988b). The slurry was consolidated to a verti-
cal pressure of 10 to 20 psi under K_o conditions. At the end of
consolidation, a specimen of 63.5 mm in diameter and 25.5 mm in
height was trimmed from the consolidated cake for the oedometer
test. To ensure full saturation all oedometer tests were carried
out under a back pressure of 30 psi. Since pore pressure measure-
ments were not required, drainage was allowed from both top and
bottom of the specimen. The index properties and the parameters
obtained from the consolidation tests are given in Table 2.6. The
e/e_L vs. $\log\sigma_v'$ lines resulting from these experiments fall within
the range of the other data (Figure 2.12). Eq. 2.14 proposed by
Nagaraj and Srinivasamurthy (1986) was essentially the same as the
average of the normalized lines, as shown in Fig. 2.12.

2.3.4   Estimation of OCR

Wroth (1979) used the critical state model shown in Fig. 2.10
to predict OCR in offshore deposits, assuming $C_r/C_c = 0.2$. Similar
predictions are possible with the $e/e_L - \log\sigma_v'$ model. From Eq.
2.15, the "unique" (i.e. average) consolidation line can be plotted
in the e/e_L versus $\log\sigma_v'$ plot. This is the normally consolidated-
virgin compression line with the slope of C_c. By estimating the
ratio C_r/C_c ratio, the slope of the swelling line is known and it
can be drawn through any point (such as $\sigma_v' = 1000$ kPa in Fig.
2.13). Then, for OCR values of 2, 5, 10, etc., lines can be drawn

Table 2.6   Properties of Experimental Clays

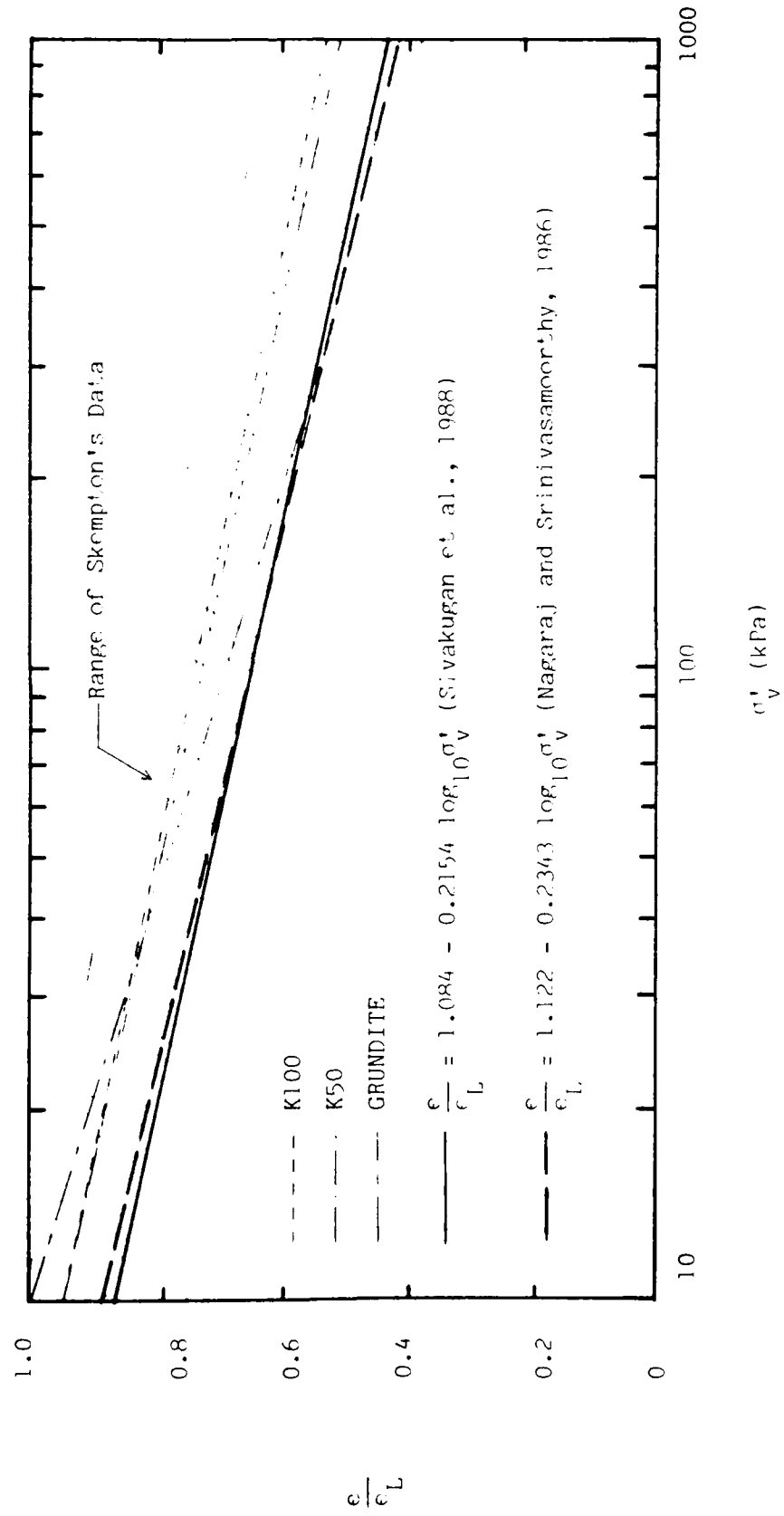| Soil	LL	PL	G_s	C_c	C_r	e_1	e_L
Kaolinite	63	36	2.65	0.35	0.106	1.93	1.67
K50	37	23	2.69	0.22	0.022	1.17	1.00
Grundite	51	29	2.75	0.36	0.060	1.76	1.40

Figure 2.12 Experimental Results on the Normalized Consolidation Plot

parallel to the NC line, through points with σ_v' of 500, 200, 100 kPa, respectively, on the swelling line. The rationale for this is provided by the critical state model, i.e. K_o consolidated and other over consolidation lines are parallel to the isotropic consolidation line. Prediction charts are given in Figs. 2.13 and 2.14, where the OCR contours, which are straight lines parallel to the virgin consolidation line, are shown for C_r/C_c of 0.1 and 0.2, respectively.

When taking samples from saturated clay deposits, disturbance should not cause a significant change in water content. Therefore, a good prediction of in situ void ratio at any depth is possible. e_L can be obtained from liquid limit test on the remolded soil, and σ_v' can be estimated if the soil profile and the densities of each strata are known. Thus, knowing e/e_L and σ_v' at a given depth, the corresponding point can be located in Figures 2.13 or 2.14 to provide an estimate of the OCR. The estimate is not sensitive to the assumed value of the ratio C_r/C_c, at least in the range 0.0 - 0.2.

2.3.5 Summary

This review and evaluation of test data confirmed that, when normalized with respect to the void ratio at liquid limit, consolidation lines fall in a narrow band. Based on this, a simple procedure was described to predict OCR of saturated clays using an average normalized virgin consolidation line. Since the OCR estimate is not sensitive to the C_r/C_c ratio, a good OCR prediction is possible from the knowledge of e/e_L and σ_v'.
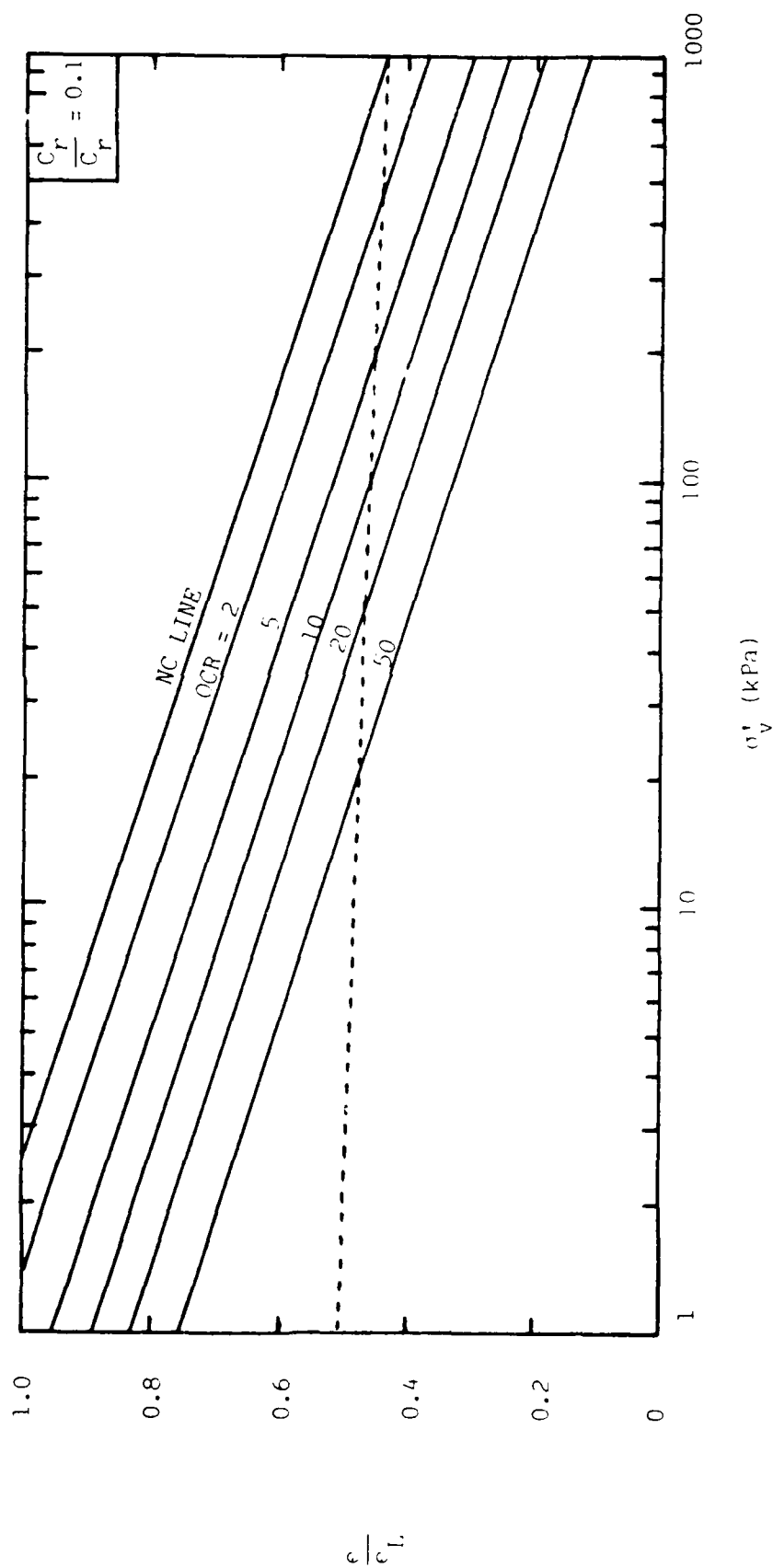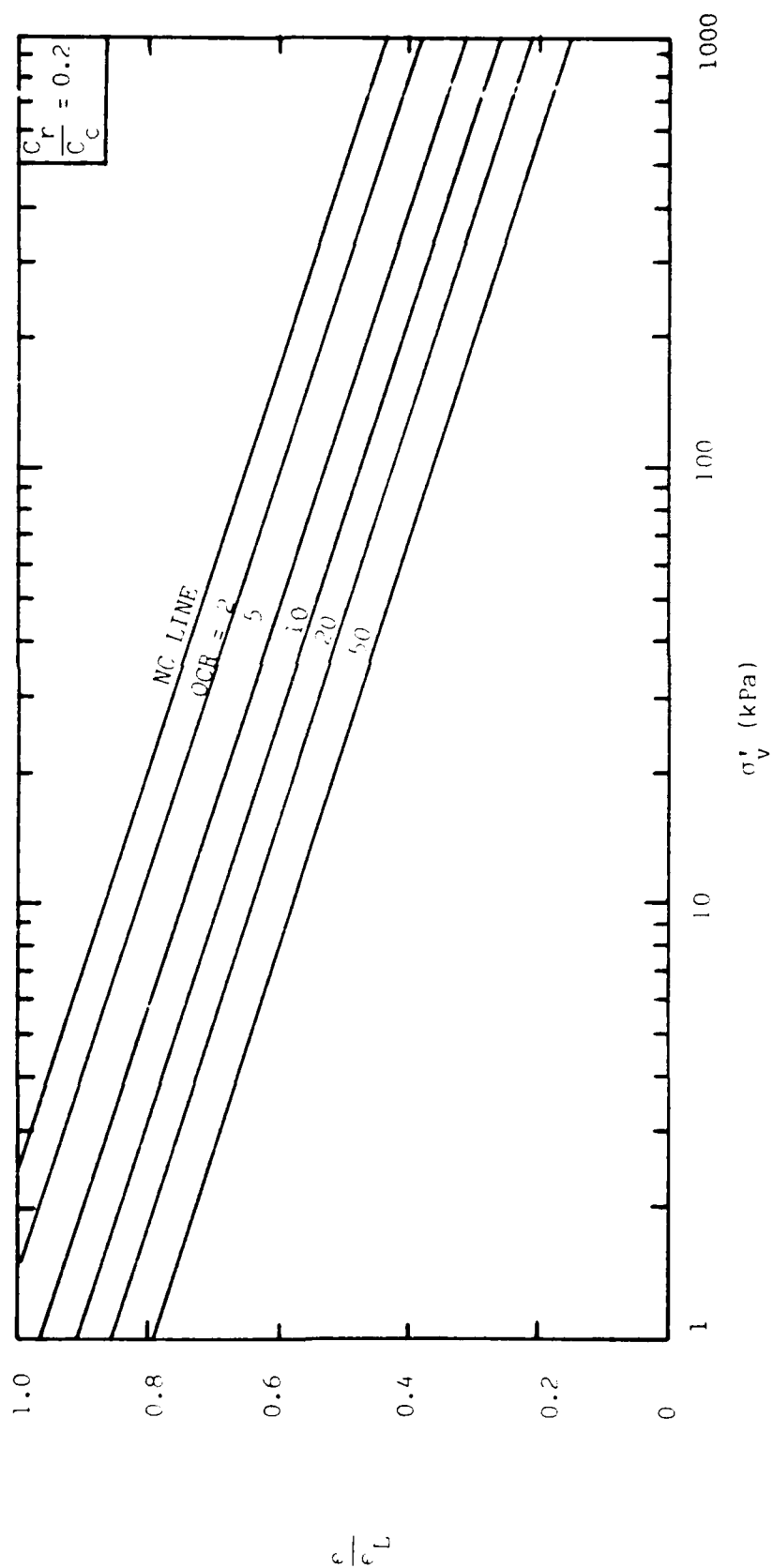
Figure 2.13 OCR Prediction Chart for $C_r/C_r = 0.1$

Figure 2.14 OCR Prediction Chart for $C_r/C_c = 0.2$

CHAPTER 3

MODELLING ANISOTROPY OF CLAYS - A NOVEL APPROACH

3.1 Introduction

Experimental studies conducted in the past have demonstrated
the significance of anisotropy on shear behavior of natural clays
(e.g. Duncan and Seed, 1966, Lewin, 1973, Mitchell, 1972, Saada,
1976, Saada and Bianchini, 1975, Tavenas and Leroueil, 1977, Ting,
1968). Lewin's stress probe experiments (1973) showed differences
between lateral and axial strains during isotropic consolidation of
an initially anisotropic specimen of clay. Anisotropy can also be
induced; Ting (1968) showed that an anisotropically consolidated
sample reaches an asymptotic isotropic state at an isotropic stress
about 3 times higher than its initial vertical stress. Experimen-
tal data (e.g., Tavenas and Leroueil, 1977, Graham et al., 1983)
show that the yield loci of natural deposits of clays are centered
around the K_o line in triaxial stress space.

These fundamental aspects of soil anisotropy must be taken
into account by geotechnical researchers and engineers if major
improvements in the interpretation and use of in situ measurements
are to be made. A simple model that captures the basic facets of
anisotropy and offers closed form solutions for strength and other
parameters at failure along various stress paths would be a valu-
able tool to accomplish this. In addition, the fundamental issues
involved in in situ testing can be best investigated, if this model

allows for sophistication without loss of the physical basis of the model.

3.2 Limitations of the Current Thinking.

Since the pioneering work of Roscoe and his co-workers (e.g., Roscoe, Schofield and Thurairajah 1963, Roscoe and Burland 1968), significant improvements have been made in modelling soil behavior. Yet, none of the models existing to date can be used routinely in the interpretation of pressuremeter and especially self boring pressuremeter (SBPM) tests. Simple models such as the MCC model (as discussed in Chapter 2) suffer from their inability to capture the above features of anisotropy. More sophisticated soil models (e.g., Prevost, 1978, Dafalias and Herrman, 1980, and Kavvadas, 1982) require extensive calibration parameters that would prevent routine use or mask the outcome of the investigations of in situ devices. Some of these models (e.g., Prevost, 1978 and 1979) are limited to the deviatoric stress space and thus cannot be used in situations where pore pressures are involved.

Perhaps, more importantly, a common shortcoming of all these models is that they do not provide a better understanding of the physical basis of the model, such as the work assumption used in the isotropic MCC model. With these shortcomings, one is left with the dissatisfaction that the important aspects such as mode of failure, possibility of radial cracking, effects of disturbance, etc., in SBPM testing can not be studied at a best rational level.

A research program has been undertaken with the aim of
addressing the above shortcomings, i.e. of creating a model that
captures the anisotropic features of clays and is applicable to
SBPM interpretation. Four stages are contemplated for this work:

   a.   Develop a simple anisotropic theory built on a sound physical
        basis.

   b.   Build upon this model to a sophisticated level without loss
        of generality.

   c.   Use (a) and/or (b) to interpret SBPM data.

   d.   Use (b) to study the fundamental issues of SBPM.

Stages (a) and (c) are well underway. An outline of the essential
features of the theory and its application to pressuremeter prob-
lems are reported in the following; details are given in Thevanay-
agam (1988a,b).

3.3   New Theoretical Developments

The purpose of this section is to provide the essential
features of a plasticity model that captures the behavior of aniso-
tropic clays at the critical state. The emphasis is upon: i) The
anisotropic nature of the yield surface; ii) The effect of induced
anisotropy; iii) The prediction of the failure parameters of clays,
using simple parameters (ϕ_c and OCR); and iv) The ability to inter-
pret any measured in situ strength, and transform it to any other

stress path applicable to a given design problem.

Test results published in the literature are used for validation. These includes many natural soils that have been tested in triaxial compression/extension (TC/TE), plane strain compression/extension (PSC/PSE), model pressuremeter (PM) and simple shear (SS).

3.3.1   Background Material: The Axi-symmetric Model

The notations are that of critical state soil mechanics (Schofield and Wroth 1968); they are appended to this chapter (Section 3.7).   Elastic isotropy is assumed, and elastic shear strains are assumed to exist.   The parameters κ and λ refer to the slope of the swelling and virgin K_o lines in e vs. lnp plane.   All stresses are effective stresses.   Compressive stresses and strains are taken positive and tensor notation is used.   Due to the mode of deposition, natural clays are generally cross anisotropic; the vertical axis is assumed to be the axis of cross anisotropy.

The original Cam Clay theory (Roscoe, Schofield and Thurairajah, 1963) began with the work assumption:

$$p\ \dot{\epsilon}_v^p + q\ \dot{\epsilon}_q^p = M\ p\ \dot{\epsilon}_q^p \tag{1}$$

Considering the continuity requirements of work relation, Eq.1 was modified to the form of the modified cam clay model, MCC, (Roscoe and Burland, 1968):

$$p\dot{\varepsilon}_v^P + q\dot{\varepsilon}_q^P = p \left| (\dot{\varepsilon}_v^P)^2 + (M\dot{\varepsilon}_q^P)^2 \right|^{1/2} \tag{2}$$

which, assuming the associative flow rule, resulted in an isotropic yield surface of the form:

$$f_{iso} = p^2 - pp_o + \frac{q^2}{M^2} = 0 \tag{3}$$

Dafalias (1987) introduced a modification to the work assumption:

$$p\dot{\varepsilon}_v^P + q\dot{\varepsilon}_q^P = p \left| (\dot{\varepsilon}_v^P)^2 + (M\dot{\varepsilon}_q^P)^2 + 2\alpha\dot{\varepsilon}_v^P\dot{\varepsilon}_q^P \right|^{1/2} \tag{4}$$

where α is a nondimensional parameter with an absolute value less than that of M. Dafalias (1987) considered the term α to account for anisotropic internal residual stresses and coupling of $\dot{\varepsilon}_v^P$ and $\dot{\varepsilon}_q^P$. However, it can be shown that irrespective of the nature of the soil (whether it is isotropic or not), Eq.4 is strictly true and has a definite meaning if the following relationship is used for α (Thevanayagam, 1988a):

$$2\alpha = 2r_i + (r_i^2 - M^2)\frac{\dot{\varepsilon}_q^P}{\dot{\varepsilon}_v^P} \tag{5}$$

The selection of the parameter α dictates the importance of the coupling term in Eq. 4, and also the shape of the yield locus as deduced from the work equation. If the normality condition is assumed, then α is related to the shape of the yield locus, f, by (from Eq. 5):

$$2 \alpha = 2 r + (r_n^2 - M^2) \frac{\partial f / \partial q}{\partial f / \partial p} \tag{6}$$

Thus, in general, α must be a function of M, p, q and r_n, i.e. $\alpha = g_1 (M,p,q,r_n)$. The assumptions $\alpha = g_1 (r_n)$ (Dafalias, 1987) or $\alpha = 0$ (Roscoe and Burland, 1968) are obviously special cases of this more general formulation for α.

When assuming a constant value of α, it is appropriate to relate it to the end of K_o virgin consolidation of clay from a slurry. At that stage, the following conditions must be satisfied:

$$\frac{\dot{\varepsilon}_v}{\dot{\varepsilon}_q} = 3/2 \; ; \quad \frac{\dot{\varepsilon}_v^p}{\dot{\varepsilon}_q^p} = \frac{\dot{\varepsilon}_v - \dot{\varepsilon}_v^e}{\dot{\varepsilon}_q - \dot{\varepsilon}_q^e}; \quad \text{and} \quad r_o = \frac{\dot{q}}{\dot{p}} = \frac{3 (1 - K_o)}{(1 + 2 K_o)} \tag{7}$$

where r_o refers to the slope of the virgin K_o line in p-q plane. Using the assumption of elastic isotropy and e vs. lnp relationships for the elastic strains, the following relationships exist:

$$K = \frac{\dot{p}}{\dot{\varepsilon}_v^e} = \frac{(1 + e)p}{\kappa}; \quad \dot{\varepsilon}_q^e = \dot{q}/(3G) \; , \quad \frac{G}{K} = \frac{3 (1 - 2 \nu)}{2 (1 + \nu)} \tag{8}$$

where K, G and ν are the elastic bulk modulus, shear modulus and Poisson's ratio of the clay, respectively. Using Eqs. 5 and 7-8, α at the end of K_o virgin consolidation, α_o, is given by:

$$\alpha_o = \frac{3 a_1 r_o + \eta_o^2 - M_c^2}{3 a_1}; \text{with } a_1 = \frac{1 - \kappa/\lambda}{1 - \left| \frac{\kappa \eta_o (1+\nu)}{3 \lambda (1 - 2\nu)} \right|} \tag{9a}$$

If the elastic shear strain is neglected in Eq.7, $a_1 = 1 - \kappa/\lambda$, and α_o

reduces to:

$$\alpha_o = \frac{3(1-\kappa/\lambda)\eta_o + \eta_o^2 - M_c^2}{3(1-\kappa/\lambda)} \qquad (9b)$$

If the clay is isotropically consolidated ($\dot{\varepsilon}_q = \dot{\varepsilon}_q^p = 0$), α_o becomes zero. It may be noted that no assumption on the shape of the yield surface or on the flow rule is necessary to derive α_o.

Assuming a constant value of α, i.e. $\alpha = \alpha_o$, the shape of the yield locus function is deduced from the work equation as:

$$\frac{p}{p_i} = \frac{M^2 + \eta_i^2 - 2\alpha \eta_i}{M^2 + \eta^2 - 2\alpha \eta} \qquad (10a)$$

where p and p_i correspond to any two positions on the yield surface, $f = 0$ (Fig. 1a). However, M takes the value M_c (compression side) for points located above point A in Figure 1a, and M_e (extension side) for points below A. Point A corresponds to the condition of zero increment in plastic shear strain, i.e. $\partial f/\partial q = 0$. At that point, the value of η is equal to α (from Eq. 6 with $\partial f/\partial q = 0$). The equations for the state boundary surface can be derived from Eq. 10a as:

$$(\eta-\alpha)^2 = -(M-\alpha)^2 + \frac{(M^2-\alpha^2)}{(M_c^2-\alpha^2)} \left|(\eta_o-\alpha)^2+(M_c^2-\alpha^2)\right| \exp\left|\frac{N_o-v_\lambda}{\lambda-\kappa}\right| \quad (10b)$$

$$\left(\frac{q}{p_e}-\alpha\frac{p}{p_e}\right)^2 = -(M-\alpha)^2\left|\frac{p}{p_e}\right|^2 + \frac{(M^2-\alpha^2)}{(M_c^2-\alpha^2)} \left|(\eta_o-\alpha)^2+(M_c^2-\alpha^2)\right|\left|\frac{p}{p_e}\right|^{\frac{\lambda-2\kappa}{\lambda-\kappa}} (10c)$$

The parameters p_e, N_o, and v_λ are defined as shown in Fig.1b and in

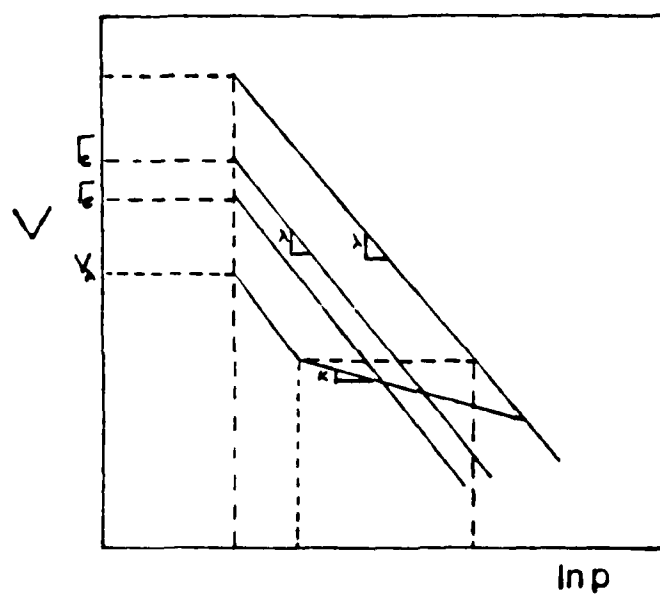Fig. 1a.   A Typical Anisotropic Yield Surface in the
Triaxial p-q Space

Fig. 1b. Critical State Parameters

Section 3.7.

Equations 10b and 10c are plotted in Figs. 2 and 3 for kaolin using the following parameters: $N_o = 3.23$, $\lambda = 0.19$, $\kappa = 0.06$, $M_c = 0.85$, $M_e = -0.85$, and $r_o = 0.43$. The state boundary surface predicted from these equations are compared to experimental data on stress paths obtained by Atkinson et al. (1987). This comparison shows that the model with a constant α captures the main features of the state boundary surface with some deviations. The first deviation occurs in the initial part of the triaxial extension (TE) stress path, as this part of the TE stress path lies inside the state boundary surface; however, this is not completely unexpected, at least in the initial part of the stress path, as the initial part of the TE stress path remains within the yield locus and thus must be elastic (Thevanayagam and Prapaharan, 1988). Therefore, this initial part of the TE stress path is expected to lie inside the state boundary surface. The stress path in triaxial compression (TC) closely follows the state boundary surface up to the peak deviatoric stress and then the most significant deviation occurs beyond this point (clearly illustrated in Figs. 2 and 3). These deviations at large strains are attributed to the effects of induced anisotropy.

The comparison between predictions and experimental data in Figs. 2 and 3 demonstrates that the proposed model provides a good representation of the material behavior; however, if the post peak behavior in TC and large strain behavior in TE are of interest then the induced anisotropy should be accounted for in the model. In
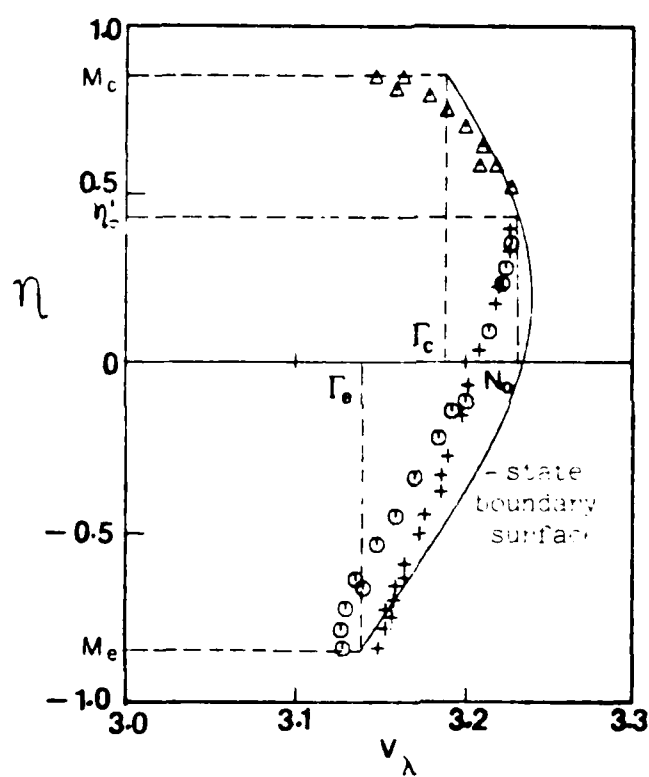
Fig. 8   Normalized Stress Paths and State Boundary
         Surface (Compression: Constant p' △;
         Extension: Undrained Triaxial ⊙;
         Constant p' +,: 'Measured - after Atkinson
         et al., 1987)
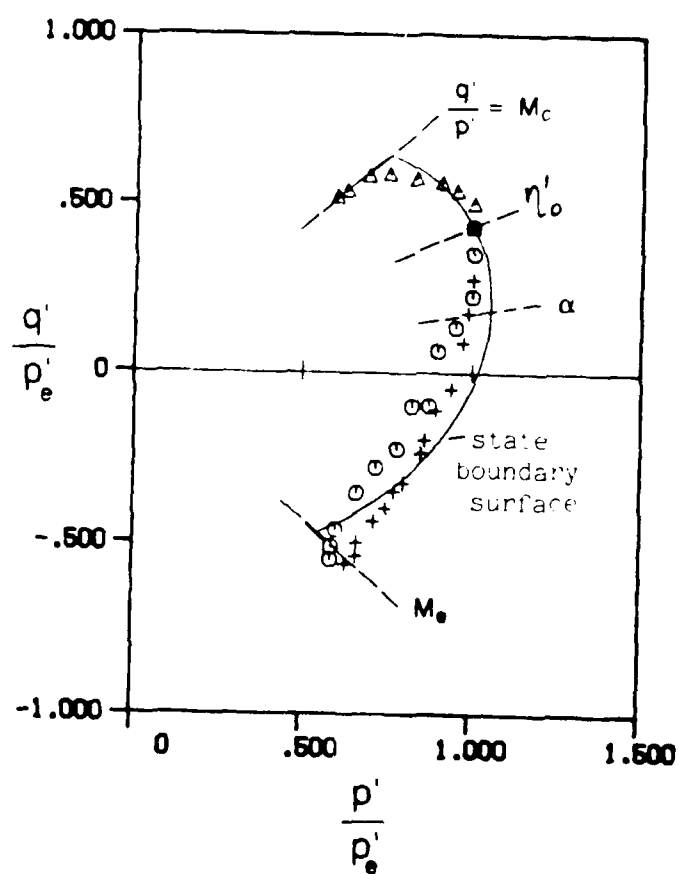
Fig. 3   Normalized Stress Paths and State
          Boundary Surface (Compression:
          Constant p' Δ; Extension: Undrained
          Triaxial ⊙: Constant p' +): Measured
          after Atkinson et al., 1987)

what follows, the effects of induced anisotropy are introduced by considering that α does not remain constant, but varies during shearing proportionally to the initial value α_o. The other assumptions of the model, related to the other evolution characteristics of the yield surface f, are: (i) the projection of the yield surface on the e vs. lnp plane has a constant slope κ, and (ii) the hardening is such that point E (i.e. p_E in Fig.1a) projected on the e vs. lnp plane remains on the $K_o NC$ line, independent of plastic loading.

The expressions for undrained strength ratio in TC and TE are developed first. Assuming that the value of α is given by $\alpha = \gamma\alpha_o$ (i.e. proportional to α_o) at failure, the values of γ in TC and TE are obtained by calibrating the theoretical expressions for strength ratio using experimental data. This is followed by the development of a 3-D model. The results of the axisymmetric and 3-D models are used to obtain closed form solutions for failure parameters of clays. Predictability is demonstrated by comparison with experimental data. Subsequently the application of this model to the pressuremeter will be illustrated.

3.3.2 Undrained Shear in Triaxial Compression

Referring to Table 1, the undrained strength in TC is given by:

Use Eqns. Eq.	TC, Fig.20a	TE, Fig.20b
(10) A1	$\dfrac{p_o}{p_\alpha} = \dfrac{M_c^2 - \alpha^2}{M_c^2 + \eta_o^2 - 2\eta_o\alpha},\quad \dfrac{p_f}{p_\alpha} = \dfrac{M_c^2 - \alpha^2}{2M_c^2 - 2M_c\alpha}$	$\dfrac{p_o}{p_\alpha} = \dfrac{M_c^2 - \alpha^2}{M_c^2 + \eta_o^2 - 2\eta_o\alpha},\quad \dfrac{p_f}{p_\alpha} = \dfrac{M_e^2 - \alpha^2}{2M_e^2 - 2M_e\alpha}$
$q_f = Mp_f$ A2	$\tau_f = \dfrac{q_f}{2} = \dfrac{M_c p_f}{2}$	$\tau_f = \dfrac{q_f}{2} = \dfrac{M_e p_f}{2}$
e vs. ln(p) A3	$e_o = e_f - \kappa \ln\left(\dfrac{p_o}{p_f}\right)$	$e_o = e_f - \kappa \ln\left(\dfrac{p_o}{p_f}\right)$
A4	$e_o = e_f - \kappa \ln\left(\dfrac{p_{max}}{p_{oc}}\right) - \lambda \ln\left(\dfrac{p_o}{p_{max}}\right)$	$e_o = e_f - \kappa \ln\left(\dfrac{p_{max}}{p_{oc}}\right) - \lambda \ln\left(\dfrac{p_o}{p_{max}}\right)$
A1–A4 A5	$\left(\dfrac{\tau_f}{\sigma_{vo}}\right)_{TC} = \dfrac{M_c}{6}\cdot(1+2K_{o,nc})\cdot\left|\dfrac{M_c^2+\eta_o^2-2\eta_o\alpha}{2M_c^2-2M_c\alpha}\right|^\Lambda \cdot \left|\dfrac{1+2K_{o,oc}}{1+2K_{o,nc}}\right|^\Lambda \cdot OCR^\Lambda$	$\left(\dfrac{\tau_f}{\sigma_{vo}}\right)_{TE} = \dfrac{M_e}{6}\cdot(1+2K_{o,nc})\cdot\left|\dfrac{M_c^2+\eta_o^2-2\eta_o\alpha}{2M_c^2-2M_e\alpha}\right|^\Lambda \cdot \left|\dfrac{M_e^2-\alpha^2}{M_c^2-\alpha^2}\right|^\Lambda \cdot \left|\dfrac{1+2K_{o,oc}}{1+2K_{o,nc}}\right|^\Lambda \cdot OCR^\Lambda$
		$\left(\dfrac{\tau_f}{\sigma_{vo}}\right)_{TE} = \dfrac{M_e}{M_c}\cdot\left|\dfrac{M_e^2-\alpha^2}{M_c^2-\alpha^2}\right|^\Lambda \cdot \left(\dfrac{\tau_f}{\sigma_{vo}}\right)_{TC}\cdot\left|\dfrac{M_c^2-M_c\alpha}{M_e^2-M_e\alpha}\right|^\Lambda$
A2,A5 A6	$A_f = \dfrac{1}{3} - \left|\dfrac{1 - \dfrac{6}{M_c(1+2K_{oc})}\left(\dfrac{\tau_f}{\sigma_{vo}}\right)_{TC}}{\eta_{oc} - \dfrac{6}{(1+2K_{oc})}\left(\dfrac{\tau_f}{\sigma_{vo}}\right)_{TC}}\right|$	$A_f = \dfrac{-1}{3} - \left|\dfrac{1 - \dfrac{6}{M_e(1+2K_{oc})}\left(\dfrac{\tau_f}{\sigma_{vo}}\right)_{TE}}{\eta_{oc} - \dfrac{6}{(1+2K_{oc})}\left(\dfrac{\tau_f}{\sigma_{vo}}\right)_{TE}}\right|$

Note: $\left(\dfrac{\tau_f}{\sigma}\right)_{TF}$ is negative.

$$\left(\frac{\tau_f}{\sigma_{vo}}\right)_{TC} = \left(\frac{\tau_f}{\sigma_{vo}}\right)_{nc} \left|\frac{1+2K_{o,oc}}{1+2K_{o,nc}}\right|^{\frac{\kappa}{\lambda}} \left|OCR\right|^{\Lambda}; \quad \Lambda = 1 - \frac{\kappa}{\lambda} \qquad (11a)$$

$$\text{where} \left(\frac{\tau_f}{\sigma_{vo}}\right)_{nc} = \left(\frac{1+2K_{o,nc}}{6}\right) M_c \ D_1; \quad D_1 = \left|\frac{M_c^2 + r_o^2 - 2\alpha \ r_o}{2M_c^2 - 2\alpha \ M_c}\right|^{\Lambda} (11b)$$

σ_{vo} is the initial vertical stress before shearing, α represents the anisotropic state at failure, and nc and oc stands for normally consolidated clay and overconsolidated clay, respectively. The shear strength τ_f is as defined in Table 1. If α is set to zero, Eq.11b reduces to the strength expressions for CK_oUC strength and CIUC (when $r_o=0$, for $K_o=1$) strength of the MCC model (Wroth 1984, also see Chapter 2 of this report). If desired, simplifications to Eq.11 can be made as follows.

The relationship between the slope of the virgin consolidation line and swelling line in e vs lnp plane (denoted by λ and k) and those in e vs $ln\sigma_v$ plane (denoted by λ_v and k_v) are given by (Thevanayagam, 1988a):

$$\lambda = \lambda_v \quad \text{and,} \quad \kappa = \left|\frac{\ln(OCR)}{\ln\left|\frac{(1+2K_{o,nc})\ OCR}{1+2K_{o,oc}}\right|}\right| \kappa_v \qquad (12)$$

Using typical K_o-OCR relationships (e.g. Brooker and Ireland, 1965) for clays, Eq.12 reduces to:

$$\kappa = 1.3 \, \kappa_v \tag{13}$$

Thus, Λ in Eq. 11.b can be written as:

$$\Lambda = 1 - \frac{1.3 \, k_v}{\lambda} \tag{14}$$

Furthermore, substituting Eq.13 in Eq.11, $(\frac{\tau}{\sigma_{vo}})_{TC}$ can be expressed as:

$$(\frac{\tau_f}{\sigma_{vo}})_{TC} = D_2 \, (\frac{\tau_f}{\sigma_{vo}})_{nc} \, (OCR)^{\Lambda_v} \tag{15}$$

$$\text{with} \quad D_2 = \frac{\left| \frac{1 + 2 \, K_{o,oc}}{1 + 2 \, K_{o,nc}} \right|^{\frac{1.3\kappa_v}{\lambda}}}{\left| OCR \right|^{\frac{0.3\kappa_v}{\lambda}}}$$

$$\text{and} \quad \Lambda_v = 1 - \frac{\kappa_v}{\lambda}$$

For typical values of soil parameters, $k_v/\lambda \simeq 0.1 - 0.3$ and typical K_o-OCR relationships (e.g. Brooker and Ireland, 1965), D_2 is close to 1.0, reducing Eq. 15 to:

$$(\frac{\tau_f}{\sigma_{vo}})_{TC} = (\frac{\tau_f}{\sigma_{vo}})_{nc} \, \left| OCR \right|^{\Lambda_v} \tag{16}$$

The form of Eq.16 is similar to the empirical relationship proposed by Ladd, et al. (1977) and the theoretical relationship for isotropic clays (Wroth 1984).

3.3.3 Undrained Shear in Tiiaxial Extension

Similarly, the undrained shear strength in TE is given by (see Table 1):

$$\left(\frac{\tau_f}{\sigma_{vo}}\right)_{TE} = \frac{M_e}{M_c} \cdot \frac{M_e^2 - \alpha^2}{M_c^2 - \alpha^2} \left(\frac{\tau_f}{\sigma_{vo}}\right)_{TC} \left| \frac{M_c \ (M_c - \alpha)}{(M_e - \alpha) \ M_e} \right| \left(1 - \frac{1.3 \kappa_v}{\lambda}\right) \qquad (17)$$

where $(\tau_f/\sigma_{vo})_{TC}$ is given by Eqs.11 or 16; in this case, α represents the anisotropic state at the critical state after shearing in TE. Note that the value of M_e is negative. Classically, critical state parameters M_c and M_e are obtained using the expressions (Roscoe and Burland 1968, Dafalias 1987): $M_c = 6\sin\phi/3 - \sin\phi$ and $M_e = -6\sin\phi/3 + \sin\phi$, where the ϕ angle is the angle of friction at failure obtained from TC ($\sin \phi = (\sigma_1 - \sigma_3)/(\sigma_1 + \sigma_3)$ at $(\sigma_1 - \sigma_3)_{max}$). However, this expression is valid only for truly isotropic clays. Existing data (e.g. Saada et al., 1975) show that the friction angle in TE is generally greater than that in TC. In this report, using the failure criteria developed later in Eq.23b, a better relationship was obtained for ϕ_c and ϕ_e (demonstrated in Eq.23c), and comparison with experimental data showed very good agreement. Using this information, Eq.17 reduces to a simple expression (absolute value of τ_f in TE is taken):

$$\left(\frac{\tau_f}{\sigma_{vo}}\right)_{TE} = \left| \frac{M_c - \alpha}{M_c + \alpha} \right| \left(1 - \frac{1.3 \ \kappa_v}{\lambda}\right) \left(\frac{\tau_f}{\sigma_{vo}}\right)_{TC} \qquad (18)$$

3.3.4 Effect of Induced Anisotropy and Variations in Soil Parameters

The effects of variability on soil parameters ν and (k_v/λ) on the expressions for strength ratio in TC and TE were studied. Using the experimental data on many clays the values of γ in TC and TE were calibrated. The following three cases were considered:

a. $\alpha = 0$ (i.e. isotropic MCC model);

b. Initial value of α, α_o, given by Eq. 9b and α at critical state given by $\alpha = \gamma \, \alpha_o$;

c. Case (b), but using Eq. 9a for α_o.

Case (a) when compared to cases (b) and (c) is used to study whether the initial anisotropy is an important factor in the undrained strength ratio of clays. Cases (b) and (c) were chosen to study the influence of Poisson's ratio on the strength ratio. Using these cases, the values of γ for TC and TE were calibrated from experimental data on peak strength.

A reasonable variation of the ratio k_v/λ in the range 0.1-0.3 showed that the above relationships were fairly insensitive to this ratio, and most calculations were thus made with $k_v/\lambda = 0.20$. For the TC strength (Eqs.11-16), case (c) was virtually unaffected by any variation in ν, and the results were very similar to that of case (b). Based on regression analysis, case (b) was found to be the best, thus indicating that Eq.9b is appropriate for α_o. The single most influential parameter was ϕ_c. The comparison of the

model prediction with experimental data at peak strength in TC showed that α is not a very sensitive parameter in TC, and thus, as a first approximation, $\gamma = 1.0$ is a reasonable assumption in TC. The predictability of residual strength of clays was not studied at this stage; it is expected that $\gamma = 1.0$ will not be a satisfactory assumption if the strength at very large strains is of interest. Also the rate effects were not considered in the process of calibration.

For TE, the influence of induced anisotropy was significant. A value of $\gamma = 0.6$ was found to be most appropriate for the data evaluated, resulting in Fig.4. However, since the term $(\tau_f/\sigma_{vo})_{TC}$ in Eq.18 is not very sensitive to α , for simplicity in expressing the strength ratio in terms of that in TC, it can be sufficient to substitute $\alpha = \gamma\alpha_o$ only in the first term of Eq.18. For highly overconsolidated clays, since most of the stress path lies inside the yield locus, the induced anisotropy may be expected to be small, i.e. γ may tend towards 1.0. Further simplifications can be made to Eq.18 as follows; Using a typical value of $k_v/\lambda = 0.2$, taking a Taylor series expansion, and neglecting higher order terms Eq.18 reduces to:

$$(\frac{\tau_f}{\sigma_{vo}})_{TE} \cong (\frac{M_c - 0.5\,\alpha}{M_c + \alpha})\ (\frac{\tau_f}{\sigma_{vo}})_{TC} \tag{19}$$

where the relationships:

$$\alpha = \gamma\,\alpha_o \quad \text{and} \quad \gamma = 0.6 \tag{20}$$
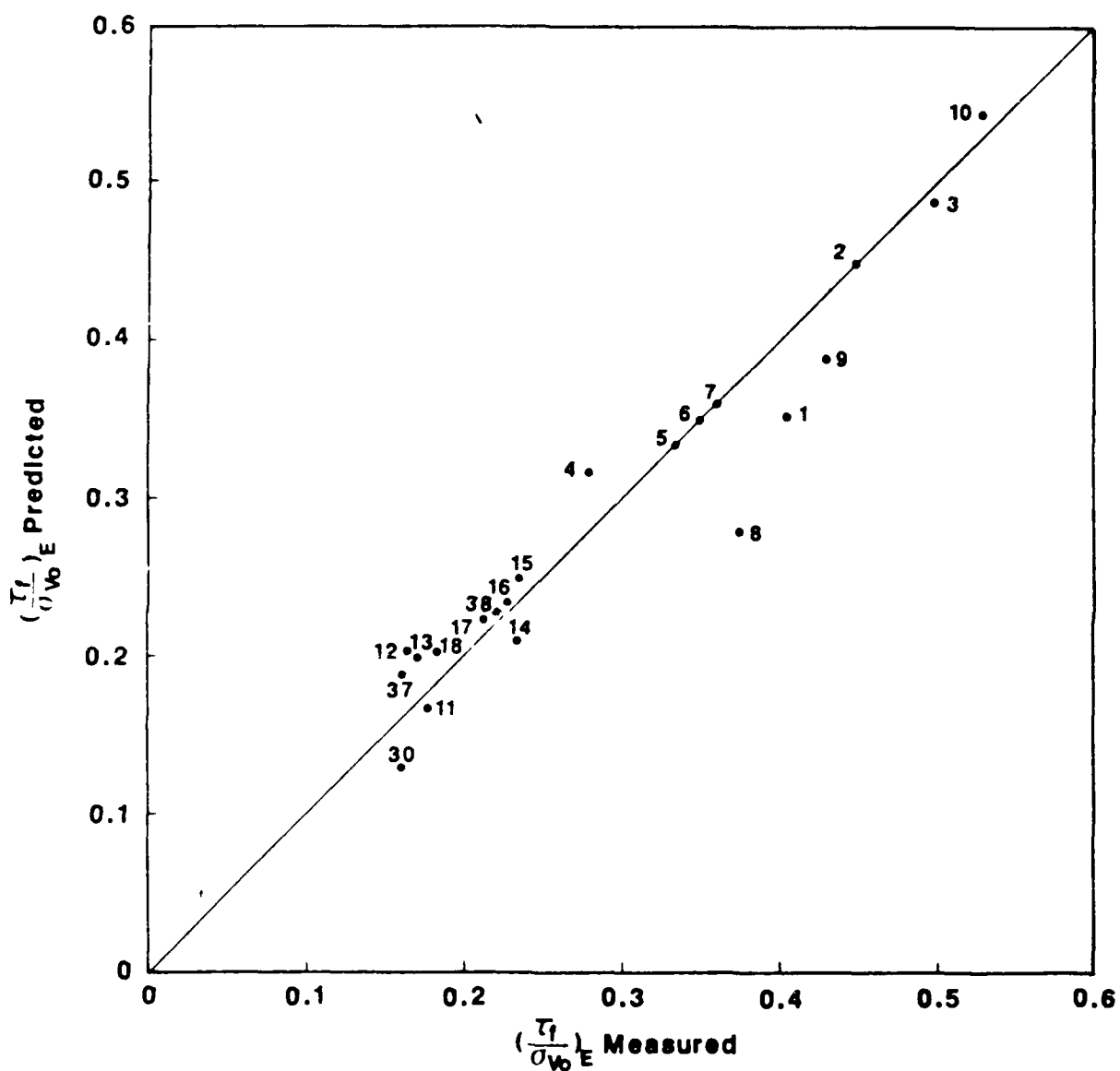
Fig. 4 Predicted Versus Experimental Undrained Strength

Ratio $(\frac{\tau_f}{\sigma_{vo}})_{TE}$ (Numbers Refer to Cases in Table 8)

appear applicable to many clays.

Using Eqs. 11 to 19 and $q_f = Mp_f$ at failure, the stresses and shear induced pore pressure parameters at failure can be derived for both TC and TE (Table 2). Table 1 contains the expression for Skempton's A-parameter as well.

The determination of failure parameters for modes of failure other than TC and TE is presented in the next sections. Two important aspects are discussed: (i) development of the necessary theoretical relationships required to obtain failure parameters in any mode of failure; and (ii) rationale for failure criteria of an anisotropic material, and physical explanation for the forms chosen in this development.

3.3.5 General 3-D Behavior of Clays at Critical State

Let the failure criterion for a clay, given by $f^f = 0$, satisfy the critical state condition, and be dependent on the initial state of the clay. For any arbitrary point A on this failure criterion, the corresponding state of the yield surface is given by f_A^y. No point can lie outside the failure criterion, and no intersection of yield and failure criteria is possible except tangentially. Using the associative flow rule, the gradient of f_A^y at A is perpendicular to the hydrostatic stress axis, as no plastic volumetric strain takes place at critical state. Since f_A^y and f^f are in contact tangentially at A, it follows that the gradient of $f_d^f = 0$ is parallel to the gradient of f_A^y at A, where $f_d^f = 0$ is the

TABLE 2 Failure Parameters at Critical State of a Clay

MODE AT FAILURE / STATE OF STRAIN	TC	C'	PSC	PSE	S-S	PM
STATE OF STRAIN AT FAILURE	$\sigma_{22}=\sigma_{33};\ \sigma_{11}$; $\varepsilon_{11}>0$; $\varepsilon_{ij}=0\ i\neq j$	$\sigma_{22}=\sigma_{33}$; σ_{11} ; ε_{11} ; $\varepsilon_{ij}=0\ i\neq j$	σ_{33} ; σ_{11} ; $\varepsilon_{22}=0$; $\varepsilon_{ij}=0\ i\neq j$	$\sigma_{33}=\sigma_{11}$; $i=j$; $\varepsilon_{22}=0$; $\varepsilon_{ij}=0\ i\neq j$	$\varepsilon_{ij}=0;\ i=j$; σ_{13} ; σ_{33} ; σ_{11}	$\sigma_{11}=0$; $\sigma_{22}=-\sigma_{33}$; $\varepsilon_{ij}=0\ i\neq j$
τ_f	$\left(\dfrac{\sigma_1-\sigma_3}{2}\right)_{max}$	$\left(\dfrac{\sigma_3-\sigma_1}{2}\right)_{max}$	$\left(\dfrac{\sigma_1-\sigma_3}{2}\right)_{max}$	$\left(\dfrac{\sigma_3-\sigma_1}{2}\right)_{max}$	$\left(\dfrac{\sigma_1-\sigma_3}{2}\right)_{max}$	$\left(\dfrac{\sigma_2-\sigma_3}{2}\right)_{max}$
$\left[\dfrac{\tau_{fxx}}{\tau_{ftc}}\right]$	1.0	$\dfrac{(M_c-0.5\alpha)}{(M_c+\alpha)}$	$\dfrac{(1.15M_c+1.04\alpha)}{(M_c+\alpha)}$	$\dfrac{(1.15M_c-0.46\alpha)}{(M_c+\alpha)}$	$\dfrac{1.5\alpha}{(M_c+\alpha)}$	$\dfrac{(2M_c+0.5\alpha)}{\sqrt{3}\,(M_c+\alpha)}$
$\left(\dfrac{\sigma_1}{\sigma_{vo}}\right)$	$\dfrac{4M_c+6}{3M_c}\cdot\left(\dfrac{\tau_f}{\sigma_{vo}}\right)_c$	$\dfrac{6-4M_c}{3M_c}\cdot\dfrac{M_c-0.5\alpha}{M_c+\alpha}\cdot\left(\dfrac{\tau_f}{\sigma_{vo}}\right)_c$	$\left[\dfrac{x}{M_c\sqrt{2}}+1.15M_c+1.29\alpha\right]\cdot\dfrac{1}{M_c+\alpha}\cdot\left(\dfrac{\tau_f}{\sigma_{vo}}\right)_c$	$\left[\dfrac{x}{M_c\sqrt{2}}+0.71\alpha-1.15M_c\right]\cdot\dfrac{1}{M_c+\alpha}\cdot\left(\dfrac{\tau_f}{\sigma_{vo}}\right)_c$	--	$\left[\dfrac{\sqrt{3x^2+2.25}}{M}+x-0.5\right]\cdot\dfrac{\alpha}{M_c+\alpha}\cdot\left(\dfrac{\tau_f}{\sigma_{vo}}\right)_c$
$\left(\dfrac{\sigma_2}{\sigma_{vo}}\right)$	$\dfrac{6-2M_c}{M_c}\cdot\left(\dfrac{\tau_f}{\sigma_{vo}}\right)_c$	$\dfrac{6+2M_c}{3M_c}\cdot\dfrac{M_c-0.5\alpha}{M_c+\alpha}\cdot\left(\dfrac{\tau_f}{\sigma_{vo}}\right)_c$	$\left(\dfrac{x}{M_c\sqrt{2}}-0.5\alpha\right)\cdot\dfrac{1}{M_c}\cdot\left(\dfrac{\tau_f}{\sigma_{vo}}\right)_c$	$\left(\dfrac{x}{M_c\sqrt{2}}-0.5\alpha\right)\cdot\dfrac{1}{M_c+\alpha}\cdot\left(\dfrac{\tau_f}{\sigma_{vo}}\right)_c$	--	$\left[\dfrac{\sqrt{3x^2+2.25}}{M}+1\right]\cdot\dfrac{\alpha}{M_c+\alpha}\cdot\left(\dfrac{\tau_f}{\sigma_{vo}}\right)_c$

	$(\frac{\sigma_2}{\sigma_{vo}})$	$(\frac{\sigma_3}{\sigma_{vo}})$	$\sin(\phi_{xx})$	$(\frac{\Delta U_{sh}}{\sigma_{vo}})_{xx} = \frac{(P_o - P_f)}{\sigma_{vo}}$	x
	—	$\frac{\|\sqrt{3x^2+2.25} - x - 0.5\|}{3} \cdot \frac{\alpha}{M_c+\alpha} \cdot (\frac{\tau_f}{\sigma_{vo}})_c$	$\frac{2x}{(\frac{2}{\sqrt{3x^2+2.25}} - 1)\frac{M_c}{M_c}}$	$\frac{1+2K_{o,ocr}}{3} - \frac{\sqrt{3x^2+2.25}}{M_c} \cdot \frac{\alpha}{M_c+\alpha} \cdot (\frac{\tau_f}{\sigma_{vo}})_c$	$\frac{2M_c + 0.5\alpha}{\sqrt{3}\alpha}$
	—	$(\frac{x}{M_c\sqrt{}} - 0.21\alpha + 1.15M_c) \cdot \frac{1}{M_c+\alpha} \cdot (\frac{\tau_f}{\sigma_{vo}})_c$	$\frac{2.31M_c - 0.92\alpha}{x\frac{\sqrt{2}}{M_c} + 0.5\alpha}$	$\frac{1+2K_{o,ocr}}{3} - (\frac{x}{(M_c+\alpha)M_c\sqrt{2}}) \cdot (\frac{\tau_f}{\sigma_{vo}})_c$	$(7.98M_c^2 - 6.35M_c\alpha + 2.39\alpha^2)^{1/2}$
	—	$(\frac{x}{M_c\sqrt{}} - 1.15M_c - 0.79\alpha) \cdot \frac{1}{M_c+\alpha} \cdot (\frac{\tau_f}{\sigma_{vo}})_c$	$\frac{2.31M_c + 2.08\alpha}{x\frac{\sqrt{2}}{M_c} + .5\alpha}$	$\frac{1+2K_{o,ocr}}{3} - (\frac{x}{M_c\sqrt{2}}) \cdot \frac{1}{M_c+\alpha} \cdot (\frac{\tau_f}{\sigma_{vo}})_c$	$(7.98M_c^2 + 14.35M_c\alpha + 7.61\alpha^2)^{1/2}$
	—	$(\frac{\sigma_1}{\sigma_{vo}})$	$\frac{3M_c}{6-M_c}$	$\frac{1+2K_{o,ocr}}{3} - (\frac{2}{M_c} \cdot \frac{M_c - 0.5\alpha}{M_c+\alpha}) \cdot (\frac{\tau_f}{\sigma_{vo}})_c$	—
		$(\frac{\sigma_2}{\sigma_{vo}})$	$\frac{3M_c}{6+M_c}$	$\frac{1+2K_{o,ocr}}{3} - \frac{2}{M_c} (\frac{\tau_f}{\sigma_{vo}})_c$	—

deviatoric component of the failure criterion, obtained by projecting f^f at a given initial state onto the deviatoric plane in stress space. Since f^f is dependent on the initial state of the clay, the function f_d^f is also dependent on the initial state. The general form of f^f in 3-D stress space may be obtained by the evolution of the intersection of f_d^f and another, non deviatoric surface, $f_p^f = 0$. In this development f_p^f is assumed to be independent of the initial state of the clay. The resulting failure surface f^f is given by:

$$f^f = f_d^f + f_p^f = 0, \text{ with, } f_d^f = 0, \text{ and } f_p^f = 0 \text{ at failure.} \quad (21)$$

The strain increment upon loading at failure (i.e. at critical state) is given by:

$$\dot{\epsilon}_{ij} = \beta \, \frac{\partial f_d^f}{\partial \sigma_{ij}} \quad (22)$$

where β is a proportionality constant. In undrained shearing only 5 of the 6 components of strain are independent. Therefore, Eq. 22 yields only five independent equations. The functions $f_d^f = 0$ and $f_p^f = 0$ offer two more independent equations. The unknowns are the failure stresses (6 components) and the proportionality constant β. Therefore with the knowledge of the strain increment at failure $\dot{\epsilon}_{ij}$, and Eqs. 21 and 22, the failure stresses σ_{ij} can be solved for in closed form, i.e. the strain path and Eqs. 21 and 22 lead to the solution for failure stresses.

The choices made for f_d^f and f_p^f and their physical meanings are as follows. The form of f_d^f is given by a general Mises criteria type:

$$f_d^f = \frac{3}{2}(S_{ij}-\alpha_{ij})(S_{ij}-\alpha_{ij}) - k^2 = 0 \qquad (23a)$$

$$\text{with } S_{ij} = \sigma_{ij} - \frac{1}{3}\sigma_{kk}\delta_{ij}$$

where δ_{ij} is the Kronecker delta, σ_{ij} the stress tensor, S_{ij} the deviatoric stress tensor, and α_{ij} represents the anisotropic state of the material at failure, with k and α_{ij} dependent on the initial state of the material only. If the clay is initially cross-anisotropic (e.g. natural 1-D consolidated clays) the axes of stresses and strains are chosen to coincide with the axes of aniso-tropy (Fig.5). If a different coordinate system is chosen, the results of this study should be used with appropriate direction cosines (as later indicated by Eq. 25). For cross anisotropic clays, $\alpha_{33} = \alpha_{22} = -\alpha_{11}/2$, and $\alpha_{ij}=0$ for $i\neq j$.

The form for f_p^f is given by an extended von Mises type:

$$f_p^f = (\sigma_1-\sigma_2)^2+(\sigma_2-\sigma_3)^2+(\sigma_3-\sigma_1)^2-\frac{2H^2}{9}(\sigma_1+\sigma_2+\sigma_3)^2=0 \qquad (23b)$$

where σ_1,σ_2 and σ_3 are principal stresses and H is a constant. The failure criteria given in Eqs. 23a and 23b are interpretable within the context of mechanics. The terms α_{ij} can be considered to represent the deviatoric component of residual stresses in the clay, that is locked-in stresses indicative of the anisotropic
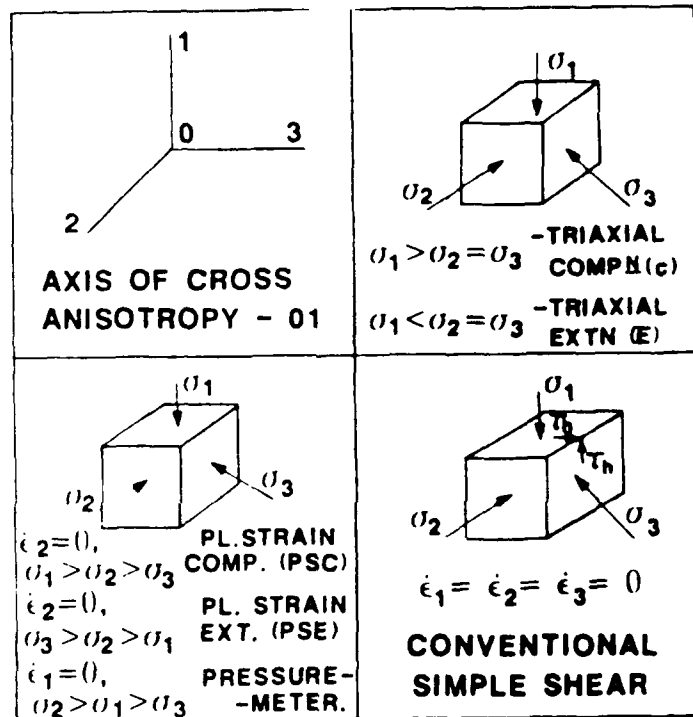
Fig. 5   Axis System for Different Tests

nature of the soil. The deviatoric stresses internally available in the soil are given by $(S_{ij} - \alpha_{ij})$. From an energy standpoint, Eq. 23a can be interpreted in terms of the shear strain energy internally stored in the soil, while Eq. 23b shows that the strain energy externally available to do work is dependent on the mean stress. Taken together, those equations imply that the mean and deviatoric stresses at failure are dependent on the orientation of the failure plane.

The general 3-D failure criteria, Eqs. 23a-b, should satisfy some specific conditions: (i) $q_f = M\ p_f$ in TC and TE; and (ii) the results obtained using the axisymmetric model given earlier. These conditions can be used to solve for the model parameters α_{ij}, k, and H. The first condition implies that $H^2 = M^2$, and it can be used to obtain the relationship between ϕ_c and ϕ_e:

$$\sin\phi_e = \frac{\sin\phi_c}{1 - \frac{2}{3}\sin\phi_c} \qquad (23c)$$

The predictions made with Eq. 23c are given in Fig. 6 (dashed line) for the experimental data used earlier. This agreement between predicted and experimental values is very good. For comparison, the prediction made using the work by Lade and Mussante (1977 and 1978), and Matsuoka and Nakai (1982) are also given in Fig. 6. For a given ϕ_c, these relationships tend to underpredict the value of ϕ_e. The results in Fig. 6 indicate that, based upon the TC and TE failure modes, the proposed criteria are satisfac-
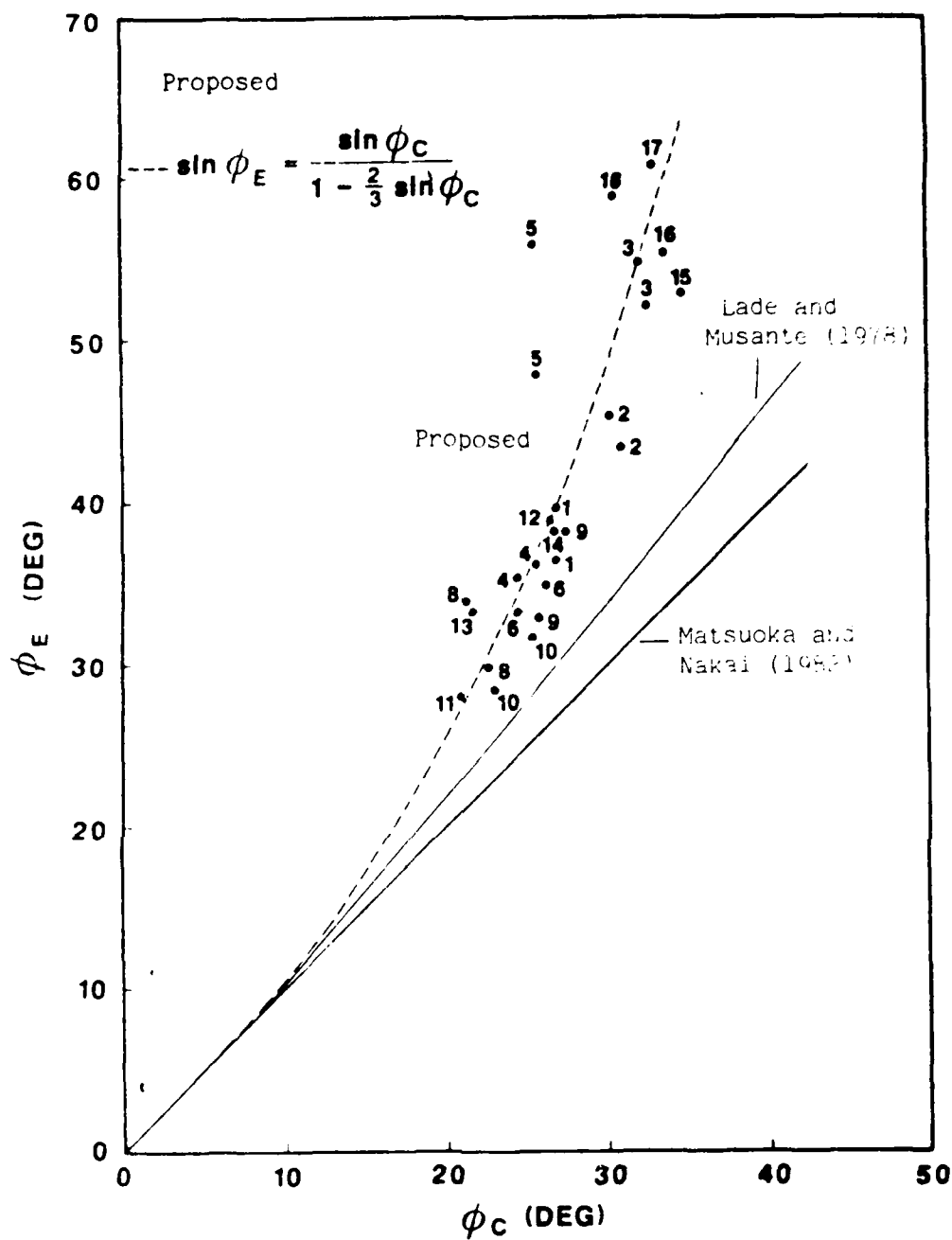
Fig. 6   Proposed Relationship Between ϕ_e and ϕ_c for 1-D
Consolidated Clays (Numbers Refer to Cases in
Table 8)

tory. However, alternate forms could be explored based upon data for other modes of failure.

Using the second condition that the failure criteria must satisfy, i.e. the axisymmetric results in TC and TE, the two unknowns α_{11} and k in Eq.23a can be solved for (Thevanayagam, 1988a):

$$\frac{k}{\sigma_{vo}} = \frac{2 \ M_c + 0.5\alpha}{M_c + \alpha} \ (\frac{\tau_f}{\sigma_{vo}})_{TC} \qquad (24a)$$

and

$$\frac{\alpha_{11}}{\sigma_{vo}} = \frac{\alpha}{M_c + \alpha} \ (\frac{\tau_f}{\sigma_{vo}})_{TC} \qquad (24b)$$

where $(\tau_f/\sigma_{vo})_{TC}$ is given by Eqs.11 or 16.

3.4 Summary of the New Model.

As indicated earlier, with the knowledge of strain increments at failure, Eqs. 22 to 23a-b gives seven independent equations. There are 7 unknowns (σ_{ij}'s and β). Using OCR, $M_c = \frac{6 \sin \phi_c}{3 - \sin \phi_c}$, Eqs. 9b, 11 or 16, 24, $\alpha = \gamma \ \alpha_o$, and σ_{vo}, all the model parameters can be determined. Consequently, using Eq. 22 and 23a-b, the failure stresses in any mode of failure can be solved for in closed form. As noted earlier, if a coordinate system different from that shown in Fig. 5 is chosen, appropriate direction cosines must be applied to Eqs. 22 and 23a-b. For example, if the strain incre-ments at failure are known in a new coordinate system different

from that in Fig. 5, Eq. 22 should be modified as follows:

$$\dot{\varepsilon}_{mn} = \beta \; l_{im} \; l_{jn} \; \frac{\partial f_d^f}{\partial \sigma_{ij}} \tag{25}$$

where σ_{ij} are stresses in the coordinate system shown in Fig. 5, l_{ij} are the direction cosines, i.e. cosine of the angle between axis i in the system shown in Fig. 5 and axis j in the new system, and $\dot{\varepsilon}_{ij}$ is the strain increment at failure in the new coordinate system.

Using Eqs. 15, and 21-24, the strength relationships for some of the most commonly encountered modes of failure are given by (see Table 2):

$$\left(\frac{\tau_f}{\sigma_{vo}} \right)_{SS} = \frac{1.5 \; \alpha}{M_c + \alpha} \; \left(\frac{\tau_f}{\sigma_{vo}} \right)_{TC} \tag{26a}$$

$$\left(\frac{\tau_h}{\sigma_{vo}} \right)_{SS} = 0.9 \; \frac{2 \; M_c + 0.5 \; \alpha}{\sqrt{3} \; (M_c + \alpha)} \; \left(\frac{\tau_f}{\sigma_{vo}} \right)_{TC} \tag{26b}$$

$$\left(\frac{\tau_f}{\sigma_{vo}} \right)_{PSC} = \frac{\frac{2\sqrt{3}}{3} \; M_c + 1.04 \; \alpha}{M_c + \alpha} \; \left(\frac{\tau_f}{\sigma_{vo}} \right)_{TC} \tag{27}$$

$$\left(\frac{\tau_f}{\sigma_{vo}} \right)_{PSE} = \frac{\frac{2\sqrt{3}}{3} \; M_c - 0.46 \; \alpha}{M_c + \alpha} \; \left(\frac{\tau_f}{\sigma_{vo}} \right)_{TC} \tag{28}$$

$$\text{with } \alpha = \gamma \; \alpha_o$$

The factor 0.9 in the above (Eq. 26b) was introduced to take into account the non-uniformity in stress distribution in simple shear (SS) tests conducted in the laboratory, which was found to reduce the strength of the clay by about 10% (Prevost and Hoeg 1976).

Additional information on stresses, friction angles, and shear induced pore pressure parameters at failure are given in Table 2 for various stress paths. Eqs. 21-23 can be used to generate the same information for any other mode of failure that is of interest. Invoking Jaky's relationship (1948) for K_o ($K_o = 1 - \sin\phi_c$), the relationships for friction angle and undrained shear strength in various modes of failure can be further simplified. Figs. 7 and 8 show these simplified relationships.

From simple shear test data on natural clays, Ladd et al. (1977) showed that the strength ratio of overconsolidated clays can be related to that in NC clays and OCR by:

$$(\frac{\tau_f}{\sigma_{vo}})_{oc} = (\frac{\tau_f}{\sigma_{vo}})_{nc} \cdot OCR^m \tag{29}$$

where m is a constant, approximately equal to 0.80. For isotropic clays, Wroth (1984) showed a similar theoretical expression for strength ratio in TC. Using the theoretical development reported herein, it is possible to show a general theoretical relationship for many modes of failure for 1-D consolidated clays. Recalling Eqs.16, 20, 26-28, the following holds true for any particular type of undrained shear in TC/TE, PSC/PSE, PM and SS:
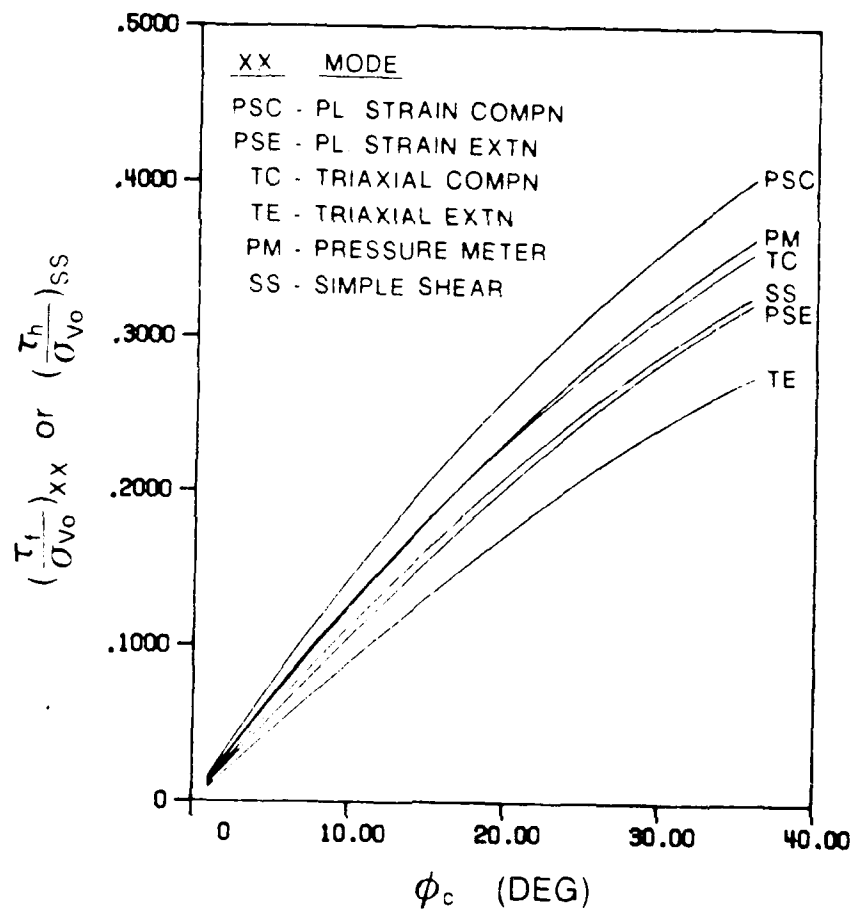
Fig. 7   Simplified Relationship for Undrained
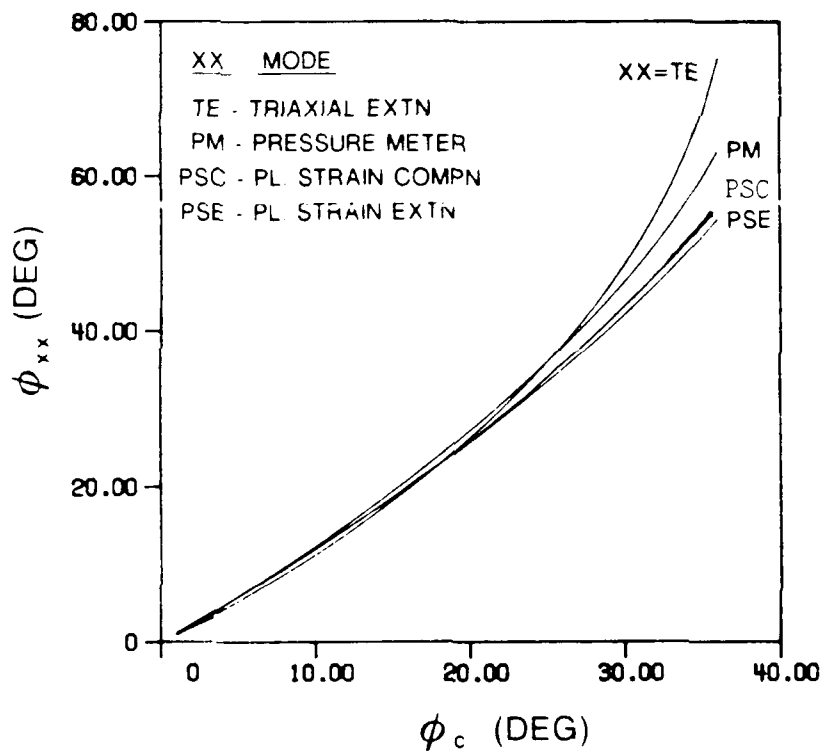Strength Ratio $(\frac{\tau_f}{\sigma_{vo}})$ for NC Clays

Fig. 8 Simplified Relationships Between Friction Angles
in Many Modes of Failure

$$\left(\frac{\tau_f}{\sigma_{vo}}\right)_{oc} = \left(\frac{\tau_f}{\sigma_{vo}}\right)_{nc} \left|OCR\right|^{\Lambda_v} \tag{30}$$

Figs. 4, 9a-b and 10 show the measured and predicted strength of several natural clays, for many different stress paths, geologic origins and OCR. The close agreement observed in these figures as well as in Fig. 6 substantiates the proposed theory and the choice of the failure criteria. The general concept of the approach and its advantages are summarized as follows:

i. The notion that mean stress at failure is dependent on the mode of undrained failure is included;

ii. One axisymmetric yield surface and a general form for the failure surface f^f are introduced, which allow the complete determination of failure parameters for any mode of failure.

iii. The initial anisotropy is properly taken into account in the yield surface and failure criteria.

iv. The effect of induced anisotropy is captured and incorporated by a calibration procedure. Given the initial conditions of the soil, the complete failure behavior at critical state (strength, pore pressures, friction angles, etc.) along any mode of failure is given by the relationships in Table 2 or Eqs. 21-23.

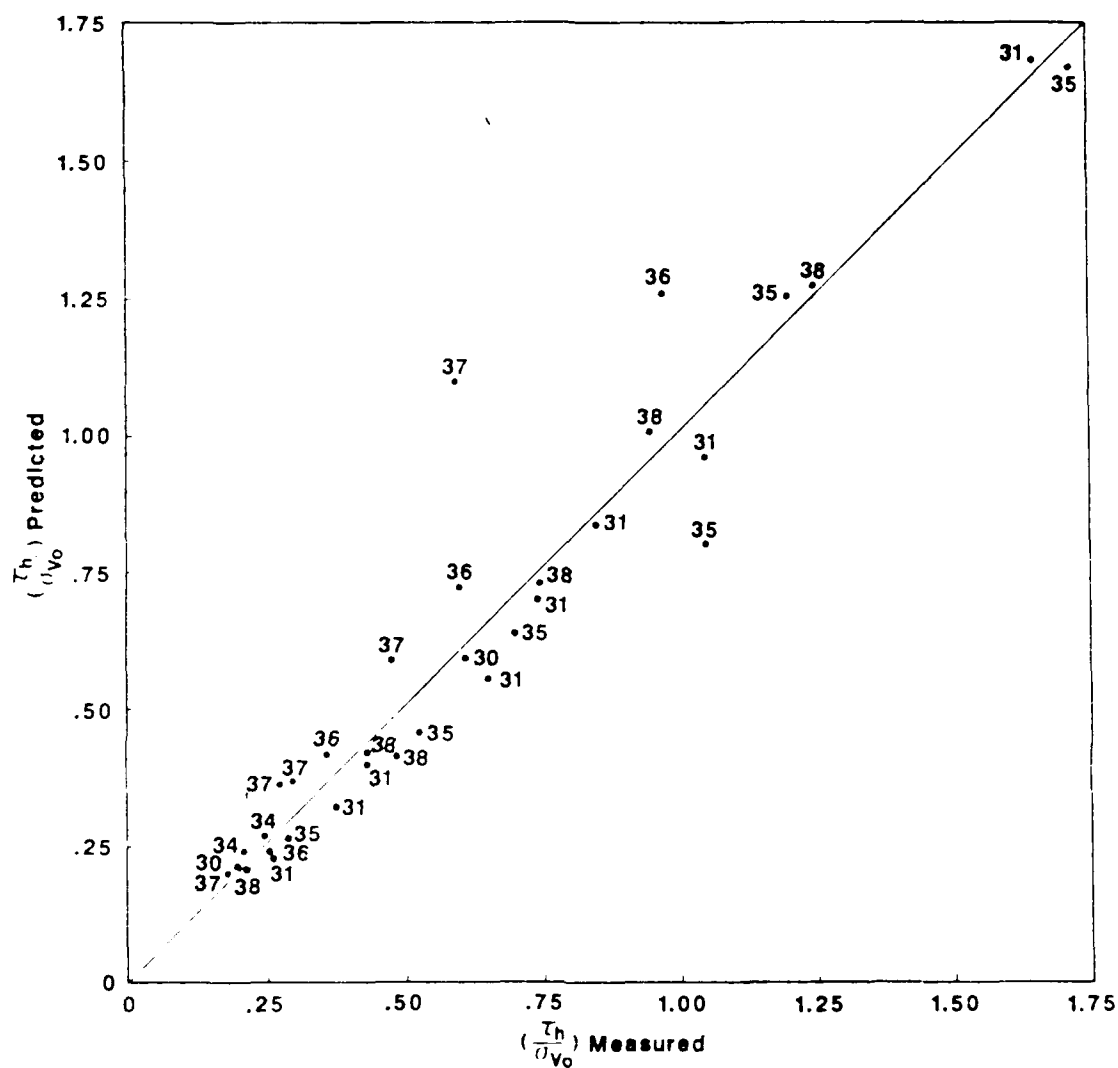v. Limited laboratory testing of soil is required to calibrate the model.

Fig. 9a Predicted Versus Measured Undrained Strength Ratio
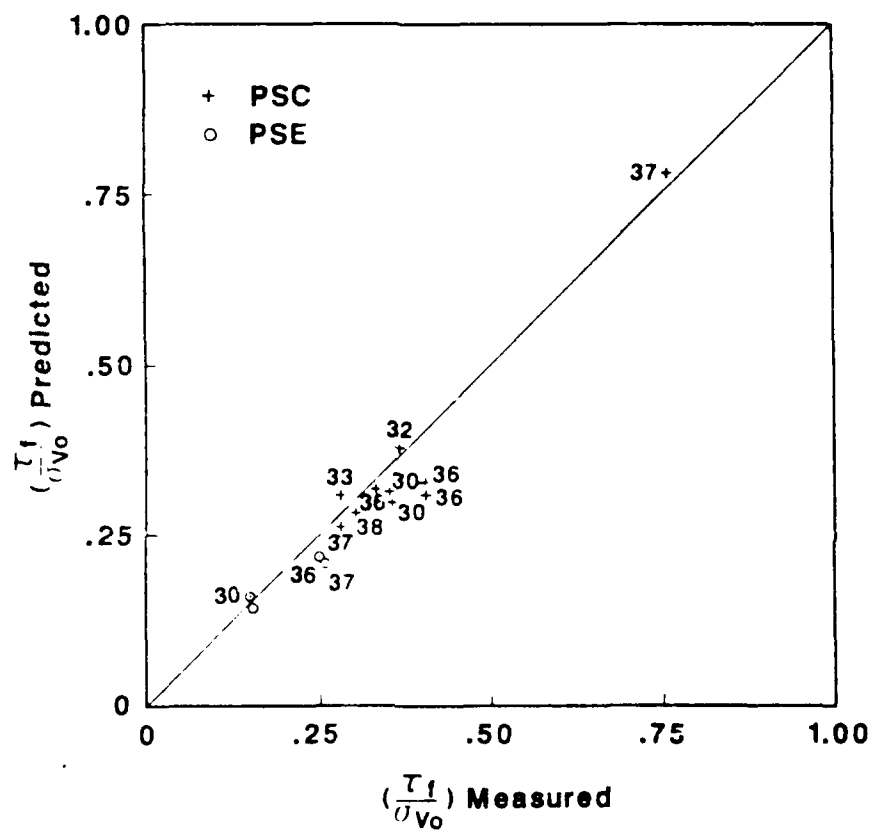in Simple Shear (Numbers Refer to Cases in Table 4)

Fig. 9. Predicted Versus Measured Undrained Strength
Ratio in Pl. Strain Compression and Extension
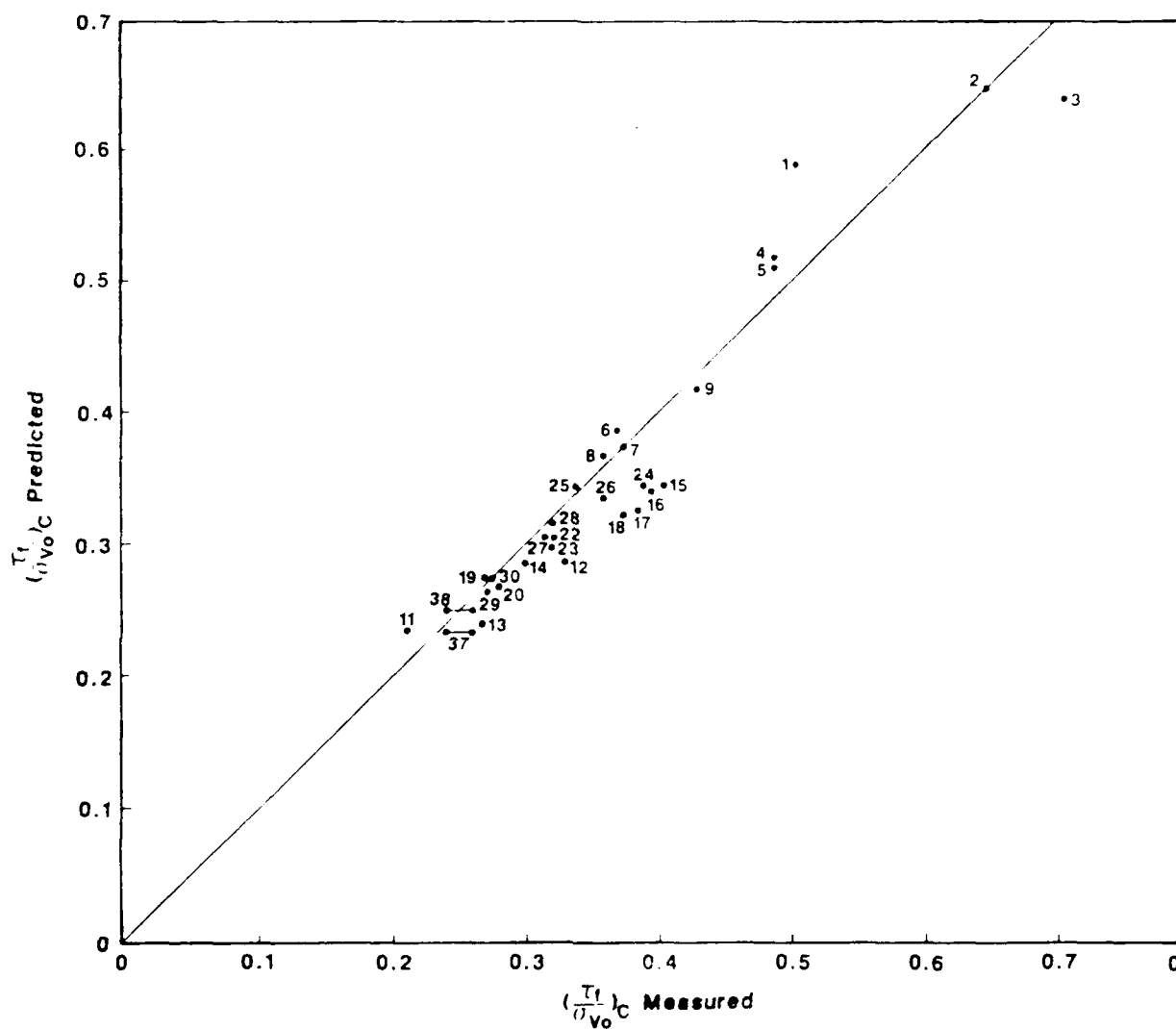(Numbers Refer to Cases in Table 8)

Fig. 10 Predicted Versus Measured Undrained Strength Ratio
in Triaxial Compression. (Numbers Refer to Cases in
Table 8)

vi.   Any relationship derived in this work can be related using
        the two most commonly used soil parameters, ϕ_c and OCR (with
        a reasonable value of κ_v / λ such as 0.2).

vii.   The model implementation is simple and could be used during
        field tests as experiments are being performed.

To the authors' knowledge, it is the first time that a model
which captures the essential features of initial and induced aniso-
tropy, yet yielding closed form solutions for all the failure
parameters of clays, is presented. Each of the steps involved in
the development is physically explained and complemented using
experimental data. The model strictly adheres to all the facets of
anisotropy known to date. Sophistication of the model thereof is
possible and is being developed.

The proposed theory can certainly be applied to a number of
geotechnical engineering problems (Thevanayagam, 1988a and 1988b),
such as:

   i.   stability analysis of embankments, retaining walls, vertical
        cuts, etc.

  ii.   interpretation of vane shear test

 iii.   study of SBPM, etc.

The potential that the theory has for SBPM interpretation is intro-
duced in the next section.

Table 3:   Some Selected Forms of Failure Criteria

	Case I	Case II	Case III
f^f	$f_p^f + f_d^f = 0$	$f_p^f + f_d^f = 0$	$f_p^f + f_d^f = 0$
f_p^f	$1/2\,[(\sigma_1 - \sigma_2)_f^2 + (\sigma_2 - \sigma_3)_f^2 + (\sigma_1 - \sigma_3)_f^2] = M^2 p^2$	Max of $(\sigma_i - \sigma_j)$ $= Mp$	Max of S_{ij} $= 2/3\ Mp,\ i=j$
f_d^f	$3/2(s_{ij} - \alpha_{ij})$ $(s_{ij} - \alpha_{ij}) - k^2 = 0$	$3/2(s_{ij} - \alpha_{ij})$ $(s_{ij} - \alpha_{ij}) - k^2 = 0$	$3/2(s_{ij} - \alpha_{ij})$ $(s_{ij} - \alpha_{ij}) - k^2 = 0$

Note: Case I corresponds to Eqs. 23a-b in Sec. 3.3.5.

Since the induced anisotropy factor γ was calibrated using data on peak strength in TC and TE, the model is not applicable to obtain the residual strength of clays. Also, calibrated values of γ = 1.0 for TC and γ = 0.6 for TE were deduced from experimental data for many clays. For individual clays these values may be slightly different. If data is available for a clay of interest, then using the theoretical development of this report the value of γ may be calibrated and used in Eqs. 21-24 to obtain failure parameters in any mode of failure that is of interest to the analyst for that particular clay.

In this development two other forms were also considered for f_p^f. They are shown in Table 3. These forms also give the relationship between φ_c and ϕ_e given by Eq.23c. Without further data on the failure stresses of clays, the relative merits of these different criteria could not be studied. Eq.23b was selected because of its interpretability in terms of shear strain energy and mathematical simplicity. Based on existing data, it is shown (e.g. see predictions in Table 5a-b) that f_p^f in Eq.23b predicts failure stresses reasonably well, and appears to perform better than the other two possibilities shown in Table 3. An experimental program to study the relative merits of these criteria will certainly be highly revealing.

3.5 Some Novel Applications to Pressuremeter Problem

Applications of this theory are focusing on a study of the

following aspects of self boring pressuremeter measurements.

1. State of stresses at failure and mode of failure;

2. Possibility of radial cracking;

3. Methods to determine ϕ_c and OCR using SBPM data;

4. Development of a solution technique to interpret disturbed
    SBPM data;

5. Possible effects of rate of testing, creep and relaxation
    time on SBPM data, and

6. Possible effects of partial drainage.

Promising results were obtained to date with regard to aspects
1,2,3 and 4. They are summarized in the following; Details can be
found in Thevanayagam (1988b).

3.5.1 State of Stress

The stress path during the pressuremeter test is not fully
agreed upon and much speculation has been offered (e.g. Prevost,
1979, Ladd et al., 1980, Wroth, 1984, Ladanyi, 1977, Wood and
Wroth, 1977). A clear understanding of the mode of deformation
during testing is instrumental to the development of a superior
interpretation method. Using the theory reported herein and a
"bending mechanism", the mode of failure in pressuremeter testing
of clays was identified. The axisymmetric nature of loading in

pressuremeter tests requires that the soil elements around the probe be within two extreme modes of deformation, plane strain and plane stress. The state of stress and behavior of clays at failure for these two extreme cases i) plane strain, $\dot{\epsilon}_1 = 0$, and (ii) plane stress, σ_v = constant, will be analyzed first. This information and available experimental data (Wood and Wroth 1977, Huang 1986) will then be used to develop plausible arguments to show that the assumption of plane strain $\dot{\epsilon}_1 = 0$ is usually satisfactory in the interpretation of pressuremeter data. Conditions for which the plane strain state may not prevail are identified.

For undrained plane strain shearing with $\dot{\epsilon}_z = 0$ and $\dot{\epsilon}_2 = -\dot{\epsilon}_3$ (subsequently denoted by the subscript pm), the methodology of this work, Eqs.21-23, yields the following relationships for stresses at failure (also see Table 2):

$$\left(\frac{\sigma_r - \sigma_\theta}{2\sigma_{vo}}\right)_{pm} = \left(\frac{\tau_f}{\sigma_{vo}}\right)_{pm} = \frac{2 M_c + 0.5 \alpha}{\sqrt{3} (M_c + \alpha)} \left(\frac{\tau_f}{\sigma_{vo}}\right)_{TC} \tag{31a}$$

$$\left(\frac{\sigma_r - \sigma_v}{2\sigma_{vo}}\right)_{pm} = \frac{M_c - 1.05 \alpha}{\sqrt{3} (M_c + \alpha)} \left(\frac{\tau_f}{\sigma_{vo}}\right)_{TC} \tag{31b}$$

$$\left(\frac{\sigma_v - \sigma_\theta}{2\sigma_{vo}}\right)_{pm} = \frac{M_c + 1.55 \alpha}{\sqrt{3} (M_c + \alpha)} \left(\frac{\tau_f}{\sigma_{vo}}\right)_{TC} \tag{31c}$$

$$\text{where} \quad \sigma_v = \sigma_{11}, \quad \sigma_r = \sigma_{22}, \quad \sigma_\theta = \sigma_{33} \tag{31d}$$

The expression for $(\sigma_r/\tau_f)_{pm}$ is given by:

$$\left(\frac{\sigma_r}{\tau_f}\right)_{pm} = \frac{\left|\dfrac{(3X^2+2.25)^{1/2}}{M_c} + X - 0.5\right|}{X};$$ (31e)

$$\text{with } X = \frac{2M_c + 0.5\,\alpha}{\sqrt{3}\,\alpha}$$

and the relationships for σ_r, σ_θ and σ_v are:

$$\left|\frac{\sigma_r}{\sigma_{vo}}\right|_{pm} = \left|\frac{\sqrt{3X^2 + 2.25}}{M_c} + X - 0.5\right| \cdot \left|\frac{\alpha}{M_c + \alpha}\right| \left|\frac{\tau_f}{\sigma_{vo}}\right|_{TC}$$ (31f)

$$\left|\frac{\sigma_v}{\sigma_{vo}}\right|_{pm} = \left|\frac{\sqrt{3X^3 + 2.25}}{M_c} + 1\right| \left|\frac{\alpha}{M_c + \alpha}\right| \left|\frac{\tau_f}{\sigma_{vo}}\right|_{TC}$$ (31g)

$$\left|\frac{\sigma_\theta}{\sigma_{vo}}\right|_{pm} = \left|\frac{\sqrt{3X^2 + 2.25}}{M_c} - X - 0.5\right| \left|\frac{\alpha}{M_c + \alpha}\right| \left|\frac{\tau_f}{\sigma_{vo}}\right|_{TC}$$ (31h)

The stresses at failure can also be obtained using the other choices for f_p^f given earlier in Table 3; they are shown in Table 4. Only results obtained with the failure criterion in Eqs. 23a-b are reported in the following discussion.

Eqs. 31a-c imply that, independent of OCR and initial magnitudes of principal stresses in horizontal and vertical directions, the following inequalities hold true:

$$\sigma_r > \sigma_v > \sigma_\theta \quad \text{at failure.}$$ (32)

and that the r-θ plane is always the failure plane. Figs. 11a and

Table 4: Stress Parameters at Failure in Plane Strain $\varepsilon_z=0$ Test in Clays

Eqn	Case I	Case II	Case III
B1 f^f	$f_p^f + f_d^f = 0$	$f_p^f + f_d^f = 0$	$f_p^f + f_d^f = 0$
B2 f_p^f	$1/2[(\sigma_1-\sigma_2)_f^2+(\sigma_2-\sigma_3)_f^2+(\sigma_1-\sigma_3)_f^2] = M^2 p^2$	Max of $(\sigma_1 - \sigma_j)$ $= Mp$	Max of S_{ij} $= 2/3\ Mp,\ i=j$
B3 f_d^f	$3/2(s_{ij}-\alpha_{ij})\cdot(s_{ij}-\alpha_{ij})-k^2=0$	$3/2(s_{ij}-\alpha_{ij})\cdot(s_{ij}-\alpha_{ij})-k^2=0$	$3/2(s_{ij}-\alpha_{ij})\cdot(s_{ij}-\alpha_{ij})-k^2=0$
B4 $\left(\dfrac{\tau_f}{\sigma_{vo}}\right)_{PM} = \left(\dfrac{\sigma_r-\sigma_\theta}{2\sigma_{vo}}\right)_{PM}$	$\dfrac{M_c+0.5\alpha}{\sqrt{3(M_c+\alpha)}}\cdot\left(\dfrac{\tau_f}{\sigma_{vo}}\right)_{TC}$	$\dfrac{M_c+0.5\alpha}{\sqrt{3(M_c+\alpha)}}\cdot\left(\dfrac{\tau_f}{\sigma_{vo}}\right)_{TC}$	$\dfrac{M_c+0.5\alpha}{\sqrt{3(M_c+\alpha)}}\cdot\left(\dfrac{\tau_f}{\sigma_{vo}}\right)_{TC}$
B5 $\left(\dfrac{\sigma_z}{\sigma_{vo}}\right)_{PM}$	$\left[\dfrac{\sqrt{3x^2+2.25}}{M_c}+1\right]\cdot\dfrac{\alpha}{M_c+\alpha}\cdot\left(\dfrac{\tau_f}{\sigma_{vo}}\right)_{TC}$	$\left[\dfrac{3}{2M_c}(x+0.5\alpha)+1\right]\cdot\dfrac{\alpha}{M_c+\alpha}\cdot\left(\dfrac{\tau_f}{\sigma_{vo}}\right)_{TC}$	$\left[\dfrac{2x}{M_c}+1\right]\cdot\dfrac{\alpha}{M_c+\alpha}\cdot\left(\dfrac{\tau_f}{\sigma_{vo}}\right)_{TC}$
B6 $\left(\dfrac{\sigma_r}{\sigma_{vo}}\right)_{PM}$	$\left[\dfrac{\sqrt{3x^2+2.25}}{M_c}+x-0.5\right]\cdot\dfrac{\alpha}{\ \ }\cdot\left(\dfrac{\tau_f}{\ \ }\right)$	$\left[\dfrac{3}{2M_c}(x+0.5)+x-0.5\right]\cdot\dfrac{\alpha}{\ \ }\cdot\left(\dfrac{\tau_f}{\ \ }\right)$	$\left[\dfrac{2x}{M_c}+x-0.5\right]\cdot\dfrac{\alpha}{\ \ }\cdot\left(\dfrac{\tau_f}{\ \ }\right)$

Table 4: (cont'd)

B7 $(\frac{\sigma_g}{\sigma_{vo}})_{PM}$	$\dfrac{[\frac{\sqrt{3x^2+2.25}}{M_c} - x - 0.5]}{\frac{\alpha}{M_c} + \alpha \cdot (\frac{\tau_f}{\sigma_{vo}})_{TC}}$	$\dfrac{[\frac{3}{2M_c}(x+0.5) - x - 0.5]}{\frac{\alpha}{M_c} + \alpha \cdot (\frac{\tau_f}{\sigma_{vo}})_{TC}}$	$\dfrac{[\frac{2x}{M_c} - x - 0.5]}{\frac{\alpha}{M_c} + \alpha \cdot (\frac{\tau_f}{\sigma_{vo}})_{TC}}$
B8 $\sin(\phi_{pm})$	$\dfrac{2X}{[2\sqrt{\frac{3x^2+2.25}{M_c}} - 1]}$	$\dfrac{2X}{[\frac{3}{M_c}(x+0.5) - 1]}$	$\dfrac{2X}{[\frac{4x}{M_c} - 1]}$
B9 $\dfrac{\Delta U_{sh}}{\sigma_{vo}}$	$\dfrac{1+2K_{ocr}}{3} - \dfrac{[\frac{\sqrt{3x^2+2.25}}{M_c}]}{\frac{\alpha}{M_c} + \alpha \cdot (\frac{\tau_f}{\sigma_{vo}})_{TC}}$	$\dfrac{1+2K_{ocr}}{3} - \dfrac{[\frac{3}{2M_c}(x+0.5)] \cdot}{\frac{\alpha}{M_c} + \alpha \cdot (\frac{\tau_f}{\sigma_{vo}})_{TC}}$	$\dfrac{1+2K_{ocr}}{3} - \dfrac{[\frac{2x}{M_c}]}{\frac{\alpha}{M_c} + \alpha \cdot (\frac{\tau_f}{\sigma_{vo}})_{TC}}$
B10 $(\dfrac{\sigma_r}{\tau_{fpm}})$	$\dfrac{[\frac{\sqrt{3x^2+2.25}}{M_c} + x - 0.5]}{X}$	$\dfrac{[\frac{3}{2M_c}(x+0.5) + x - 0.5]}{X}$	$\dfrac{[\frac{2x}{M_c} + x - 0.5]}{X}$
B11 X	$\dfrac{2M_c + 0.5\alpha}{\sqrt{3}\alpha}$	$\dfrac{2M_c + 0.5\alpha}{\sqrt{3}\alpha}$	$\dfrac{2M_c + 0.5\alpha}{\sqrt{3}\alpha}$

Note: Case I corresponds to Eqs. 23a-b in Sec. 3.3.5.

87

11b show the variation of σ_r/σ_{vo}, σ_v/σ_{vo} and $\sigma_\theta/\sigma_{vo}$ for NC and OC clays (OCR = 10) as a function of ϕ_c. Fig. 11c gives the variation of $\sigma_\theta/\sigma_{vo}$ for various values of OCR and ϕ_c, and for γ values of 0.6 and 1.0. Table 5a-b, Figs. 12a and 12b compare measured values of failure stresses for Spestone kaolin (Wood and Wroth, 1977) to those predicted by Eqs. 31f-h. Evaluation of these results lead to the following implications:

1. As long as the plane strain condition, $\dot{\varepsilon}_z = 0$, is maintained, the stresses σ_r and σ_θ become the major and minor principal stresses respectively, irrespective of the initial state of stress;

2. There exists a critical OCR, called OCR_c, at which (σ_v/σ_{vo}) at failure remains equal to 1.0. For most of the clays, this OCR_c lies in a narrow range of 1.5-2.5 (Fig.13). For a clay with OCR < OCR_c, σ_v decreases sharply and becomes the intermediate principal stress at failure. The stress σ_r may increase or decrease depending on the characteristics of the clay (for very weak clays σ_r decreases), and σ_θ decreases becoming the minor principal stress at failure (Figs.11a-c). If OCR = OCR_c, then σ_r increases and σ_θ decreases, while σ_v remains constant and becomes the intermediate principal stress. If OCR > OCR_c, σ_v and σ_r increase while σ_θ decreases. The increase in σ_v depends on the value of OCR and the clay. However, the changes in σ_v and σ_r are such that σ_v always becomes the intermediate principal stress. For any
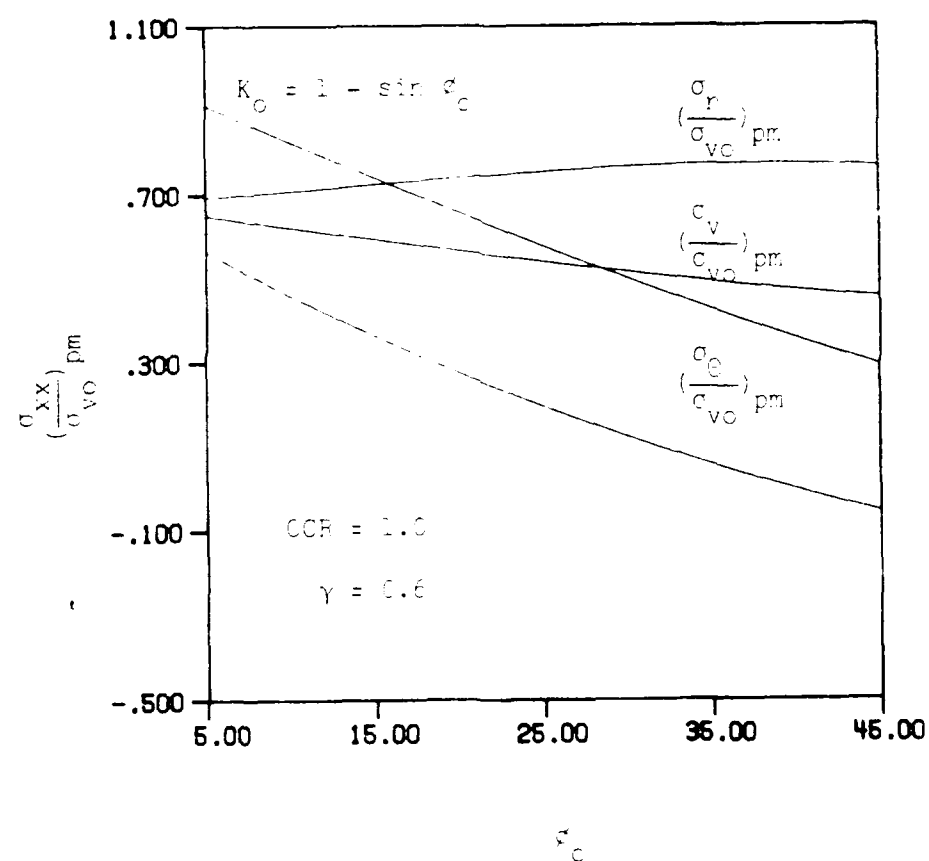
Fig. 11a $(\frac{\sigma_{xx}}{\sigma_{vo}})_{pm}$ vs. ϕ_c Relationship for NC Clays
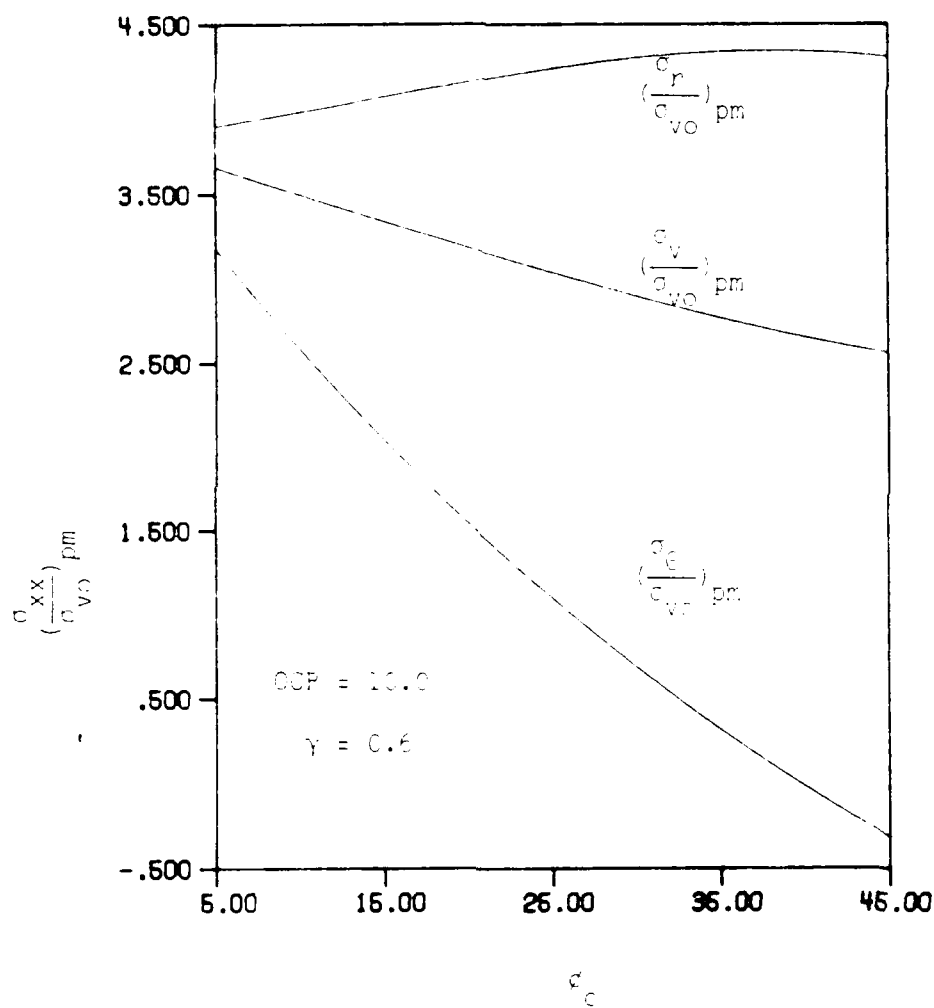
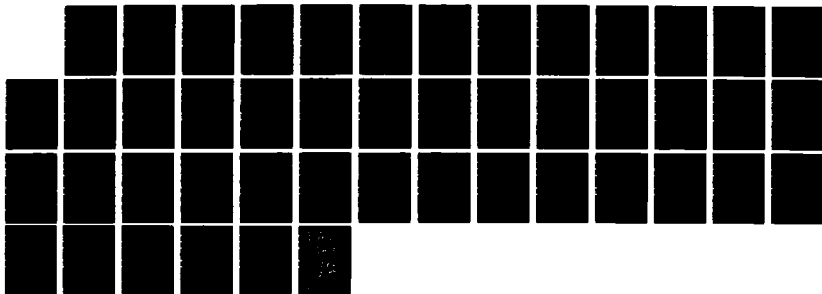Fig. 11b $(\frac{\sigma_{xx}}{\sigma_{vo}}$ vs. $\varnothing_c$ Relationship for OC Clays

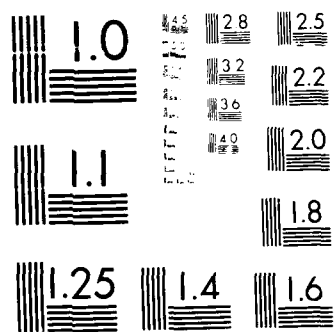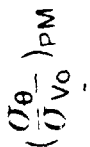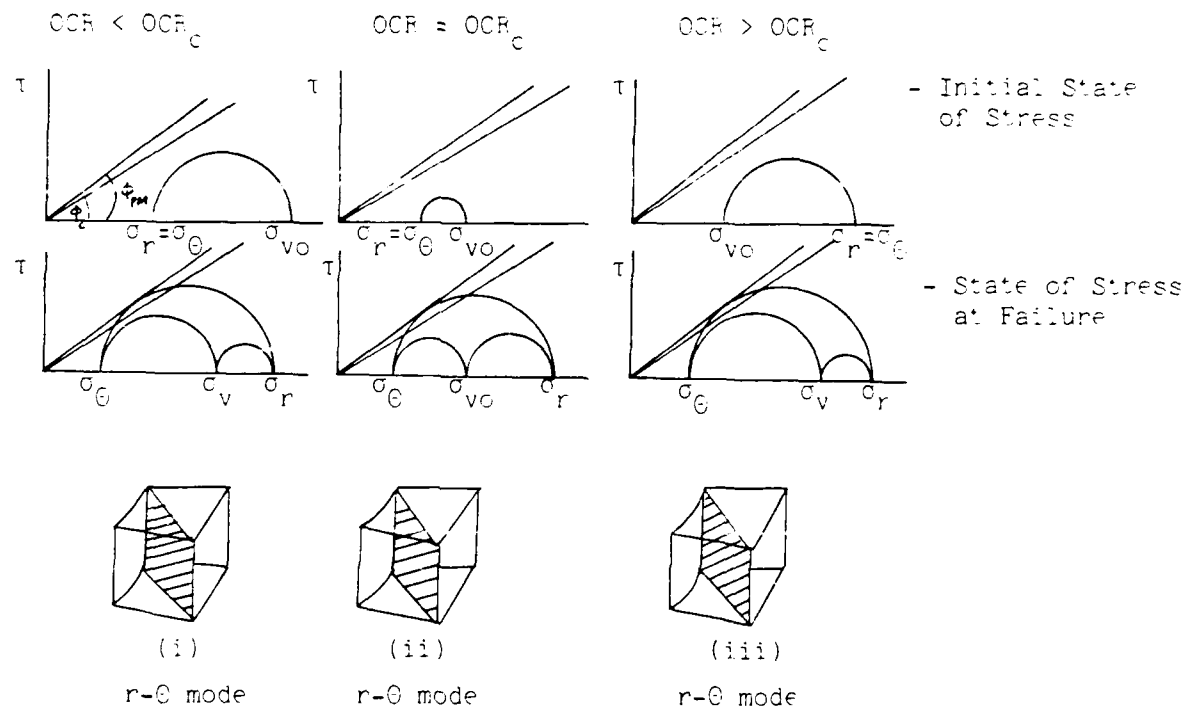Fig. 11c Simplified $(\frac{\sigma_\theta}{\sigma_{vo}})_{pm}$ vs ϕ_c Relationship

Fig. 11d   State of Stress and Orientation of Failure
Planes (Proposed Theory)

Table 5a: Numerical Prediction of Stress Parameters at Failure in Plane Strain ($\epsilon_v = 0$) Path (Test Data - Wood et al., 1977).

Case	Test No	OCR	Prd'td $\left(\dfrac{\sigma_v}{\sigma_{vo}}\right)$	Meas'd $\left(\dfrac{\sigma_v}{\sigma_{vo}}\right)$	Prd'td $\left(\dfrac{\sigma_r}{\sigma_{vo}}\right)$	Meas'd $\left(\dfrac{\sigma_r}{\sigma_{vo}}\right)$	Prd'td $\left(\dfrac{\sigma_\theta}{\sigma_{vo}}\right)$	Meas'd $\left(\dfrac{\sigma_\theta}{\sigma_{vo}}\right)$	Prd'td (ϕ_{pm})	Meas'd (ϕ_{pm})	Prd'td $\dfrac{2\sigma_v}{\sigma_r+\sigma_\theta}$	Meas'd $\dfrac{2\sigma_v}{\sigma_r+\sigma_\theta}$
I	K4	1.0	0.576	0.51	0.727	0.674	0.324	0.316	22.5	22.5-26.0	1.10	1.11
	K2	2.5	1.19	1.02	1.513	1.19	0.674	0.516	22.5	22.5-26.0	1.10	1.15
	K3	5.46	(2.14)	1.44	(2.4)	1.91	(1.07)	0.77	22.5	22.5-26.0	1.10	1.1
	K3	5.46	2.24	1.44	2.8	1.91	1.26	0.77	22.5	22.5-26.0	1.10	1.1
II	K4	1.0	0.617	0.51	0.767	0.674	0.364	0.316	20.8	22.5-26.0	1.09	1.11
	K2	2.5	1.28	1.02	1.59	1.19	0.757	0.516	20.8	22.5-26.0	1.09	1.15
	K3	5.46	2.4	1.44	2.98	1.91	1.415	0.77	20.8	22.5-26.0	1.09	1.1
III	K4	1.0	0.654	0.51	0.804	0.674	0.4	0.316	19.5	22.5-26.0	1.09	1.11
	K2	2.5	1.36	1.02	1.67	1.19	0.83	0.516	19.5	22.5-26.0	1.09	1.15
	K3	5.46	2.54	1.44	3.12	1.91	1.55	0.77	19.5	22.5-26.0	1.09	1.1

Note a: ( ) denotes that $\alpha = \alpha_o$ was assumed.

Note b: Case I corresponds to Eqs. 23a-b in Sec. 3.3.5.

Table 5b: Predicted and Measured Critical OCR.

	Predicted	Measured
OCR_c	2.0	<2.5

Note: Measured value was intepreted by the writers using the experimental data from Wood et al. (1977).

Figure 12a Theoretical Versus Measured Stress Ratio at
           Failure in Undrained Pl. Strain $\epsilon_z = 0$

           Shearing of Clays (Measured after Wood and
           Wroth 1977)
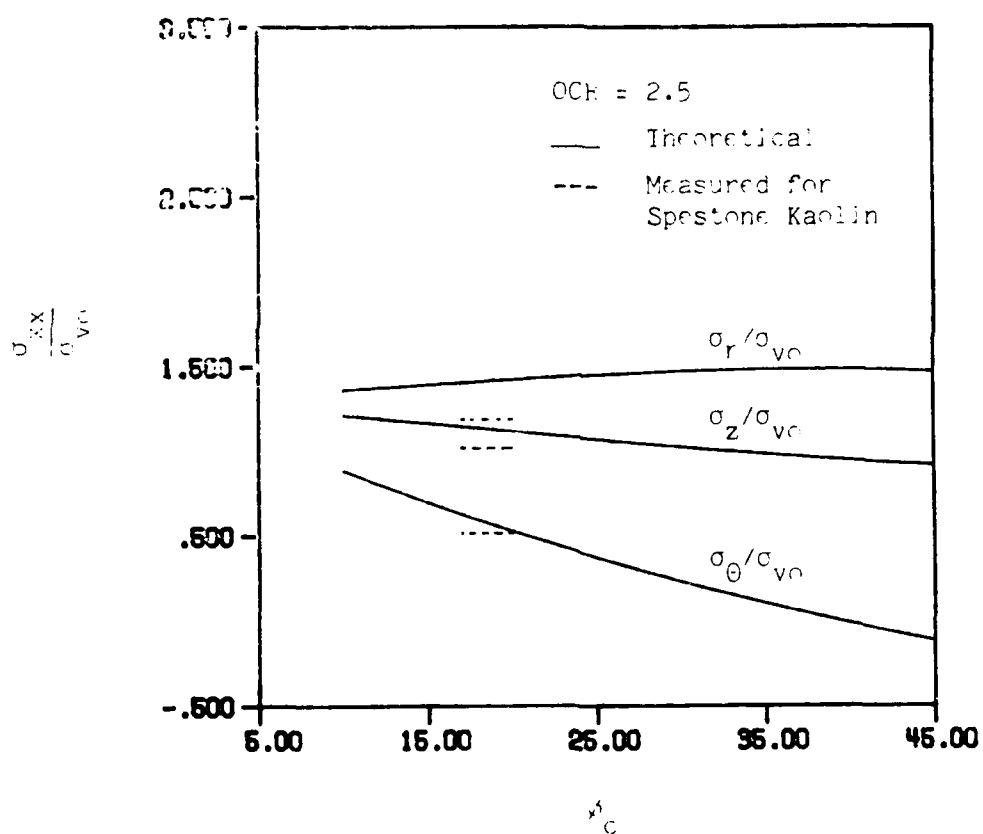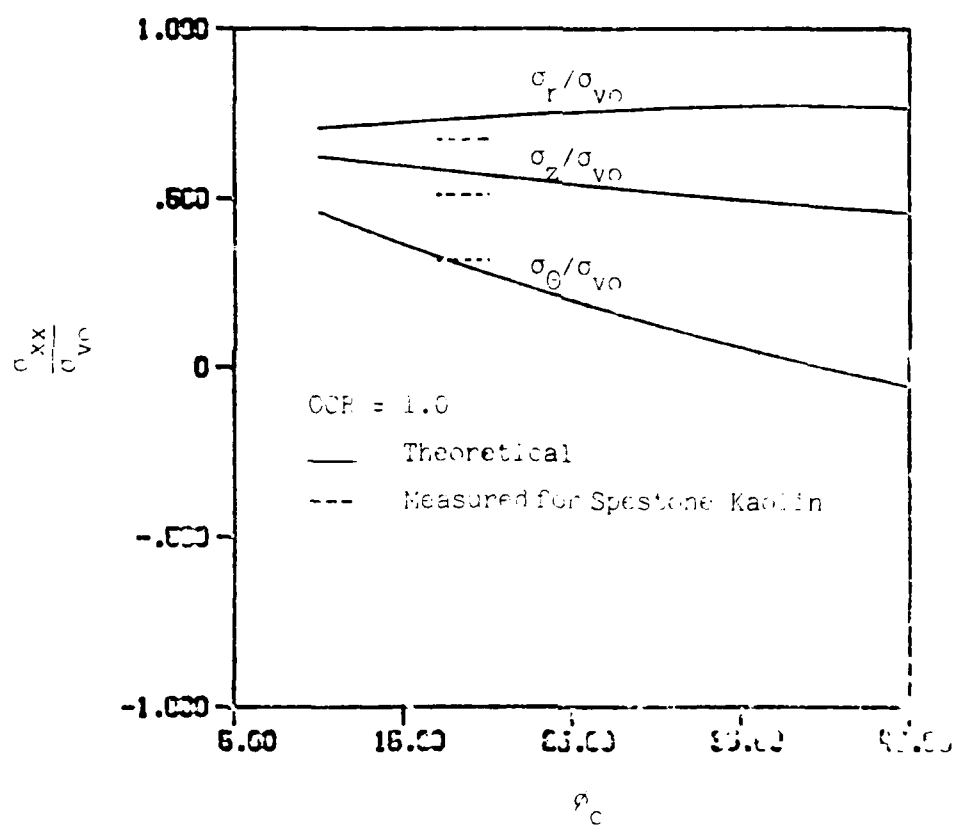
Figure 12b   Theoretical Versus Measured Stress Ratio at
              Failure in Undrained Pl. Strain $\varepsilon_z = 0$

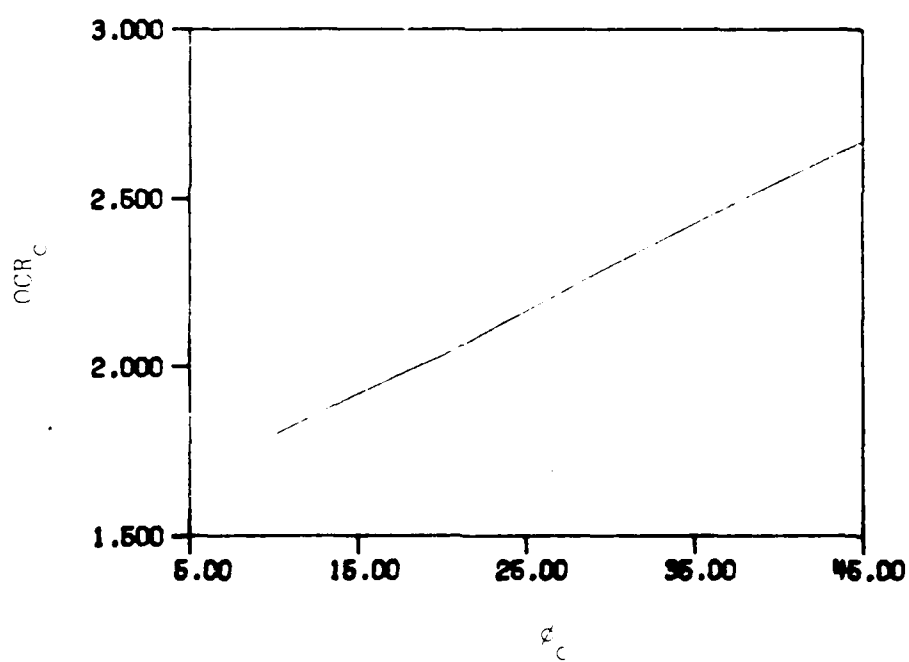   Shearing of Clays (Measured after Wood and Wroth,
              1977)

Fig. 13 OCR_c vs ϕ_c Relationship

value of OCR, the failure takes place in the r-θ plane. This is summarized in Fig. 11d. Experimental data obtained by Wood and Wroth (1977) (Figs. 12a-b) support these trends.

3. The mean principal stress, in general, does not remain constant. For lightly OC clays the mean principal stress decreases whereas it increases for highly OC clays;

4. The angle ϕ_{pm} is always greater than the corresponding angle ϕ_c obtained in TC (Fig.8).

5. Fig. 11c indicates that, for $\phi_c > 37°$, σ_θ becomes negative. Also, the chances for negative value of σ_θ increases with γ approaching 1.0. Since γ is expected to be close to 1.0 for highly OC clays, the likelihood for negative σ_θ is slightly higher for OC clays than for NC clays.

The solution for failure stresses σ_r/σ_{vo}, $\sigma_\theta/\sigma_{vo}$ and $\dot{\varepsilon}_z/\dot{\varepsilon}_r$ in undrained plane stress shear of clays (σ_v = constant, $\dot{\varepsilon}_r > 0$) can be obtained by solving the following set of equations:

$$(2\sigma_v - \sigma_r - \sigma_\theta - 3\alpha_{11})^2 + (2\sigma_r - \sigma_v - \sigma_\theta + 1.5\,\alpha_{11})^2$$

$$+ (2\sigma_\theta - \sigma_r - \sigma_v + 1.5\,\alpha_{11})^2 - 6\,k^2 = 0 \qquad (33a)$$

$$(\sigma_v - \sigma_\theta)^2 + (\sigma_v - \sigma_r)^2 + (\sigma_r - \sigma_\theta)^2 -$$

$$\frac{2M_c^2}{9}(\sigma_r + \sigma_\theta + \sigma_v)^2 = 0 \tag{33b}$$

$$\frac{\dot{\varepsilon}_z}{\dot{\varepsilon}_r} = \frac{2\sigma_v - \sigma_r - \sigma_\theta - 3\alpha_{11}}{2\sigma_r - \sigma_v - \sigma_\theta + 1.5\,\alpha_{11}} \tag{33c}$$

where $\sigma_{11} = \sigma_v$, $\sigma_{22} = \sigma_r$, $\sigma_{33} = \sigma_\theta$, $\dot{\varepsilon}_{11} = \dot{\varepsilon}_z$ (vertical strain increment), and $\dot{\varepsilon}_{22} = \dot{\varepsilon}_r > 0$. These equations can be solved numerically. Fig. 14 shows the variation of $\dot{\varepsilon}_z/\dot{\varepsilon}_r$ as a function of ϕ_c for various values of OCR. This figure shows that, in general, the vertical strain increment is compressive for lightly OC clays, whereas it is tensile for highly OC clays. For each value of ϕ_c, there exists an OCR at which the incremental vertical strain is zero (i.e. plane strain). This value of OCR is the value of OCR_c deduced earlier using the results for plane strain shearing of clays.

Let us consider the application of radial stresses in a cylindrical cavity wall as shown in Fig. 15. For the purpose of discussion, the element A_1 is chosen as a reference point if end effects are neglected, or any other element A_i below A_1 can be selected if end effects are assumed to exist. In deep tests, the soil above the level A_1 can be considered as a thick plate clamped at some distance away from the probe. Using the above descriptions of clay behavior in plane stress and plane strain shearing, the mode of failure and the mechanism causing it in pressuremeter tests can be deduced from the following reasoning.
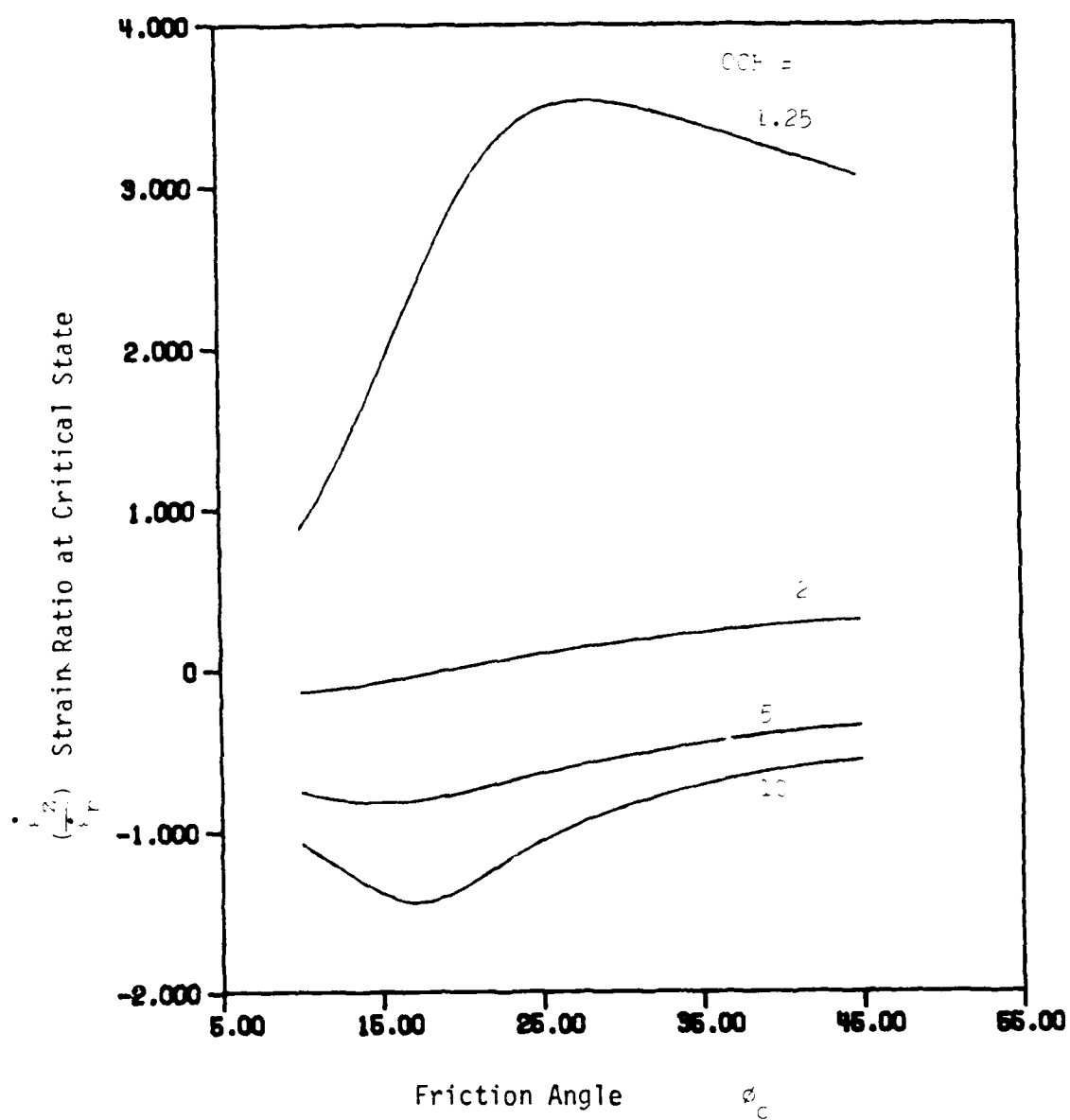
Fig. 14: Strain Ratio Vs. Friction Angle at Critical State

in Plane Stress $\sigma_v = \sigma_{vo}$ Shearing (PSS)

TANK SEALING CAP

EXHAUST COCK

GAS
CYLINDER

WATER TANK

DRAIN
COCK

PRESSURE COCK

A_1

A_2

A_3

MONO CELL PROBE

$2r_o$

$\sigma_z > \sigma_{vo}$ for $OCR > OCR_c$

$\sigma_z < \sigma_{vo}$ for $OCR < OCR_c$

σ_z

σ_{vo}

0

1

r/r_o
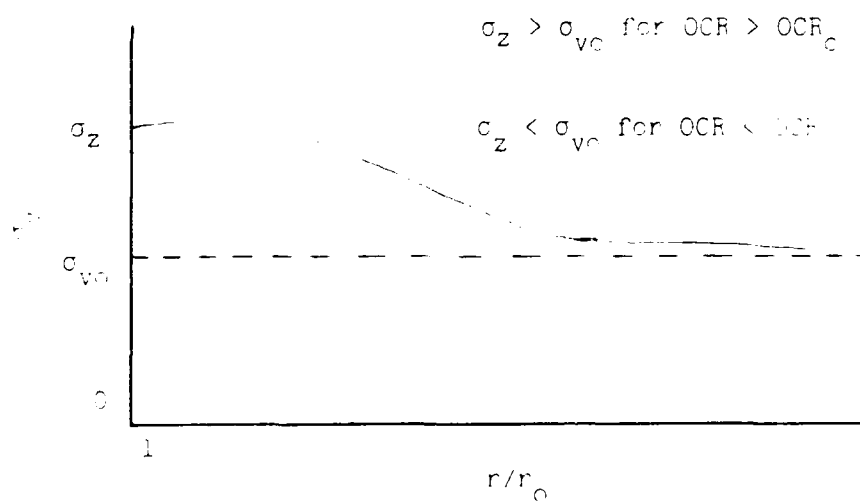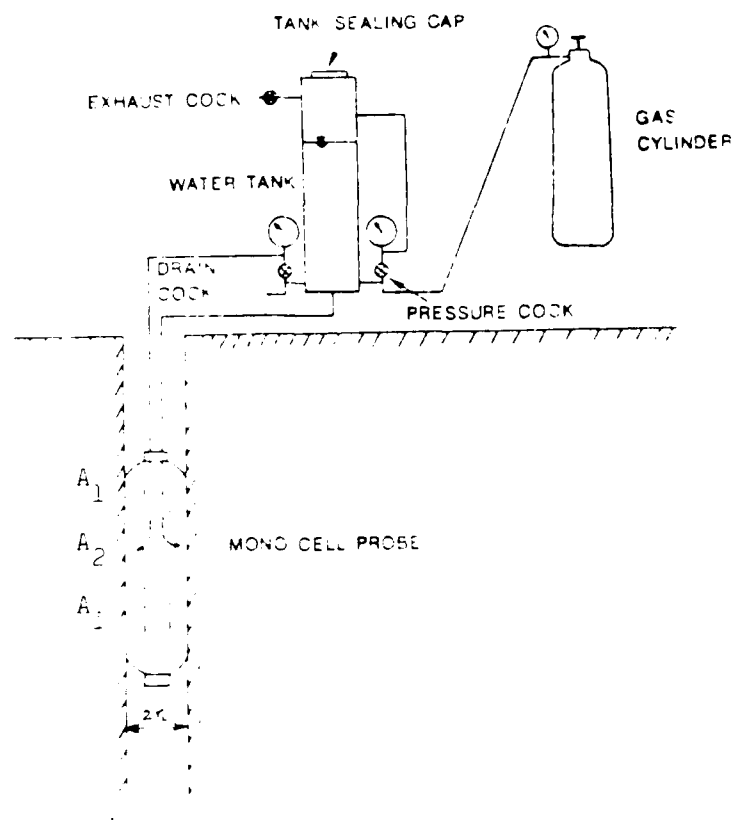
Vertical Stress Distribution Along the
Horizontal Plane Through A.

Figure 15   A Schematic Diagram of Pressuremeter Testing and
Vertical Stress Distribution Around the Cavity

Assuming that plane stress conditions prevail, the results in Fig. 14 indicates that depending on the value of OCR, $\dot{\epsilon}_z$ can be tensile (highly OC), zero (at OCR_c), or compressive (lightly OC). Considering the soil layer above the level A_1 as a thick plate, a compressive strain increment, $\dot{\epsilon}_z$, requires that the plate with a central hole deflect downwards. Since the flexural rigidity of the plate is large, a small amount of deflection requires a substantial reduction in the stress distribution σ_v under the plate, i.e. in the horizontal plane at the level of A_1. This contradicts the original assumption that plane stress in vertical direction prevails. The same argument but using a hogging type of movement can be used for the case of highly OC clays. It should be remembered that this argument is valid only if the plate is very thick. However, in the case of OCR = OCR_c, this bending mechanism is absent ($\dot{\epsilon}_z = 0$), and the soil elements satisfy both plane stress and plane strain conditions, independently of the depth at which the test is performed. Therefore, the soil elements around the probe in pressuremeter testing at large depths cannot be expected to experience the plane stress mode of failure except when OCR = OCR_c.

Assuming that plane strain conditions prevail, for OCR = OCR_c σ_v remains equal to σ_{vo}, and the mode of failure is both plane strain and plane stress shearing, as already discussed above. If OCR > OCR_c, the theory reported herein (see Figs. 11a-c) and limited experimental data (Wood and Wroth, 1977) imply that σ_v increases. To achieve this, an upward movement of the thick plate

of soil is necessary. Therefore, the soil elements around the probe would apparently deviate from the plane strain condition. However, considering the high flexural rigidity of the plate, this increase in σ_v is possible with a very small upward deflection of the thick plate at level A_1; thus, this upward deflection is in fact negligible and the element at level A_1 can be considered to be in plane strain. Similar argument (with downward deflection, and decrease in σ_v) is plausible for a case of OCR < OCR_c. Therefore, it can be concluded that for pressuremeter testing of clays at relatively large depths, the soil elements closely experience a state of plane strain shearing. The "bending mechanism" of the thick plate of soil above the pressuremeter probe is responsible for this. However, the argument will not hold true for testing at shallow depths except when OCR = OCR_c. With further development of the model reported herein, a complete numerical analysis of this problem is possible and is proposed for further study. Nevertheless, based on the plausible arguments stated herein the following conclusions can be drawn without loss of generality. For a clay with OCR = OCR_c, the pressuremeter data can be interpreted at any depth using the assumption of plane strain shearing. For deep tests the mode of failure is very close to that in plane strain and the theoretical results reported earlier are applicable. For shallow depths, the mode of failure is far from that in plane strain.

3.5.2   Interpretation of ϕ_c and OCR from SBPM Data

It is noted that Eq.31e depends only on the value of ϕ_c, while Eq.31a depends on both ϕ_c and OCR of the clay. Hence, using these relationships, a method to obtain ϕ_c and OCR of the insitu clay using SBPM data can be developed. A step by step example of this method is given in the following:

1. Using pressuremeter expansion and pore pressure measurements, obtain $(\tau_f)_{pm}$ and corresponding $(\sigma_r)_{pm}$ at failure.

2. Assume a value for ϕ_c; Estimate $M_c = 6\sin\phi_c/(3-\sin\phi_c)$ and α_o (from Eq.9b).

3. Use steps 1 and 2 to check that Eq. 31e is satisfied. Repeat steps 2 and 3 with a different estimate of ϕ_c until convergence is reached.

The value of OCR may be deduced from the value of ϕ_c at convergence and Eq. 31a. Using data from model pressuremeter tests simulated in a calibration chamber (Chameau et al., 1987), the parameters ϕ_c and OCR were obtained with this procedure for two clays. The predicted values are compared to those measured from TC tests in Table 6. While the predictions for normally consolidated clays is excellent, the OCR is slightly under predicted for highly OC clays (tests CP23 and CP16). This deviation is attributed to the presence of shear stresses on the pressuremeter membrane due to the consolidation around it and subsequent swelling to prepare

Table 6   Prediction of Soil Parameters Using Anisotropic Theory

TEST # SOIL	Predicted		Measured	
	ϕ_{tc}	OCR	ϕ_{tc}	OCR
CP 6 [K100]	19.5	1.02	20.7	1.0
CP 8 [K50]	20.2	0.99	23.5	1.0
CP 23 [K50]	20.8	7.5	23.5	10.0
CP 16 [K100]	23.5	7.3	20.7	10.0

ϕ_{tc} = Friction Angle in Triaxial Compression Test

Measured: Based on data from Huang, 1986.

highly OC clays in the calibration chamber tests.

3.5.3 Interpretation of Disturbed SBPM Data

The self boring technique does produce changes in the initial loading condition and the initial position of the cavity wall. Wroth and Hughes (1973) reported an outward radial movement of the cavity wall corresponding to about 0.5% of radial strain. Denby (1978) also reported similar movements of the cavity wall well before the beginning of the expansion test. Later studies using a larger size cutting shoe (Benoit and Clough, 1986) also pointed out this possibility. A recent integrated study of the problems involved in the pressuremeter tests (Prapaharan, 1987 and Prapaharan et al., 1988), showed that this initial movement is the most influential when compared to any other problems identified with the test.

This section deals with developing an interpretation technique that may be used to improve the current difficulties in interpreting pressuremeter data with initial movement (i.e. initial disturbance). An outline of this new interpretation method is given and illustrated using model pressuremeter test data. The solution procedure requires the expansion curve and pore pressure measurements at the cavity wall (for overconsolidated clays OCR is also required).

Let $\hat{\epsilon}_r$ refer to the strain obtained from measurements in the disturbed test (i.e. $\hat{\epsilon}_r$ = measured strain), and $\Delta\epsilon_o$ be the error.

The error $\Delta\varepsilon_o$ in the measured strain may be estimated in the following manner [For illustration purposes, the figures used herein were obtained by applying this technique to model pressuremeter test data (Test No. CP6) of Huang, 1986]:

1. Assume that the measured strain $\hat{\varepsilon}_r$ includes some unknown error $\Delta\varepsilon_o$:

$$\varepsilon_r = \hat{\varepsilon}_r + \Delta\varepsilon_o \qquad (34)$$

2. For several values of $\Delta\varepsilon_o$, using Eq. 34 and $\hat{\varepsilon}_r$ vs. probe pressure measurements, obtain ε_r vs probe pressure data. This data can be fitted using a spline function (i.e. one spline function for each $\Delta\varepsilon_o$).

3. For each spline fit in step 2, using the method of derivatives (e.g. Palmer, 1972, Ladanyi, 1972, Baugelin, et al., 1972) obtain the peak strength τ_{fpm}, the corresponding σ_r and strain ε_r at the cavity wall. These are shown in Table 7 and Figs. 16 and 17 for the data set considered.

4. For each value of $\Delta\varepsilon_o$, using the values in step 3, and Eqs. 31a and 31e, obtain the values of ϕ_c and OCR.

5. Establish the relationship between OCR and $\Delta\varepsilon_o$ (see example in Fig.18)

6. If the value of OCR of the clay is estimated by other means (e.g. dilatometer or piezocone data), using this OCR and Fig.18 (for the data considered), the correct value of $\Delta\varepsilon_o$
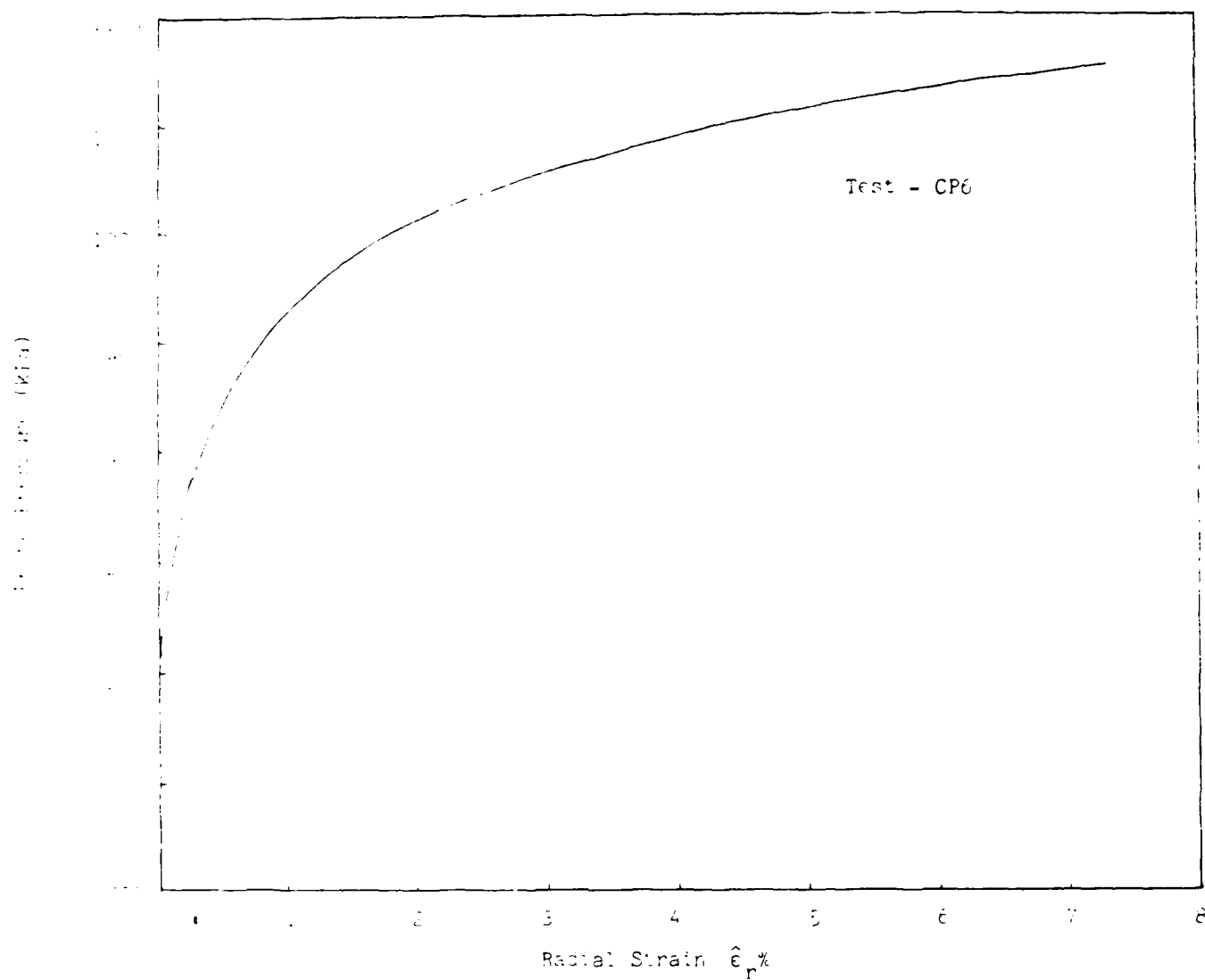
Fig. 3: Model Pressuremeter Expansion Curve (Huang 1986)

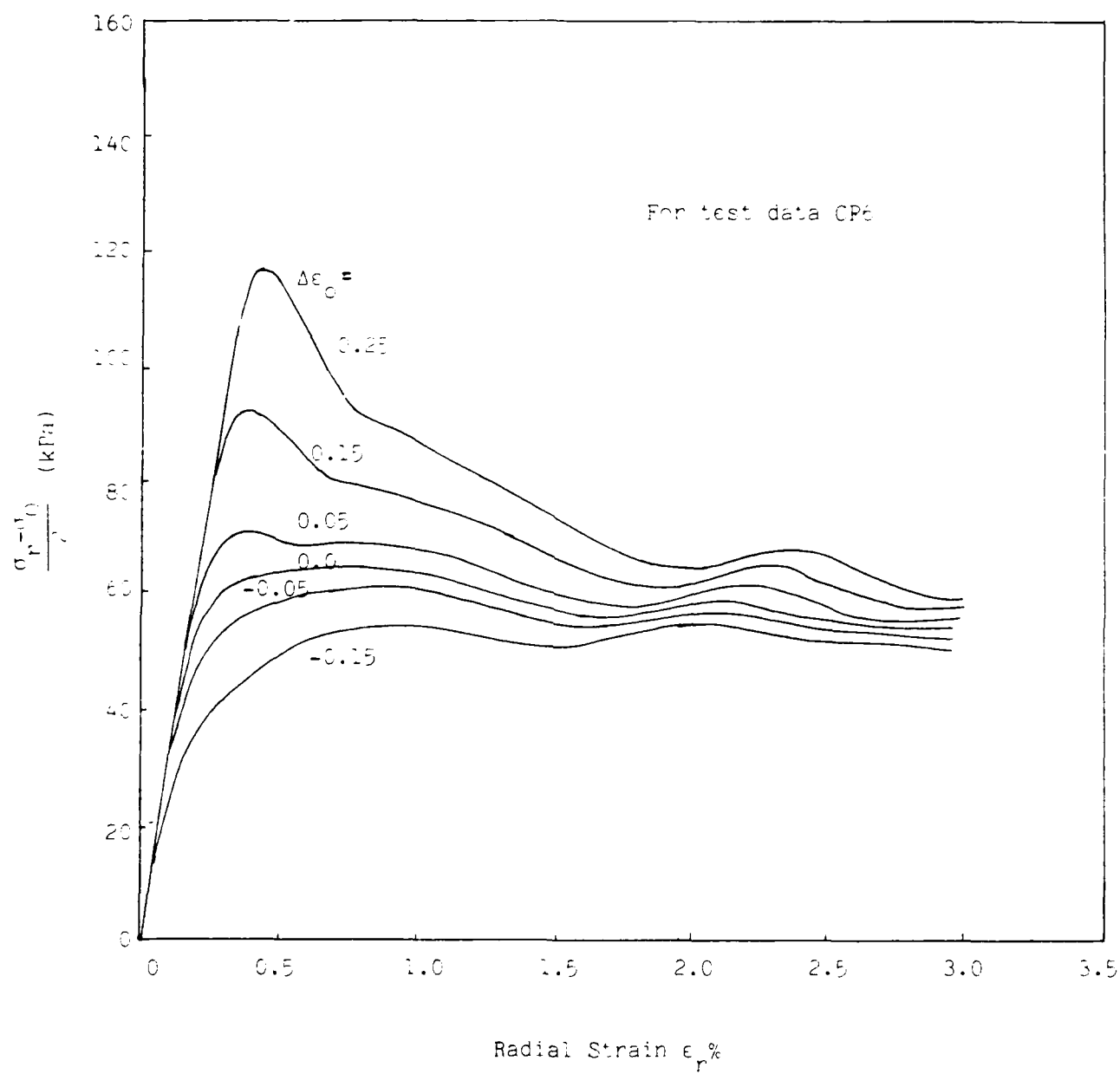Fig. 17 Derived Stress-Strain Curves for Each $\Delta\varepsilon_o$

Table 7: Resulting OCR, ϕ_c for Assumed Values of Error $\Delta\epsilon_o$

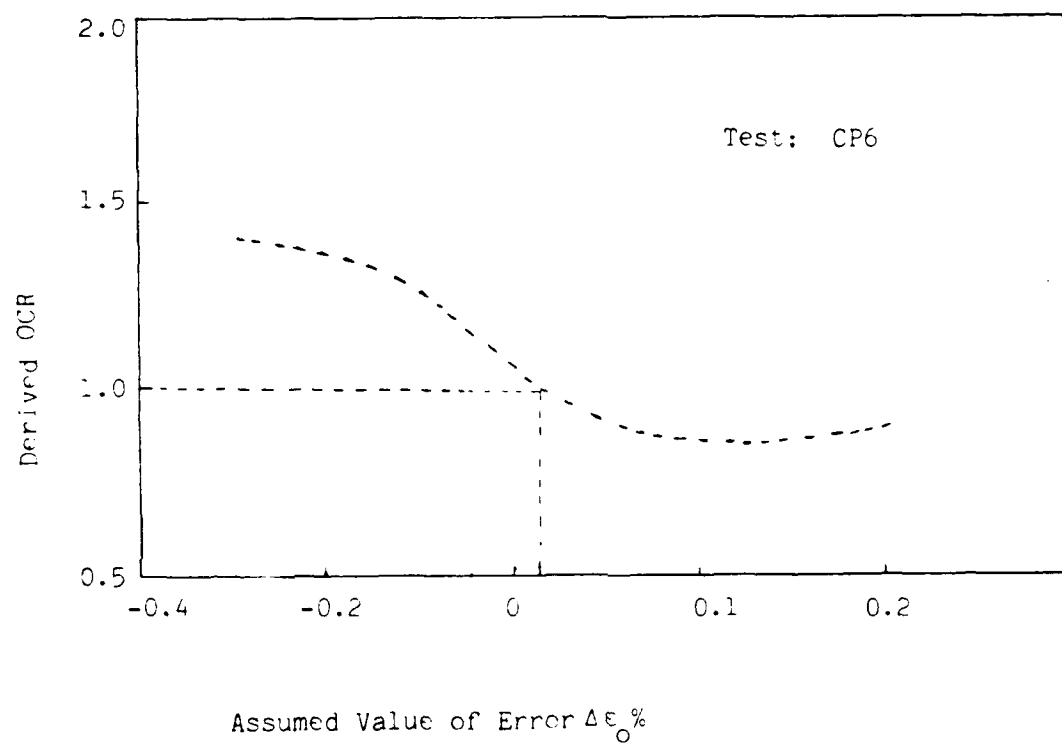| Error $\Delta\epsilon_o$ (%)	τ_{fpm} (kPa)	ϵ_r (%)	$\hat{\epsilon}_r$ (%)	σ_r (kPa)	$\dfrac{\sigma_r}{\tau_{fpm}}$	ϕ_c (deg.)	OCR
0.25	117.0	0.5	0.25	185.0	1.58	62.	0.96
0.15	91.0	0.43	0.28	185.5	2.04	38.	0.85
0.05	71.0	0.36	0.31	191.0	2.70	25.	0.90
0.0	64.4	0.50	0.50	213.3	3.31	19.	1.06
-0.05	60.0	0.7	0.75	241.9	4.03	15.	1.26
-0.15	53.3	0.8	0.95	260.	4.88	12.	1.40

Fig. 18 OCR vs $\Delta\varepsilon_0$ (Refer to Table 7)

can be determined.

For the data in this example problem, OCR is equal to 1.0, the error is found to be about $\Delta\varepsilon_o = +0.02\%$ from Fig. 18. Using this value of $\Delta\varepsilon_o$, the measured strain can be corrected, and true pressuremeter strength and material parameters deduced. For this example, they are given by:

$$\tau_{fpm} = 64.4 \text{kPa}, \quad \frac{\tau_{fpm}}{\sigma_{vo}} = 0.236, \quad \text{and} \quad \phi_c = 19.5 \text{ deg.}$$

The value of ϕ_c is in excellent agreement with that measure in TC, about 20.7°.

3.5.4 Existence of Tensile Stress σ_θ

Ladanyi (1977) indicated the possibility of radial cracking for frozen soils. Wood and Wroth (1977) observed negative value of interpreted circumferential stress σ_θ for some pressuremeter tests in clays. This was thought to lead to radial cracking. If radial cracking is present, then the mode of failure may become that of unconfined compression (Ladanyi 1977). This is a serious problem, because all the current interpretation methods and the necessary relationships to obtain the stress-strain curve of the soil are based on the assumptions that the soil around the cavity remains intact and compatibility of strain holds. If radial cracking is present, then those interpretation methods are no longer valid. This subject has not been studied analytically in detail except some model pressuremeter tests (Huang, 1986 and Chameau et al.,

1987) and simulated plane strain $\dot{\varepsilon}_z = 0$ tests on clays in true triaxial tests (Wood and Wroth, 1977). None of the simulated tests or model pressuremeter tests had any evidence of negative circum-ferential stress. The only theoretical study on mode of deformation in SBPM was done assuming soil as an isotropic-elastic material that is governed by a Mohr-Coulomb criterion with σ_{vo} remaining constant (Wood and Wroth, 1977) (Fig. 19). Clearly this is not a valid assumption for natural clays.

The theoretical results reported herein, Fig. 11c, indicates that radial cracking is possible only when ϕ_c is greater than about 37°, with slightly higher susceptibility for highly overconsoli-dated clays. Therefore, it appears that the likelihood of tensile stresses during the expansion of the probe is very small, possibly with the exception of frozen soils, however, in this case, the theory may not be applicable. This suggests that tensile stresses that have been reported based on current interpretation techniques may not be real, but only a reflection of the interpretation method. A plausible reason for these observations is proposed next.

It can be noted that, in general, whenever a case of tensile σ_θ is reported, it is always combined with an `interpreted' strength much higher than expected for that particular deposit. It is likely that, in many of these reported cases, the interpreted strength is high because the measured expansion curve contains an error in the measurements of radial strain due to initial movement
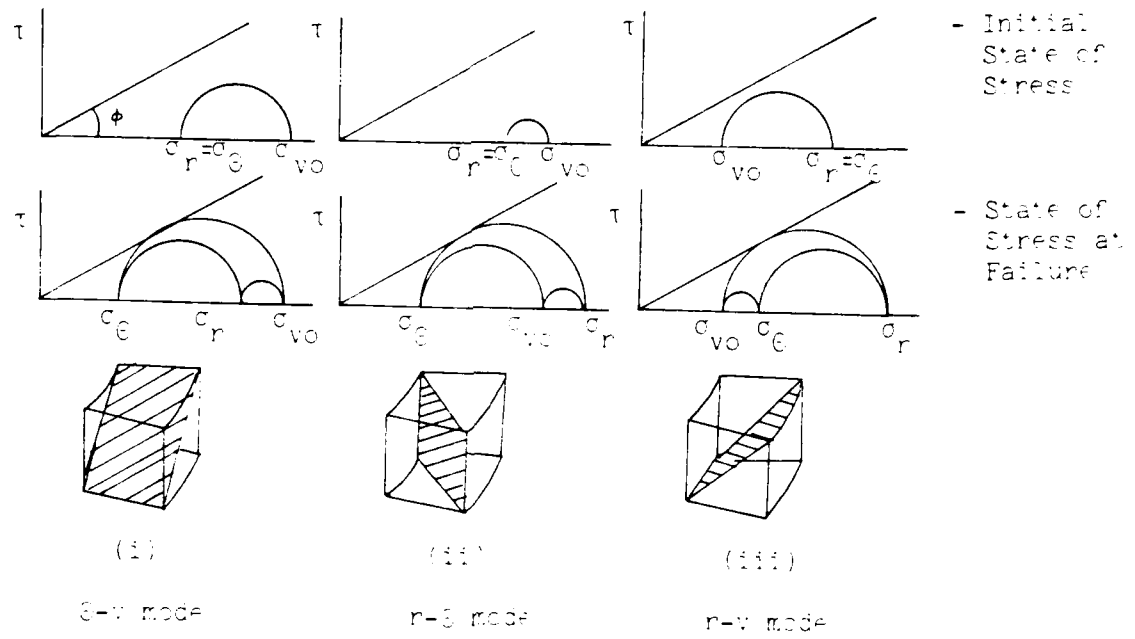
Fig. 19 Mohr-Coulomb Failure with Different Orientations of
Failure Plane (after Wood et al., 1977)

of the probe. This can lead to tensile stresses being computed erroneously as shown in the following.

Let the true material stress-strain of the material be given by:

$$\sigma_r - \sigma_\theta = q(\epsilon_r) \tag{35a}$$

Then, the "true" σ_θ is:

$$\sigma_\theta = \sigma_r - q(\epsilon_r) \tag{35b}$$

Let the interpreted stress-strain of the material be denoted by:

$$(\sigma_r - \sigma_\theta)^i = q^i(\hat{\epsilon}_r) \tag{36}$$

where $\hat{\epsilon}_r$ is the measured strain, and the superscript "i" refers to "interpreted" parameters. The interpreted circumferential stress is:

$$\sigma_\theta^i = \sigma_r - q^i(\hat{\epsilon}_r) \tag{37}$$

If the interpreted relation q^i is greater than the actual relation q, at least for some range of strain, then:

$$\sigma_\theta^i < \sigma_\theta \tag{38}$$

Thus, if q^i is interpreted high, then it is possible that σ_θ^i will reach negative values while σ_θ will in fact be positive. This condition can happen only when the interpreted strength is higher than expected and, thus, any observation related to negative stresses are most probably due to erroneous interpretation. How-

ever, since negative σ_θ is a theoretical possibility (though small) for soils with high ϕ_c, model pressuremeter tests on such clays are needed for clarification of this issue.

3.6 Conclusion

A general 3-D anisotropic model has been developed to study the behavior of clays at the critical state. The model is simple, and holds the promise of being very successful, as shown by comparisons with available data. With the developed relationships one can predict the strength and other failure parameters in any particular mode of failure. In addition, given the initial conditions, one can transform the data to predict the behavior in a different mode of deformation. Using the theoretical development of this report and the data from SBPM, the strength, friction angle, and other failure parameters, along many different modes of failure other than that of SBPM can be predicted. Also, the in situ OCR can be predicted using SBPM data and this theory. A novel approach has been presented to solve the problems caused by initial disturbance in SBPM testing. Possibility of radial cracking is shown to be a rare case. The theory holds the promise of being developed further. It offers a valuable model to study the fundamental aspects of many insitu testing devices in a new perspective.

3.7 Notations

The following symbols are used in this paper:

A_f = Skempton's A-parameter at failure;

CIUC = isotropically consolidated undrained shear test in TC;

CK_oUC = 1-D consolidated consolidated undrained shear test in TC;

CSL = critical state line;

e = void ratio;

f = $f(p,q,r_n)$ - yield surface;

G = shear modulus;

K = bulk modulus;

K_o = coefficient of earth pressure at rest;

K_oNCL = 1-D consolidated normal compression line;

N_o = specific volume intercept of the normal compression line - v vs. lnp at p=1 kPa;

M = q/p, stress ratio at critical state;

PM = pressuremeter test;

PSC = plane strain compression;

PSE = plane strain extension;

PSS = plane stress shearing;

p = mean effective stress;

P_e = exp (N_o-v/λ), equivalent pressure;

q = deviatoric effective stress;

r_n = memory variable, hardening parameter;

SS = simple shear;

TC = triaxial compression;

TE = triaxial extension;

v = 1+e, specific volume;

v_λ = $(v + \lambda \, lnp)$, equivalent specific volume;

α = anisotropic parameter;

α_o = anisotropic parameter at virgin consolid d state;

α_{ij} = anisotropic tensor;

ε_{ij} = strain tensor;

ε_v = $(\varepsilon_1 + 2\varepsilon_3)$ volumetric strain;

ε_q = $\frac{2}{3} (\varepsilon_1 - \varepsilon_3)$ deviatoric strain;

κ = slope of the swelling line in e-lnp plane;

κ_v = slope of the swelling line in e-ln(σ_v) plane;

λ = slope of the normal compression and critical state lines in e-lnp or e-lnσ_v plane;

ν = Poisson's ratio;

η = q/p, stress ratio;

η_o = $(q/p)_o$, stress ratio during virgin consolidation;

ϕ = effective angle of shearing resistance;

ψ = $\dfrac{\partial f/\partial p}{\partial f/\partial q}$

σ_{ij} = stress tensor;

Subscripts:

c = compression;
e = extension;
nc = normally consolidated clay;
oc = over consolidated clay;
vo = initial state in vertical direction;
z = vertical direction

Superscripts:

e = elastic part of ...
p = plastic part of ...
$\cdot$ = increment of ...

TABLE 8 Data Bank Used for Comparison

| NOTATION	SOIL	REFERENCE
1	Florida clay - 1	
2	Florida clay - 2	
3	Florida clay - 3	
4	Hydrite - 10-2	
5	Hydrite - 10-3	Saada, et al. (1975)
6	Girundite - 2	
7	Atchafalay clay - 1	
8	Atchafalay clay - 2	
9	Atchafalay clay - 3	
10	Atchafalay clay - 4	
11	Spestone kaolin	Parry and Nadarajah (1974)
12	Boston Blue clay	Ladd (1965)
13	Haney clay	Vaid, et al. (1974)
14	Remolded Sapparo	Mitachi and Kitago (1979)
15	Kawasaki - M-30 clay	
16	Kawasaki - M-20 clay	Nakase and Kamei (1983)
17	Kawasaki - M-15 clay	
18	Kawasaki - M-10 clay	
19	Weald clay	
20	Vicksburg Buck Shot clay	
21	Undisturbed Kawasaki clay	Ladd (1965)
22	Undisturbed Brobekkvein clay	
23	Undistrubed Skabo clay	
24	Hokkaido silt - 1	
25	Hokkaido silt - 2	Mitachi and Kitago (1976)
26	Hookaido clay	
27	Boston Blue clay	D'Appolonia, et al. (1971)
28	Kaolinite (K100)	Sivakugan (1987)
29	Kaolinite (k50)	
30	Portsmouth Sensitive Marine clay	
31	Bangkok clay	
32	San Francisco Bay mud	
33	Weald clay	Lacasse and Ladd (1973)
34	Portland Marine clay	Ladd and Edgers (1972)
35	Maine Organic clay	Dickey, Ladd and Rixner (1968)
36	Resedimented BBC	
37	Connecticut-Northampton Varved clay	
38	Atchafalay clay	
CP6	kaolin, 100%	
CP8	kaolin, 50%; silt, 50%	Huang (1986)
CP16	kaolin, 100%	
CP23	kaolin, 50%; silt, 50%	
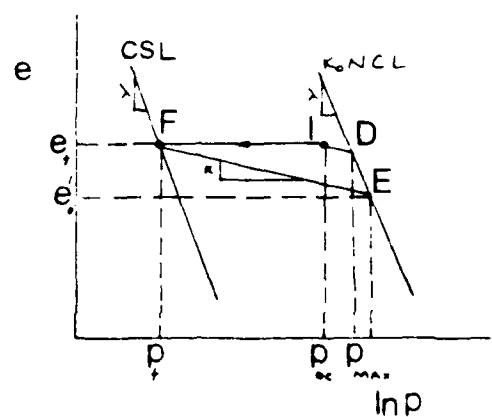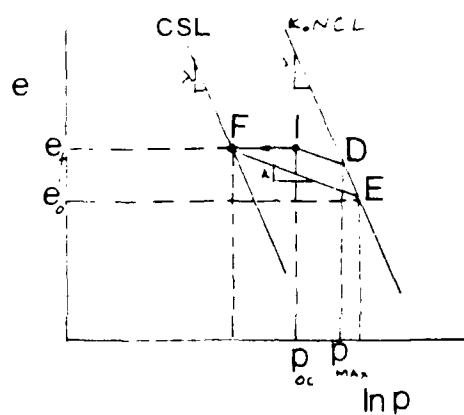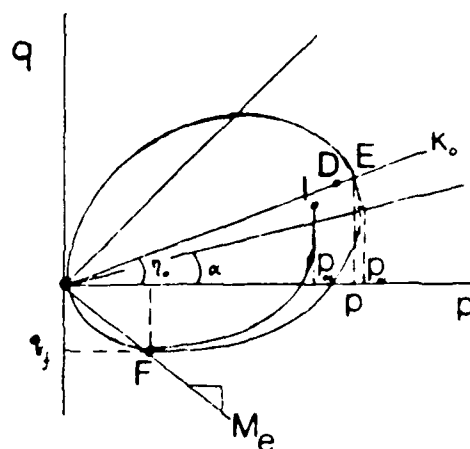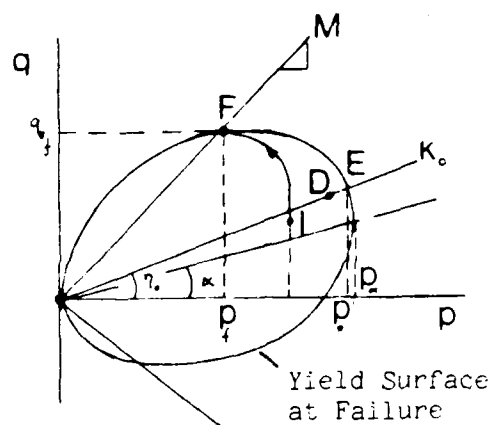
Fig. 20 Effective Stress Path Diagram in Undrained TC/TE
and Yield Surfaces at Failure (Initial state: I,
Effective stress path: IF; Failure state: F)

CHAPTER 4

CONCLUSIONS

This chapter summarizes the main conclusions drawn from this research program.

1. Although CK_oUC test and CIUC test follow different stress paths, it has been shown that a good estimate of the CK_oUC strength can be obtained from a single CIUC test on the same soil. It is a useful relation since the conventional CIUC tests are much easier to run than CK_oUC tests.

2. Expressions were derived for the normalized shear strength τ_f/σ_{vo}' using the Cam clay model, the modified Cam clay model, and the extended Cam clay and modified Cam clay models with spacing ratio. The normalized shear strength is a function of the friction angle and the consolidation characteristics of the soil. Both extended models with spacing ratio predict values that compare well with experimental data. Unlike the excellent agreement with experimental results obtained for τ_f/σ_{vo}', predictions made for Skempton's A parameter at failure A_f were marginal for all models. A_f is very sensitive to Λ, which is a function of C_c and C_r. This severely influences Λ and thus affects the predictions of A_f.

3. A simple procedure is described to predict OCR of saturated clays using normalized virgin consolidation lines. Since the OCR estimate is not sensitive to the C_r/C_c ratio, a good OCR prediction is possible from the knowledge of e/e_L and σ_v'.

4. Emphasis of this work was placed on anisotropy in clays, leading to the development of a general 3-D anisotropic model to study the behavior of clays at the critical state. To the authors' knowledge, it is the first model that captures the essential features of both initial and induced anisotropy yet yielding closed form solutions for all the failure parameters of clays. The main characteristics of the model are as follows:

i. The notion that mean stress at failure is dependent on mode of undrained failure is included;

ii. One axisymmetric yield surface and a general form for the failure surface f^f are introduced, which allow the complete determination of failure parameters for any mode of failure.

iii. The initial anisotropy is properly taken into account in the yield surface and failure criteria.

iv. The effect of induced anisotropy is captured and incorporated by a calibration procedure. Given the initial conditions of the soil, the complete failure behavior at critical state (strength, pore pressures, friction angles, etc.) along any mode of failure can be determined.

v. Limited laboratory testing is required to calibrate the model.

5. The proposed theory is applicable to a number of geotechnical problems; in this report, it was used to investigate several important issues related to the determination of in situ soil properties using the self-boring pressuremeter (SBPM):

(i) The states of stresses at failure in plane strain and plane stress were studied with the anisotropic model. Using these results it was shown that the assumption of the plane strain mode of failure is satisfactory for relatively deep tests. σ_r and σ_θ become the major and minor principal stresses respectively, irrespective of the initial state of stresses. It was also shown that the vertical stress and mean stress do not remain constant in general, in contrast to the predictions made by isotropic-elastic analysis. Currently available experimental data support these findings. All indications are that these findings settle the questions regarding the mode of deformation and the role of vertical stress during the expansion of the cylindrical cavity.

(ii) The possibility of radial cracking (negative circumferential stress) was analyzed in detail and shown to be unlikely; According to this theory, radial cracking is possible only for large friction angles, $\phi_c > 37^\circ$.

(iii) A method to obtain ϕ_c and OCR using the SBPM (ideal) data was outlined, and illustrated through a step by step solution. Using the theory developed in this work, the SBPM failure parameters can be used to determine the same parameters for many different modes of failure other than that of the SBPM.

(iv) A procedure has been proposed to evaluate the error in strain induced by initial movement of the pressuremeter cavity. It is based upon the determination of OCR using the anisotropic model and its independent estimation from other means. After evaluation of the error in strain, actual strength parameters can be calculated.

REFERENCES

[1]   Aas, G. (1965), "A Study of the Effect of the Vane Shape and
        Rate of Strain on the Measured Values of In Situ Shear
        Strength of Clays", Proceedings of the 6th International
        Conference on Soil Mechanics and Foundation Engineering,
        Montreal, Vol. i, pp. 141-145.

[2]   Atkinson, J. H. and Bransby, P. L. (1978), "The Mechanics of
        Soils: An Introduction to Critical State Soil Mechanics",
        McGraw-Hill, London, 375 pp.

[3]   Atkinson, J. H., Richardson, D., and Robinson, P. J. (1987)
        "Compression and Extension of K_o Normally Consolidated Kaolin
        Clay", J. Geotech. Engg. Div., ASCE, Vol. 113 GT12.

[4]   Azzouz, A. S., Krizek, R. J. and Corotis, R. B. (1976),
        "Regression Analysis of Soil Compressibility", Soils and
        Foundations, Vol. 16, No. 2, pp. 19-29.

[5]   Baguelin, F., Jezequel, J. F., Le Mee, E. and Le Mehaute, A.
        (1972), "Expansion of Cylindrical Probes in Cohesive Soils",
        Journal of the Soil Mech. Found. Engrg. Div., ASCE, Vol. 98,
        SM11, pp. 1129-1142.

[6]   Benoit, J. and Clough, G. W. (1986), "Self-Boring Pressureme-
        ter Tests in Soft Clay", Journal of Geotechnical Engrg. Div.,
        ASCE, Vol. 112, No. 1, pp. 60-78.

[7]   Berre, T. and Bjerrum, L. (1973), "Shear Strength of Normally
        Consolidated Clays", Proceedings of the 8th International
        Conference on Soil Mechanics and Foundation Engineering, Mos-
        cow, Vol. I, Part 1, pp. 39-49.

[8]   Bjerrum, L. and Simmons, n. E. (1960), "Comparison of Shear
        Strength Characteristics of Normally Consolidated Clays",
        Research Conference on Shear Strength of Cohesive Soils,
        ASCE, Boulder, CO, pp. 711-726.

[9]   Brooker, E. W. and Ireland, H. O. (1965), "Earth Pressure at
        Rest Related to Stress History", Can. Geotech. Journal, Vol.
        2, No. 2, pp. 1-15.

[10]   Chameau, J. L., Holtz, R. D., Sivakugan, N., and Prapaharan,
        S. (1987), "Fundamental Aspects of Pressuremeter Testing",
        Air Force Office of Scientific Research, Bolling AFB, D.C.,
        186 pp.

[11]   Cozzolina, E.V.M. (1961), "Statistical Forecasting of
        Compression Index", Proceedings of the ᵤth International

Conference on Soil Mechanics and Foundation Engineering, Vol. 1, Paris, pp. 51-53.

[12] Dafalias, Y. F. and Herrman, L. R. (1982), "A Generalized Rounding Surface Constitutive Model for Clays", chapter in Application of Plasticity and Generalized Stress-Strain in Geotechnical Engineering, pp. 78-95, R. N. Yong and E. T. Selig, eds., Special Publication Series by ASCE.

[13] Dafalias, Y. F. (1987), "An Anisotropic Critical State Clay Plasticity Model," Constitutive Laws for Engineering Materials Theory and Applications, Vol. 1, (C. S. Desai, et al., eds.), pp. 513-522.

[14] D'Appolonia, D. J., Lambe, T. W. and Poulos, H. G. (1971), "Evaluation of Pore Pressures Beneath an Embankment," Journal of the Soil Mech. Found. Engrg. Div., ASCE, Vol. 97, SM6, pp. 881-897.

[15] DeLory, F. A. and Salvas, R. J. (1969), "Some Observations on the Undrained Shearing Strength Used to Analyze a Failure", Can. Geotech. Journal, Vol. 6, No. 2, pp. 97-110.

[16] Denby, G.M. (1978), "Self-Boring Pressuremeter Study of the San Francisco Bay Mud", Ph.D. thesis, Stanford Univ., Calif., 270 pp.

[17] Dickey, J. W., Ladd, C. C. and Rixner, J. J. (1968), "A Plane Strain Shear Device for Testing Clays," Technical Report, Research Report R68-3, Soils Publication No. 237, Department of Civil Engineering, MIT, Cambridge, Massachusetts.

[18] Donaghe, R. T. and Townsend, F. C. (1978), "Effects of Anisotropic Versus Isotropic Consolidation in Consolidated Undrained Triaxial Compression Tests of Cohesive Soils", Geotech. Test. Journal, ASTM, Vol. 1, No. 14, pp. 173-189.

[19] Duncan, J. M. and Seed, H. B. (1966), "Anisotropy and Stress Reorientation in Clay," Journal of the Soil Mechanics and Foundation Engrg. Division, ASCE, Vol. 92, SM5, pp. 21-50.

[20] Egan, J. A. (1977), "A Critical State Model for Cyclic Loading Pore Pressure Response for Soils", M.Sc. Thesis, Cornell University.

[21] Graham, J., Noonan, M. L., and Lew, K. V. (1983), "Yield States and Stress-Strain Relationships in a Natural Plastic Clay", Can. Geotech. Journal, Vol. 20, No. 3, pp. 502-516.

[22] Henkel, D. J. and Sowa, V. A. (1963), "The Influence of Stress History on Stress Paths in Undrained Triaxial Tests on

Clay", Laboratory Shear Testing of Soils, ASTM, SPT 361, pp. 280-291.

[23] Holtz, R. D. and Kovacs, W. D. (1981), "An Introduction to Geotechnical Engineering", Prentice-Hall Inc., Englewood Cliffs, N.J., 733 pp.

[24] Houston, W. N. and Mitchell, J. K. (1969), "Property Inter-relationships in Sensitive Clays", Journal of the Soil Mechanics and Foundation Engineering Division, ASCE, Vol. 5, SM4, pp. 1037-1062.

[25] Huang, A. B. (1986), "Laboratory Pressuremeter Experiments in Clay Soils," Ph.D. Dissertation, Department of Civil Engineering, Purdue University, West Lafayette, IN, 236 pp.

[26] Jaky, J. (1948), "Pressures in Silos", Proceedings of the Second International Conference in Soil Mechanics and Foundation Engineering, Rotterdam, Netherlands, Vol. 1, pp. 103-107.

[27] Karube, D. (1975), "Nonstandardized Triaxial Testing Method and Its Problems", 20th Symposium in Soil Engineering, pp. 45-60 (Japanese).

[28] Kavvdas, M. (1982), "Non Linear Consolidation Around Driven Piles", D.Sc. Thesis, MIT, Cambridge, Massachusetts, 666 pp.

[29] Khera, R. P. and Krizek, R. J. (1967), "Strength Behavior of an Anisotropically Consolidated Remolded Clay", Highway Research Rec., Vol. 190, pp. 8-18.

[30] Koppula, S. D. (1981), "Statistical Estimation of Compression Index", Geotechnical Testing Journal, ASTM, Vol. 4, No. 2, pp. 68-73.

[31] Koutsoftas, D. C. and Ladd, C. C. (1985), "Design Strength for an Offshore Clay", Journal of the Geotech. Engrg. Division, ASCE, Vol. 111, GT3, pp. 337-355.

[32] Krishnamurthy, M., Nagaraj, T. S. and Sridharan, A. (1980), "Strength Anisotropy of Layered Soil System", Journal of the Geotechnical Engineering Division, ASCE, Vol. 106, GT10, pp. 1143-1147.

[33] Lacasse, S. M. and Ladd, C. C. (1973), "Behavior of Embankments on New Liskeard Varved Clay," Research Report R73-44, Soils Publication No. 327, Department of Civil Engineering, MIT, Cambridge, Massachusetts.

[34] Ladanyi, B. (1972), "Insitu Determination of Undrained
Stress-Strain Behavior of Sensitive Clays with the Pressurem-
eter", Can. Geot. Journal, Vol. 9, No. 3, pp. 313-319.

[35] Ladanyi, B. (1977), Discussion on "Undrained Stress-Strain-
Time Behavior of Clays" by J. H. Prevost, Journal of the
Geotech. Engrg. Div., ASCE, Vol. 103, GT8, pp. 933-944.

[36] Ladd, C. C. (1965), "Stress-Strain Behavior of Anisotropi-
cally Consolidated Clays During Undrained Shear," Proceedings
of the 6th International Conference on Soil Mechanics and
Foundation Engineering, Montreal, Canada, Vol. I, pp. 282-
286.

[37] Ladd, C. C. and Edgers, L. (1972), "Consolidated Undrained
Direct-Simple Shear Test on Saturated Clays," Research Report
R72-82, MIT, Cambridge, Massachusetts.

[38] Ladd, C. C., Foott, R., Ishihara, K., Schlosser, F. and
Poulos, H. G. (1977), "Stress-Deformation and Strength
Characteristics," Proc. 10th Int. Conf. Soil Mech. Found.
Engg., Vol. 1, Tokyo, Japan.

[39] Ladd, C. C., Germaine, J. T., Baligh, M. M., and Lacasse, S.
M. (1980), "Evaluation of Self-Boring Pressuremeter Tests in
Boston Blue Clay", Report No. FHWA/RD-80/052, 224 pp.

[40] Lade, P. V. and Musante, H. M. (1977), "Failure Conditions in
Sand and Remoulded Clay," Proc. 9th Int. Conf. Soil Mech.
Found. Engg., Tokyo, Japan, Vol. 1, pp. 181-186.

[41] Lade, P. V. and Musante, H. M. (1978), "Three Dimensional
Behavior of Remoulded Clay," J. Geotech. Engg. Div., ASCE,
Vol. 104, GT2, pp. 193-209.

[42] Lewin, P. I. (1973), "The Influence of Stress History on
Plastic Potential," Proceedings of the Symposium on Role of
Plasticity in Soil Mechanics, Cambridge, pp. 96-105.

[43] Lo, K. Y. and Morin, J. P. (1972), "Strength Anisotropy and
Time Effects of Two Sensitive Clays", Canadian Geotechnical
Journal, Vol. 9, No. 3, pp. 261-277.

[44] Massarsch, K. R. et al. (1975), "Measurement of Horizontal In
Situ Stresses", Proceedings of the ASCE Specialty Conference
on In Situ Measurement of Soil Properties, Raleigh, N.C.,
Vol. 1, pp. 266-286.

[45] Matsuoka, H. (1974), "Stress-Strain Relationship of Sands
Based on Mobilized Plane," Soils and Foundations, Vol. 14,
No. 2, pp. 47-61.

[46] Matsuoka, H. and Nakai, T. (1982), "A New Failure Criterion for Soils in Three Dimensional Stresses," Proceedings IUTAM Symposium, Deformation Failure of Granular Materials, Delft.

[47] Mayne, P. W. (1980), "Cam-Clay Predictions of Undrained Strength", Journal of the Geotechnical Engineering Division, ASCE, Vol. 106, GT11, pp. 1219-1242.

[48] Mayne, P. W. (1985), "Stress Anisotropy Effects on Clay Strength," Journal of the Geotechnical Engineering Division, ASCE, Vol. 111, GT3, pp. 356-366.

[49] Mitachi, T. and Kitago, S. (1976), "Change in Undrained Shear Strength Characteristics of Saturated Remolded Clay due to Swelling", Soils and Foundations, Vol. 16, No. 1, pp. 45-58.

[50] Mitachi, T. and Kitago, S. (1979), "The Influence of Stress History and Stress System on the Stress-Strain-Strength Properties of Saturated Clay," Soils and Foundations, Vol. 19, No. 2, pp. 45-61.

[51] Mitachi, T. and Kitago, S. (1980), "Undrained Triaxial and Plane Strain Behavior of Saturated Remolded Clay", Soils and Foundations, Vol. 20, No. 1, pp. 13-28.

[52] Mitchell, J. K. (1976), "Fundamentals of Soil Behavior", John Wiley & Sons, New York.

[53] Mitchell, R. J. (1972), "Some Deviations from Isotropy in Lightly O.C. Clays," Geotechnique Vol. 22, pp. No. 3, pp. 459-467.

[54] Nagaraj, T. S. and Srinivasamurthy, B. R. (1983), "Rationalization of Skempton's Compressibility Equation", Geotechnique, Vol. 33, No. 4, pp. 433-443.

[55] Nagaraj, T. S. and Srinivasamurthy, B. R. (1986), "A Critical Reappraisal of Compression Index Equations", Geotechnique, Vol. 36, No. 1, pp. 27-32.

[56] Nakase, A. and Kobayashi, M. (1971), "Change in Undrained Shear Strength of Saturated Clay due to Rebound", Proceedings of the 4th Asian Regional Conference on Soil Mechanics and Foundation Engineering, Bangkok, Thailand, Vol. 1, pp. 147-150.

[57] Nakase, A. and Kamei, T. (1983), "Undrained Shear Strength Anisotropy of Normally Consolidated Cohesive Soils," Soils and Foundations, Vol. 23, No. 1, pp. 91-101.

[58] Nakase, A. and Kamei, T. (1986), "Influence of Strain Rate on
      Undrained Shear Characteristics of K_0 Consolidated Cohesive
      Soils", Soils and Foundations, Vol. 26, No. 1, pp. 85-95.

[59] Nishida, Y. (1956), "A Brief Note on Compression Index of
      Soil", Journal of the Soil Mechanics and Foundation Engineer-
      ing Division, ASCE, Vol. 82, SM3, Paper No. 1027, 14 pp.

[60] Ohta, H. and Nishihara, A. (1985), "Anisotropy of Undrained
      Shear Strength of Clays Under Axisymmetric Loading Condi-
      tions", Soils and Foundations, Vol. 25, No. 2, pp. 73-86.

[61] Palmer, A. C. (1972), "Undrained Plane Strain Expansion of a
      Cylindrical Cavity in Clay: A Simple Interpretation of the
      Pressuremeter Test," Geotechnique, Vol. 22, No. 3, pp. 451-
      457.

[62] Parry, R. H. G. and Nadarajah, V. (1974), "Observations on
      Laboratory Prepared, Lightly Overconsolidated Specimens of
      Kaolin," Geotechnique, Vol. 24, No. 3, pp. 345-358.

[63] Pender, M. J. (1978), "A Model for the Behavior of the Over-
      consolidated Soil", Geotechnique, Vol. 28, No. 1, pp. 1-25.

[64] Prapaharan, S. (1987), "Effects of Disturbance, Strain Rate
      and Partial Drainage on Pressuremeter Test Results on Clays,"
      Ph.D. Dissertation, Department of Civil Engineering, Purdue
      University, West Lafayette, IN, 268 pp.

[65] Prapaharan, S., Chameau, J. L., Altschaeffl, A. G. and Holtz,
      R. D. (1988), "Effect of Disturbance on Pressuremeter Results
      in Clays", submitted for publication in the ASCE Journal of
      the Geotechnical Engineering Division.

[66] Prevost, J. H. and Hoeg, K., (1976), "Reanalysis of Simple
      Shear Soil Testing", Can. Geotech. Journal, Vol. 13, No. 4,
      pp. 418-429.

[67] Prevost, J. H. (1978), "Anisotropic Undrained Stress-Strain
      Behavior of Clays", Journal of the Geotech. Engrg. Div.,
      ASCE, Vol. 101, GT8, pp. 717-731.

[68] Prevost, J. H. (1979), "Undrained Shear Tests on Clays,"
      Journal of the Geotechnical Engineering Division, ASCE, Vol.
      105, GT1, pp. 49-64.

[69] Roscoe, K. H. and Poorooshasb, H. B. (1963), "A Theoretical
      and Experimental Study of Strains in Triaxial Compression
      Tests on Normally Consolidated Clays", Geotechnique, Vol. 13,
      No. 1, pp. 12-38.

[70] Roscoe, K. H., Schofield, A. N. and Thurairajah, A. (1963), "On Yielding of Clays In States Wetter Than Critical" Geotechnique, Vol. 13, No. 3, pp. 211-240.

[71] Roscoe, K. H. and Burland, J. B. (1968), "On the Generalized Stress-Strain Behavior of Wet Clay," Engineering Plasticity, (J. Heyman and F. A. Leckie, eds.), pp. 535-609, Cambridge University Press.

[72] Saada, A. S. and Bianchini, G. F. (1975), "Strength of One Dimensionally Consolidated Clays," Journal of the Geotech. Engg. Div., ASCE, Vol. 101, GT11, pp. 1151-1164.

[73] Saada, A. S. (1976), "Anisotropy in Heavily Overconsolidated Kaolin," Journal of the Geotech. Engg. Div., ASCE, Vol. 102, GT7, pp. 823-824.

[74] Schofield, A. N. and Wroth, C. P. (1968), "Critical State Soil Mechanics", McGraw-Hill Book Co., London, England, 310 pp.

[75] Sekiguchi, H. and Ohta, H. (1977), "Induced Anisotropy and Time Dependency in Clays", Proceedings of the 9th International Conference on Soil Mechanics and Foundation Engineering, Specialty Session, Tokyo, pp. 229-238.

[76] Sivakugan, N. and Holtz, R. D. (1986), Discussion of "Anisotropy of Undrained Shear Strength of Clays Under Axisymmetric Loading Conditions", by H. Ohta and A. Nishihara, Soils and Foundations, Vol. 26, No. 1, pp. 132-133.

[77] Sivakugan, N. (1987), "Effects of Stress Path and Anisotropy on the Interpretation of the Pressuremeter Test Results", Ph.D. Thesis, Purdue University, 204 pp.

[78] Sivakugan, N., Chameau, J. L. and Holtz, R. D. (1988a), "Spacing Ratio - A State Parameter for Anisotropically Consolidated Clays", in preparation.

[79] Sivakugan, N., Holtz, R. D. and Chameau, J. L. (1988b), "CK UC Shear Strength of Normally Consolidated Clays from $CIUC_0$ Tests", Journal of the Geotechnical Engineering Division, ASCE, Vol. 114, GT3, pp. 284-295.

[80] Skempton, A. W. (1944), "Notes on the Compressibility of Clays", Journal of Geological Society, Vol. 100, pp. 119-135.

[81] Skempton, A. W. and Northey, R. D. (1953), "The Sensitivity of Clays", Geotechnique, Vol. 3, No. 1, pp. 30-53.

[82] Skempton, A. W. (1954), "The Pore Pressure Coefficients A and
      B", Geotechnique, Vol. 4, No. 4, pp. 143-147.

[83] Tavenas, F. et al. (1975), "Difficulties in the In Situ
      Determination of K_o in Soft Sensitive Clays", Proceedings of
      the ASCE Specialty Conference on In Situ Measurement of Soil
      Properties, Raleigh, N.C., Vol. 1, pp. 450-476.

[84] Tavenas, F. and Leroueil, S. (1977), "Effects of Stresses and
      Time on Yielding of Clays," Proc. 9th Int. Conf. Soil Mech.
      Found. Engg., Tokyo, Japan, Vol. 1, pp. 319-326.

[85] Thevanayagam, S. (1988a), "An Anisotropic Model for Critical
      State Behavior of Clays", Internal Report CE-GEOT-88-1, Dept.
      of Civil Engineering, Purdue University, West Lafayette, IN,
      57 pp.

[86] Thevanayagam, S. (1988b), "Mechanics of Cylindrical Cavity
      Expansion in Clays", Internal Report, Dept. of Civil
      Engineering, Purdue University, West Lafayette, IN, 80 pp.

[87] Thevanayagam, S. and Prapaharan, S. (1988, to be published),
      Discussion of "Compression and Extension of K_o Consolidated
      Kaolin Clay", by J. H. Atkinson et al., Journal of the
      Geotech. Engrg. Div., ASCE, Vol. 113 GT12, Dec 1987.

[88] Ting (1968), "Some Effects of History of the Stress-Strain
      Behavior of Kaolin," Ph.D. Thesis, University of Cambridge,
      England.

[89] Vaid, Y. P. and Campanella, R. G. (1974), "Triaxial and Plane
      Strain Behavior of Natural Clay," Journal of the Geotech.
      Engrg. Div., ASCE, Vol. 100, GT3, pp. 207-224.

[90] van Echelen, H. and Potts, D. M. (1978), "The Behavior of
      Drammen Clay Under Cyclic Loading", Geotechnique, Vol. 28,
      No. 2, pp. 173-196.

[91] Wood, D. M. and Wroth, C. P. (1977), "Some Laboratory Experi-
      ments Related to the Results of Pressuremeter Tests,"
      Geotechnique, Vol. 27, pp. 181-201.

[92] Wroth, C. P. and Hughes, J.M.O. (1973), "An Instrument for
      Insitu Measurement of Properties of Soft Clays", Proc. 8th
      Intl. Conf. on Soil Mech. Found. Engrg., Vol. 1.2, Moscow,
      pp. 487-494.

[93] Wroth, C. P. and Wood, D. M. (1978), "The Correlations of
      Index Properties with Some Basic Engineering Properties of
      Soils", Canadian Geotechnical Journal, Vol. 15, No. 2, pp.
      137-145.

[94] Wroth, C. P. (1979), "Correlations of Some Engineering Pro-
     perties of Soils", Second International Conference on
     Behavior of Offshore Structures, Imperial College, London,
     pp. 121-132.

[95] Wroth, C. P. (1984), "The Interpretation of In Situ Soil
     Tests," Rankine Lecture, Geotechnique, Vol. 34, No. 4, pp.
     449-489.

[96] Youssef, M. S., El Ramli, A. H. and El Demery, M. (1965),
     "Relationship between Shear Strength, Consolidation, Liquid
     Limit, and Plastic Limit for Remolded Clays", Proceedings of
     the 6th International Conference on Soil Mechanics and Foun-
     dation Engineering, Montreal, Vol. 1, pp. 126-129.

APPENDIX I

WRITTEN PUBLICATIONS

Three Ph.D. students were partly supported by the research project. One Ph.D. dissertation has been completed:

Sivakugan, N., "Effects of Anisotropy and Stress Path on Interpretation of Pressuremeter Results in Clays", Ph.D. Thesis, December 1987.

The work reported herein will represent an important part of the Ph.D. theses of Mr. S. Thevanayagam and A. Skandarajah.

Two technical papers have already been published or accepted for publication:

[1] Sivakugan, N., Holtz, R. D. and Chameau, J. L., "CK$_o$UC Shear Strength of Normally Consolidated Clays from CIUC Tests", Journal of the Geotechnical Engineering Division, ASCE, Vol. 114, No. 3, March 1988.

[2] Sivakugan, N., Chameau, J. L., Holtz, R. D. and Altschaeffl, A. G., "Servo-Controlled Cuboidal Shear Device", Accepted for publication in the ASTM Geotechnical Journal, 1988.

There are several papers submitted for publication or in preparation which will provide adequate coverage and diffusion of the work described in this report. The following papers will acknowledge the support received from the U.S. AFOSR for this research (for the papers in preparation, tentative authors are given in parentheses in alphabetical order):

"Spacing Ratio - A New State Parameter for Anisotropically Consolidated Clays" (Chameau, Holtz, Sivakugan).

Sivakugan, N., Chameau, J. L., Holtz, R. D. and Huang A. B.,
"An Inexpensive Automatic Control System for Soils Testing",
Abstract sent to Symposium Chair, A. Wissa for inclusion in a
TRB Session - Symposium on Lab/Field Data Acquisition and Con-
trol, Annual Meeting, TRB, 1990.

Prapaharan, S., Chameau, J. L., Holtz, R. D. and Altschaeffl,
A. G., "Effect of Disturbance on Pressuremeter Results in
Clays", submitted for publication in the ASCE Journal of
Geotechnical Engineering, May 1988.

Prapaharan, S., Chameau, J. L. and Holtz, R. D., "Effect of
Strain Rate on Undrained Strength Derived from Pressuremeter
Test", submitted for publication in Geotechnique, April 1988.

"Anisotropy of Clays, a Novel Approach" (Chameau and Thevanay-
agam); this paper will be composed of two parts: Part I -
theory, and Part II - application to pressuremeter testing.

We also expect to diffuse the research results through presen-

tations at technical meetings, and interaction with our colleagues

in the geotechnical community.

END

DATE

FILMED

12-88

DTIC